$$\begin{cases} \dfrac{\mathrm{d}x}{\mathrm{d}t} = \dfrac{k_{\mathrm{B}}}{x} - \dfrac{rg}{p}\dfrac{k_{\mathrm{Fe}}}{y}, \\ \dfrac{\mathrm{d}y}{\mathrm{d}t} = \dfrac{k_{\mathrm{Fe}}}{y} - \dfrac{q}{sg}\dfrac{k_{\mathrm{B}}}{x}. \end{cases}$$

Thermochemical Boriding of Iron–Chromium Alloys

V. I. Dybkov

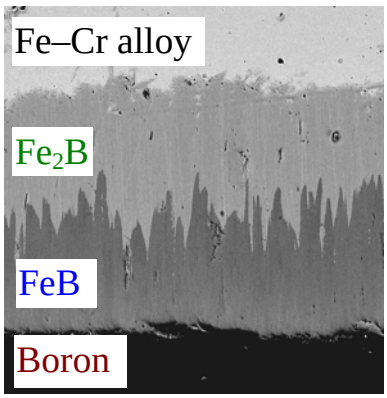

IPMS Publications
Київ 2015 Kyiv

НАЦІОНАЛЬНА АКАДЕМІЯ НАУК УКРАЇНИ

ІНСТИТУТ ПРОБЛЕМ МАТЕРІАЛОЗНАВСТВА

ім. І.М. Францевича

Thermochemical Boriding of Iron–Chromium Alloys

V.I. Dybkov

Department of Physical Chemistry of Inorganic Materials
Institute of Problems of Materials Science
National Academy of Sciences of Ukraine
Kyiv 03142, Ukraine

vdybkov@ukr.net, vdybkov@ipms.kiev.ua

www.dybkov.kiev.ua

IPMS Publications
Київ – 2015 – Kyiv

UDC 541.124:544.41:544.344:546.6/72/75

"Thermochemical boriding of iron–chromium alloys" – V.I. Dybkov.
National Academy of Sciences of Ukraine. I.M. Frantsevich Institute of Problems of Materials Science.- 124 p. (in English).
Mechanism of interfacial formation of boride layers in the course of thermochemical boriding of Fe–Cr alloys and chromium steels is considered. Experimental data on their microstructure, growth kinetics, phase identity, chemical composition, microhardness and abrasive wear resistance are presented. Addressed to researchers, engineers, post-graduates and students of chemical, physical, metallurgical and related specialties.
Illustr. - 70. Tables - 32. Refs.- 83.

УДК 541.124:544.41:544.344:546.6/72/75
"Термохімічне борування залізохромових сплавів" – В.І. Дибков.
Національна академія наук України. Інститут проблем матеріалознавства ім. І.М. Францевича.- 124 с. (Англійскою мовою).
Розглянуто механізм міжфазного утворення боридних шарів при термохімічному боруванні сплавів Fe–Cr і хромистих сталей. Представлено дослідні дані по їх мікроструктурі, кінетиці росту, фазовому і хімічному складу, а також мікротвердості та абразивній зносостійкості. Адресовано науковцям, інженерам, аспірантам і студентам хімічних, фізичних, металургійних та інших спеціальностей.
Ілюстр.- 70. Табл.- 32. Бібліогр.- 83 назви.

УДК 541.124:544.41:544.344:546.6/72/75
"Термохимическое борирование железохромовых сплавов" – В.И. Дыбков.
Национальная академия наук Украины. Институт проблем материаловедения им. И.Н. Францевича.- 124 с. (На английском языке).
Рассмотрен механизм межфазного образования боридных слоев при термохимическом борировании сплавов Fe–Cr и хромистых сталей. Представлено опытные данные по их микроструктуре, кинетике роста, фазовому и химическому составу, а также микротвердости и абразивной износостойкости. Адресовано научным работникам, инженерам, аспирантам и студентам химических, физических, металлургических и других специальностей.
Иллюстр.- 70. Табл.- 32. Библиогр.- 83 назв.

First published: July 20, 2015

Print version
ISBN: 978-966-02-7668-0

Electronic (online) version
ISBN: 978-966-02-7669-7

Contents

1. Introduction

In many practical applications, specific physical, chemical or mechanical properties are only needed for a thin surface layer, a few tens of nanometers to a few tens of micrometers thick, while the main body of a part may be made from a low-cost ordinary alloy or steel. Thermochemical boriding (or boronizing) is one of surface treatments aimed at improving service characteristics of products and parts from metals, alloys and steels [1-6]. It provides a high increase in their hardness and resistance to abrasion, wear, corrosion and oxidation.

A variety of borided parts are now routinely manufactured. Examples include agricultural machinery and aerospace components, automobile and tractor gears, pipe fittings, high wear pumps, tools and dies, steam turbine blades and many others. Such parts usually serve two to five times longer than those treated with conventional techniques such as hardening, carburizing, nitriding or nitrocarburizing. If necessary, all these may readily be combined to obtain a surface coating of desirable properties.

Generally, preliminary information needed in order to choose an optimum boriding procedure is provided by the equilibrium phase diagram of an appropriate system, if known. Phase diagram immediately indicates how many and what compounds may form as separate layers at the interface between the reactants. It should be noted, however, that it by no means dictates that these must necessarily occur simultaneously.

As seen in Fig. 1.1, two iron borides FeB and Fe_2B exist in the Fe–B binary system [7-10]. With iron, its alloys and low-alloy steels, one (either FeB or Fe_2B) or two (both FeB and Fe_2B) boride phases may therefore be expected to form in a coating on the surface of a solid substrate in the course of its thermochemical boriding, depending on temperature-time conditions and a source of boron employed.

Chemical, physical and mechanical properties of boride layers are known to be rather sensitive to the amount of alloying elements and impurities present in a base material. In the case of materials of complicated chemical composition such as multi-component alloys and steels, with which the vast majority of experiments have hitherto been carried out (see, for example, [11-42]), it is not always easy to separate the effect of a particular element on those properties from that of others. To facilitate this task, experiments with binary iron-base alloys are therefore needed.

Note that even if three or more compounds exist in a metal-boron system, in the vast majority of cases only two of them form as separate layers at the interface between reacting phases (see, for example, [43]. This firmly established experimental observation contradicts diffusional considerations [44, 45] predicting the simultaneous formation and subsequent parabolic growth of the layers of all compounds of any binary system, whatever their number, but agrees with a physico-chemical viewpoint [46-49], according to which under conditions of diffusion control one or two layers can occur and grow simultaneously between the reactants, with other compound layers being skipped for kinetic and not thermodynamic reasons.

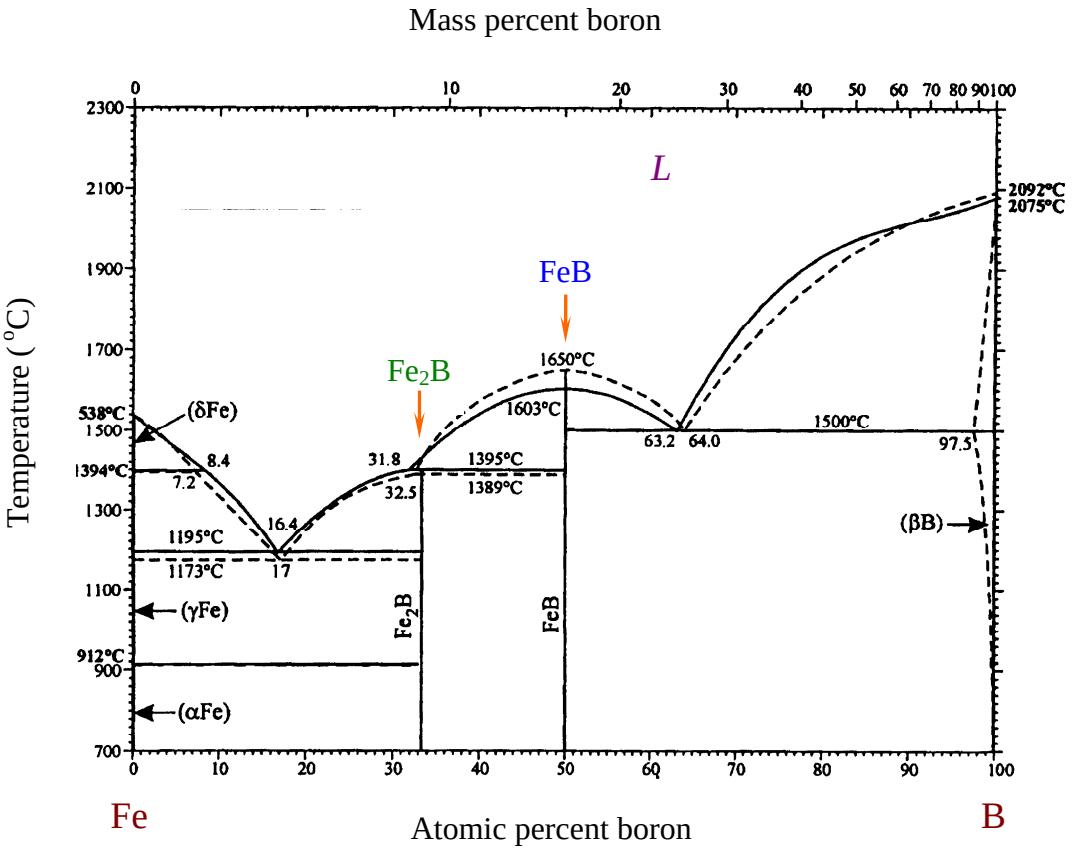

Fig. 1.1. Phase diagram of the Fe–B binary system [7-10].

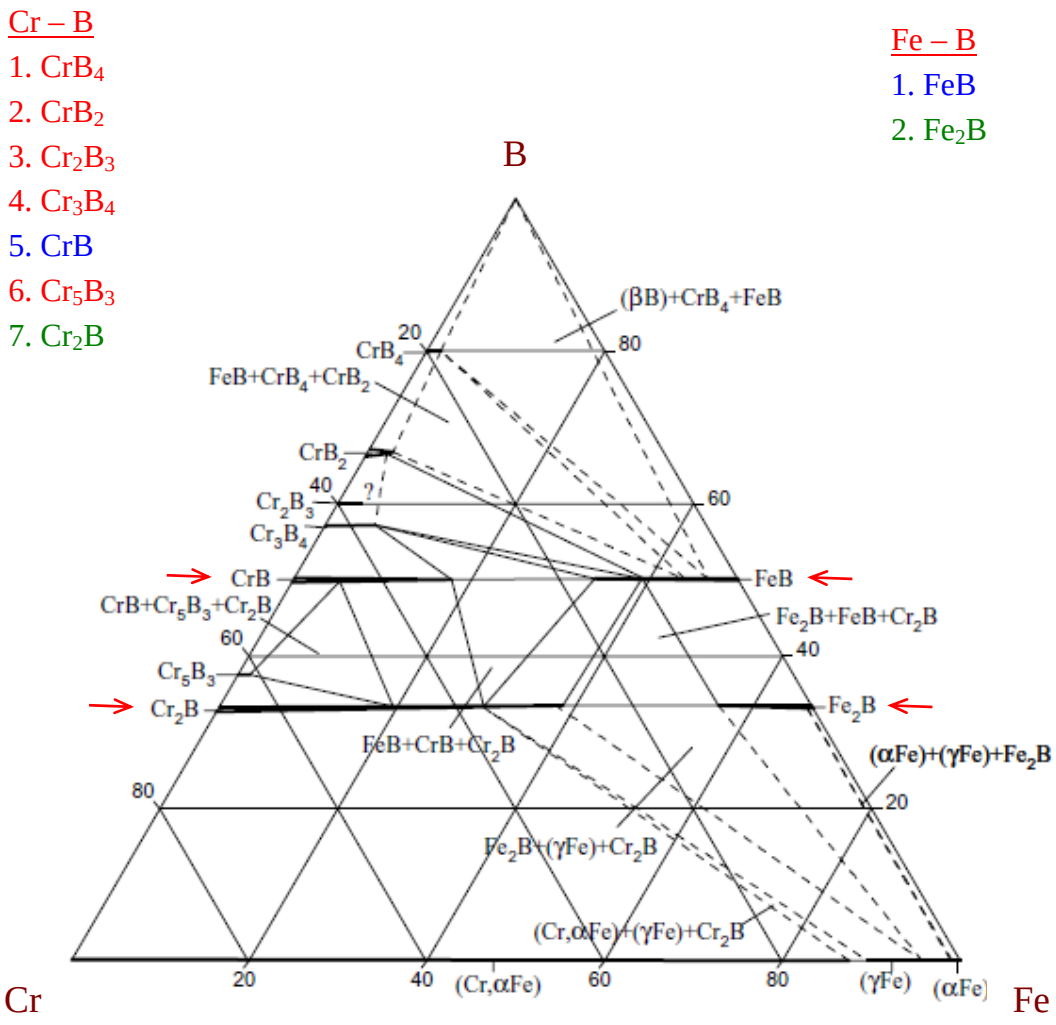

Fig. 1.2. Isothermal section of the Fe–Cr–B ternary system at 900 °C [50].

If the content of a second component of any binary alloy is not too small, ternary and two kinds of binary compounds are likely to form in the alloy-boron transition zone, either as a one-phase or as multi-phase layers. As evidenced from the isothermal section of the phase diagram of the Fe–Cr–B system shown in Fig. 1.2 [50], iron, chromium and boron do not form any ternary compound, while seven compounds CrB_4, CrB_2, Cr_2B_3, Cr_3B_4, CrB, Cr_5B_3 and Cr_2B are known to exist in the Cr–B binary system. Therefore, formation of a complicated structure of boride coatings on the surface of solid samples of Fe–Cr alloys and high chromium steels during their thermochemical boriding might be expected.

Experimental data [51-72] on the interaction of five iron-chromium alloys (5–30% Cr) and two industrial steels containing 13 and 25% Cr with boron in a mixture of amorphous boron powder and KBF_4 (activator) in the temperature range of 850–950 ^oC at reaction times up to 43200 s (12 h) are presented and discussed in this work.

First of all, attention is paid to the phase identification of boride layers formed at the interface of a solid Fe–Cr alloy or steel with boron and the determination of their chemical composition. Two types of layer microstructure (one-phase and two-phase) are shown to exist, depending upon the chromium content of an alloy or steel.

Then, mechanism of layer formation is considered in detail from a chemical viewpoint to provide evidence for the inadequacy of some too simplified physical and metallurgical imaginations existing in the available literature.

Besides, mathematical equations describing layer-growth kinetics and taking account of both the rate of chemical transformations at the layer interfaces and the rate of counter-diffusion of iron and boron atoms across their bulks are briefly analyzed to show why in many cases the solid-state growth of boride (and generally any compound) layers is neither simultaneous, nor parabolic, as follows from purely diffusional considerations.

Eventually, interconnection between the structure and mechanical properties, notably the dry abrasive wear resistance and the microhardness of boride layers formed on the surface of alloy and steel samples, is demonstrated.

Surely, any individual viewpoint is one-sided. Therefore, even though many illustrations and tables may at first sight seem to be excessive, they were nonetheless included in the book. Especially numerous are micrographs showing in detail the microstructure of boride layers in their different sections by a plane parallel and perpendicular to the interface between the reactants. Again, tables not only contain the final results of calculations carried out but also provide the experimental thickness-time relationships in numerical form. Hence, the readers, if any, will have the sufficient amount of initial data in order to draw their own substantiated conclusion about one or the other aspect of thermochemical formation of boride coatings, not necessarily coinciding with that of this or any other researcher. To facilitate, at least partly, solving this task, a detailed explanation of the procedure of calculating the diffusional growth-rate constants of boride layers with the use of parabolic relations and a system of two differential equations, including an Excel computer program, is provided at www.dybkov.kiev.ua (just click here). Clearly, this procedure can readily be applied to treat the growth kinetics not only boride but also any other compound layers.

2. Experimental procedure of thermochemical boriding of alloys and steels

2.1. Materials and samples

The materials used for the preparation of iron-chromium alloys included carbonyl iron powder (99.98% Fe) and electrolytic-grade chromium platelets (99.98% Cr). All contents are given in mass percent if otherwise not stated. Reagents were amorphous boron powder and analytical-grade KBF_4.

Initially, the boron powder contained 98.3% B, 0.04% C, 1.6% O and insignificant amounts of Si, Cu, Mg (< 0.01% each) and Fe (< 0.001%). Before the boriding experiments, the powder was first heated slowly in vacuum up to 1450 °C and then calcined at this temperature for 2 h in an atmosphere of argon at a pressure of 2.5×10^4 Pa to remove volatile oxides. Subsequently, it was cooled by filling the chamber with argon at atmospheric pressure. The average cooling rate (to 200-250 °C) was around 2 °C s^{-1}. After this treatment, no significant changes of the powder morphology and structure were revealed, except for the beginning of resolution of some broad X-ray diffraction peaks.

KBF_4 was preliminary dried stepwise in an electrical furnace at 95, 110, 130 and 170 °C in air. The holding time was 24 h at each temperature.

Cylindrical rods (Fig. 2.1) of Fe–Cr alloys (5, 10, 15, 25 and 30% chromium) were prepared by arc-melting of appropriate amounts of metals under argon, with subsequent casting of the melts into water-cooled copper crucibles. The rods were annealed at a temperature of 1100 °C for 2 h in an argon atmosphere at a pressure of 2.5×10^4 Pa to ensure their homogenization.

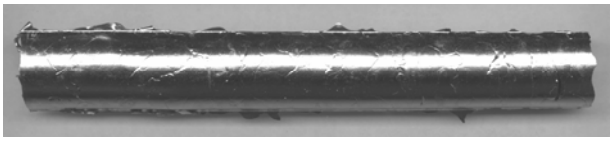

Fig. 2.1. Typical arc-melted rod of an iron-chromium alloy.

Rods (16 mm diameter) of industrial 13 and 25% Cr steels were used in the as-received condition (without any additional heat treatment). The content of main components of 13% Cr steel was 85.2% Fe, 13.6% Cr, 0.38% C, 0.30% Mn, 0.30% Si and 0.20% Ni. 25% Cr steel contained 72.8% Fe, 25.2% Cr, 0.13% C, 0.50% Mn, 0.46% Si, 0.45% Ni and 0.28% Ti. Results of determination of element contents obtained by different methods are compared for two Fe–Cr alloys and 25% Cr steel in Tables 2.1 and 2.2, respectively.

Table 2.1. Chemical composition of Fe–Cr alloy samples.

Nominal composition (%)		Rod No.	Element contents (%)			
			CA		EPMA	
Fe	Cr		Fe	Cr	Fe	Cr
85	15	1	85.1	14.5	84.8	15.2
		2	84.6	15.0	85.4	14.6
70	30	1	70.8	29.9	70.3	29.7
		2	69.6	30.2	70.1	29.9

Note: CA – chemical analysis, EPMA – electron probe microanalysis.

Table 2.2. Chemical composition of industrial 25% chromium steel (15X25T)

Method	C	Fe	Cr	Si	Mn	Ni	Ti
Certificate	0.13	72.8	25.2	0.46	0.50	0.45	0.28
CA	0.15	71.7	25.3	0.42	0.44	0.50	0.26
EPMA	-	72.4	25.1	0.49	0.48	0.43	0.29

Note: CA – chemical analysis, EPMA – electron probe microanalysis.

The microstructure of Fe–Cr alloys and steels is provided in Fig. 2.2. X-ray diffraction analysis (Table 2.3) showed it to consist of the body centered cubic α-phase (ferrite). The steels also contained fine inclusions of carbides $Me_{23}C_6$ (*Me* = Fe, Cr).

Specimens in the form of tablets, 11.28 mm diameter (1.0 cm^2 area) and 5.5 mm high, were machined from the Fe–Cr alloy and steel rods. Flat sides of the tablets were ground and polished mechanically.

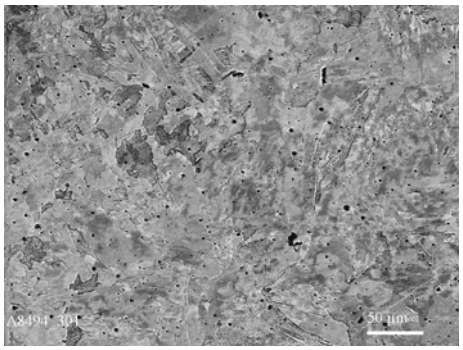

Fe–5% Cr alloy

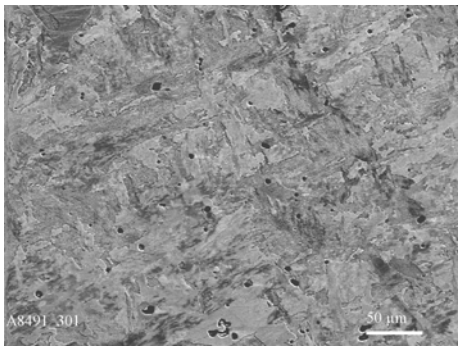

Fe–10% Cr alloy

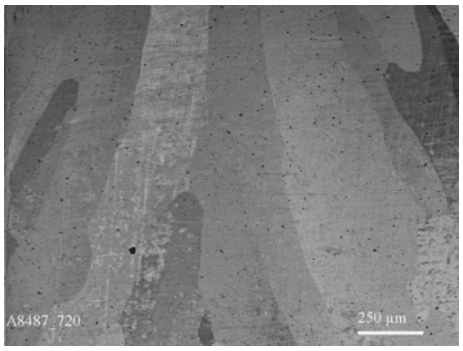

Fe–15% Cr alloy

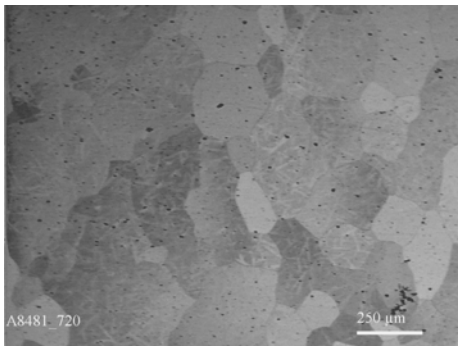

Fe–30% Cr alloy

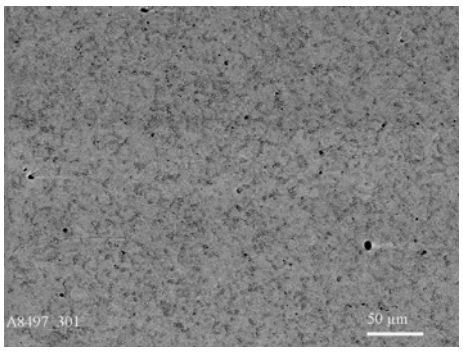

13% Cr steel

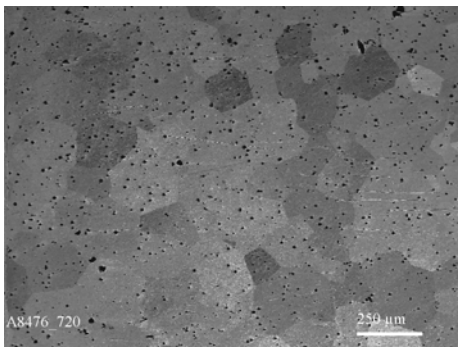

25% Cr steel

Fig. 2.2. Microstructure of Fe–Cr alloys and steels. Polished mechanically and etched for 120 s in a solution of 4 ml HF and 8ml HNO_3 in 100 ml ethanol at room temperature.

Table 2.3. Comparison of the literature values of *d* – spacing for the α-phase (ferrite) with those found experimentally for samples of two Fe–Cr alloys and industrial 25% chromium steel (*HKL* – indexes of reflections)

HKL	$D_{literature}$ for α-phase (nm)		$D_{experimental}$ for samples of two Fe–Cr alloys and industrial 25% chromium steel (nm)				
			Fe–15% Cr		Fe–30% Cr		25% Cr steel
	[73]	[74]	1[#]	2	1	2	
110	0.2027	0.2010	0.2023	0.2027	0.2027	0.2028	0.2030
200	0.1433	0.1428	0.1431	0.1433	0.1435	0.1437	0.1437
211	0.1170	0.1166	0.1170	0.1168	0.1173	0.1174	0.1173
220	0.1013	0.1010	0.1010	0.1014	0.1015	0.1016	0.1016
310	0.0906	0.0904	0.0908	0.0907	0.0908	0.0907	0.0909
222	0.0828	0.0825	0.0829	0.0824	0.0829	0.0826	0.0830

[#] Sample number.

2.2. Investigational methods

The vacuum device VPBD-2S employed for boriding Fe–Cr alloy and steel samples and its experimental cell are shown in Fig. 2.3. Experiments were carried out in an alumina crucible, 13 mm inner diameter and 40 mm high.

An alloy or steel tablet was embedded into a mixture of boron powder with 5% KBF_4 as an activator. This amount of KBF_4 is considered to be optimum [1, 43].

The mixture was then slightly pressed, and a load of 8.5 g (a low-carbon steel cylinder) was placed on top. The crucible was closed with a low-carbon steel lid and placed into a steel-sheet holder, mounted to a guide rod capable of moving in the vertical direction.

The chamber was pumped to a pressure of about 10 Pa and filled with high-purity argon (99.999 vol.% Ar). This procedure was repeated twice. Then, the chamber was again pumped and filled with argon at a pressure of 2.5×10^4 Pa, and heating was started. During heating, the crucible with its contents was in the cold zone above the furnace. After the required temperature in the range of 850-950°C had been reached in the furnace, the crucible, pre-heated to about 400°C, was moved into its middle part.

After an initial drop, the temperature attained its pre-determined value in 4–5 min and was then maintained constant within ± 1°C with the help of an automatic thermoregulator VRT-3. The temperature measurements were carried out using a Pt-PtRh thermocouple. The experiments were carried out at a temperature of 850, 900 and 950°C. Their duration was 3600–43200 s (1–12 h).

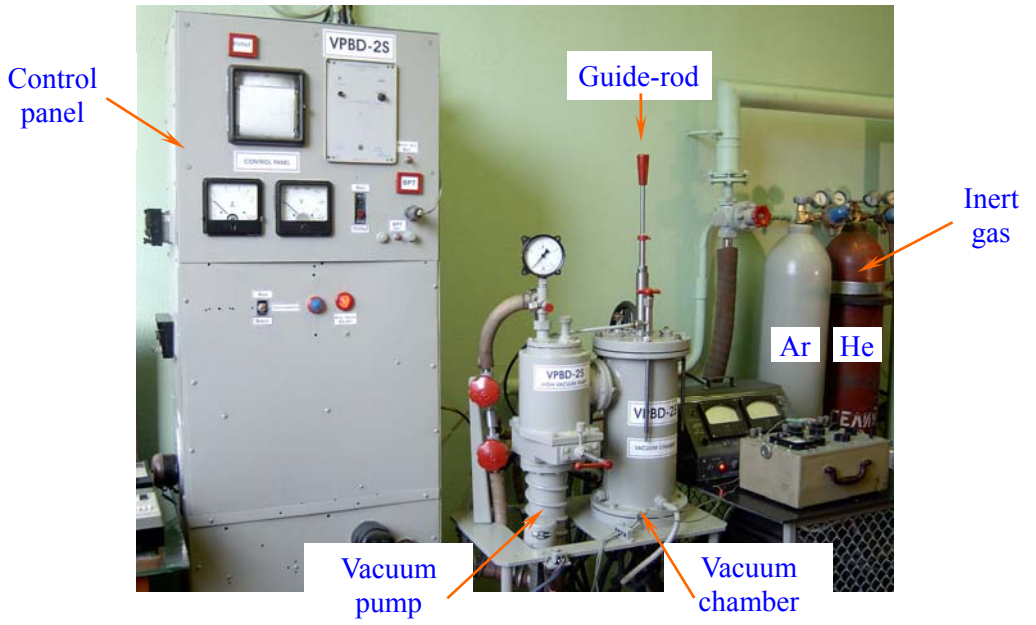

(a)

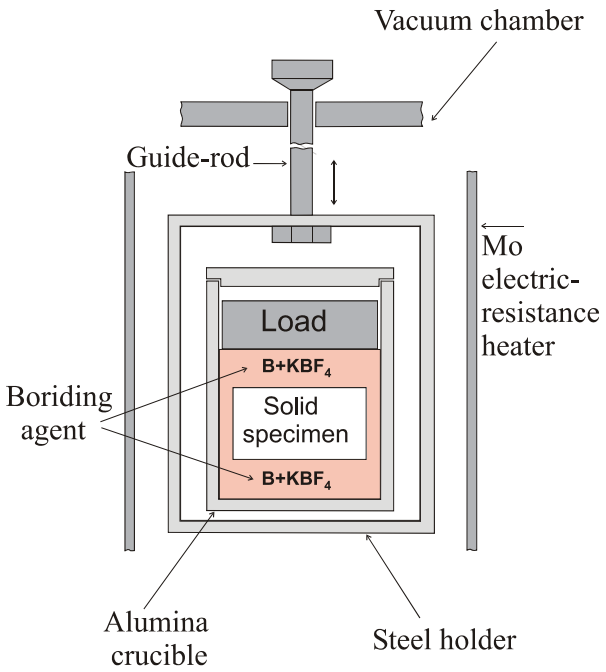

(b)

Fig. 2.3. Vacuum device VPBD-2S employed for boriding Fe–Cr alloy and steel samples: (a) general view and (b) experimental cell.

After the experiment, the tablet with boride layers was cut along the cylindrical axis into two unequal parts (4 mm and 7 mm) using an electric-spark machine, as shown in Fig. 2.4. Its greater part was embedded into a cold-setting epoxy resin and used to prepare a metallographic cross-section. The lesser part was used for X-ray diffraction investigations (plan-view samples).

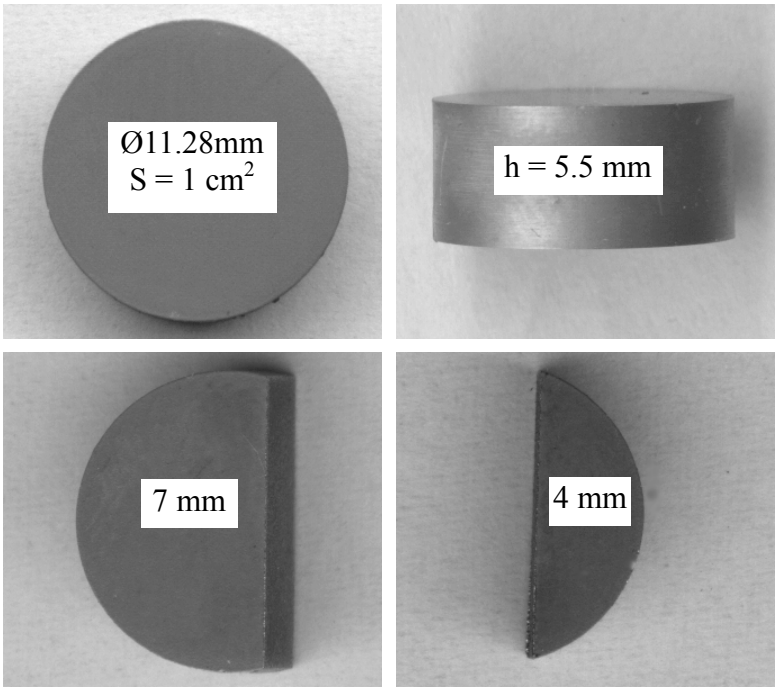

Fig. 2.4. Typical borided tablet of an iron-chromium alloy or steel.

Characterization of initial alloys and steels investigated and boride layers formed was carried out with the help of metallography, X-ray diffraction (XRD) and chemical (CA) analyses, and electron probe microanalysis (EPMA). The thickness of boride layers was evaluated using the pictures obtained on an optical microscope MIM-7 equipped with a HP Photosmart 720 camera. Typically, six pictures were taken at different places of the interface (~ 1 cm long on any cross-section) between the reacting phases. The thickness of each boride layer was calculated by dividing the area occupied by that layer by the length of a region under examination, and the average value of six measurements was found.

Micrographs (backscattered electron images – BEI), contents of boron, iron and chromium in boride layers, and concentration profiles of these elements in the transition zone between reacting phases were obtained using an electron probe microanalyzer JEOL Superprobe 733. Accelerating voltage was 15 kV, while the current was 2×10^{-7} A. The beam spot diameter and the phase volume analyzed at each point were estimated to be about 1 μm and 2 μm^3, respectively.

Boron, iron and chromium standards (≥99.99% each) were employed. Measurements of element contents were treated using a versatile ZAF (atomic number, absorption and fluorescence corrections) program PACM. All three elements (B, Fe and Cr) were determined simultaneously, and the composition was then normalized to 100%. Non-normalized values usually fall in the range 98-102%, providing evidence for a rather good accuracy of measurements, especially in view of the huge difference (more than two orders of magnitude) in intensity of radiation from boron and that from iron or chromium.

X-ray diffraction (XRD) patterns were taken immediately from the surface of tablet plan-view samples on a DRON-3 apparatus equipped with both a computer and a self-recording potentiometer KSP-4. These were obtained at a step of 0.02^{o}, detector rotational speed $0.0167^{o}\ s^{-1}$ ($1^{o}\ min^{-1}$) and sample rotational speed 62.83 rad s^{-1} (600 rpm). The counting time was 10 s at 400 imp s^{-1} and the velocity of the tape movement was 0.167 mm s^{-1} (600 mm h^{-1}). Use was made of Cu K_{α} radiation.

Before taking the first X-ray diffraction pattern, both flat surfaces of a borided tablet sample were slightly polished just to smoothen available elevations around 1 μm high. This practically as-received surface of the tablet was considered to be Section 0 of the sample. Then, 10 to 30 μm of a boride layer (depending upon its total thickness) was removed from the flat surface of the tablet by grinding and subsequent polishing, and another X-ray diffraction pattern was taken (Section I). This procedure was repeated at a step of 30-50 μm until the base material was reached. Five to eight X-ray diffraction patterns were thus taken on each borided alloy or steel sample.

Microhardness measurements on metallographic cross-sections were carried out using a standard PMT-3 tester with the diamond pyramid (Vickers indenter). The load was 0.98 N (100 g).

Dry abrasive wear resistance tests of borided alloy and steel samples were carried out in the sliding mode on P180 SiC emery paper (EP) tape (main fraction grain size 63 μm, maximum 90 μm) using an AWRD-5 device shown in Fig. 2.5. The velocity of continuous movement of the tape (25.0 m long, 0.12 m wide) was 0.35 m s^{-1}, while the gauge length during each test was 22.0 m. The load was 50 N (5.1 kg). Each test was carried out along a fresh track on the tape to ensure identical conditions for all samples. The wear resistance was determined by means of weighing a sample and measuring its height before and after the test.

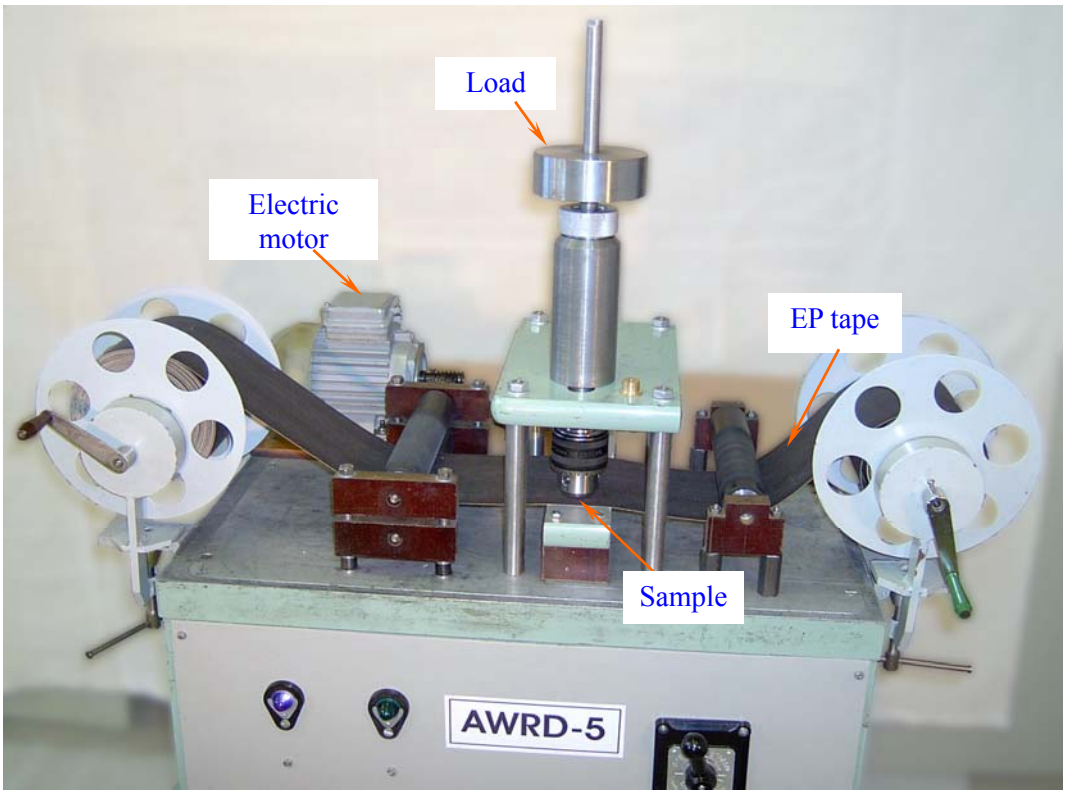

Fig. 2.5. AWRD-5 device for dry abrasive wear resistance tests of borided samples.

3. Phase identity and chemical composition of boride layers

3.1. Constituent phases of boride layers

With all alloys and steels investigated, two continuous boride layers were found to form at the interface between the reactants at a temperature of 850, 900 and 950°C, even though not always their formation was simultaneous. The constituent phases of the layers were identified by plan-view layer-by-layer X-ray diffraction analysis as shown schematically in Fig. 3.1 for Fe–5% Cr and Fe–25% Cr alloys. This figure exhibits two different types (one-phase and two-phase) of layer microstructure that will be analyzed in detail later.

Comparison of experimental X-ray patterns obtained with the available literature data for iron and chromium borides [73-78] indicates that the outer layer bordering boron consists of a solid solution (Fe,Cr)B based on the FeB chemical compound, whereas the inner layer adjacent to the solid substrate consists of a solid solution $(Fe,Cr)_2B$ based on the Fe_2B chemical compound as exemplified in Fig. 3.2 for a Fe–15% Cr alloy. Numerical values of angle 2θ, spacing *d* and peak intensity *I* for boride layers formed on the surface of samples of Fe–5% Cr and Fe–30% Cr alloys and a 25% Cr steel and those for the FeB and Fe_2B phases are additionally provided in Tables 3.1 to 3.6. Literature and experimental values of spacing *d* are seen to agree fairly well, while appropriate peak intensities disagree very considerably. This tendency was observed with all alloys and steels studied.

The strongest reflections were found to be {002} and, to a lesser extent, {020} for the orthorhombic FeB phase, and {002} for the tetragonal Fe_2B phase. It should be noted that with isotropic microcrystalline samples the strongest reflections are {111} (d = 0.21863 nm) {021, 200} (0.20086 nm) and {210} (0.19002 nm) for FeB and {211} (d = 0.20126 nm), {310} (0.16159 nm) and {213} (0.12039 nm) for Fe_2B [73-76].

3.2. Formation of layer texture

Both boride layers possess a pronounced {002} texture and therefore consist of columnar crystals oriented preferentially in the direction of diffusion. This is considered to be a consequence of the existence of paths of enhanced diffusion in the crystal lattices of FeB and Fe_2B phases [1, 22]. If such paths are not available (close rates of diffusion along all crystallographic directions), almost flat boride layers are formed (see, for example, [43]).

The change in intensities of most characteristic reflections with increasing distance from the surface of a borided Fe–15% Cr alloy tablet is illustrated in Fig. 3.3 as an example. Numerical values of intensities presented in Tables 3.7 provide evidence that the larger orientation order is observed for the inner portions of both boride layers compared to their near-interface portions.

This is easily explainable because near-interface portions of any growing boride layer are less equilibrated compared to its bulk portions. Therefore, near-interface crystals have less time to align in the preferred direction. The process of gradual ordering of Fe_2B crystals of the inner boride layer eventually resulting in the formation of its texture is illustrated in Fig. 3.4 [1, 22]. Similarly, texture of the outer FeB layer is formed with passing time.

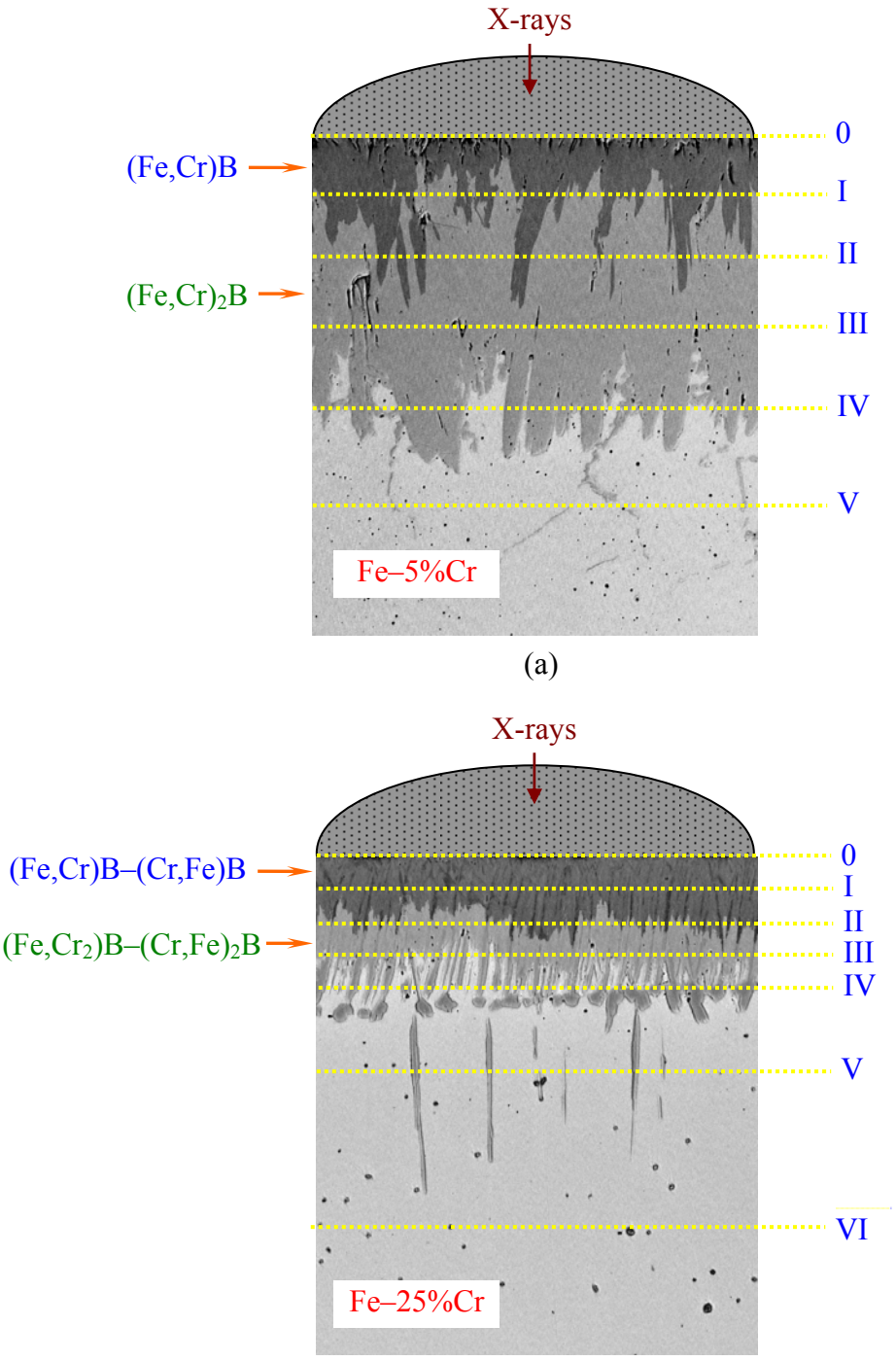

Fig. 3.1. Microstructure and scheme of X-ray diffraction investigations of borided (a) Fe–5% Cr and (b) Fe–25% Cr alloy samples. Boriding conditions: 950°C, 21600 s (6 h). Both boride layers in Fig. 3.1a are one-phase, while those in Fig. 3.1b are two-phase.

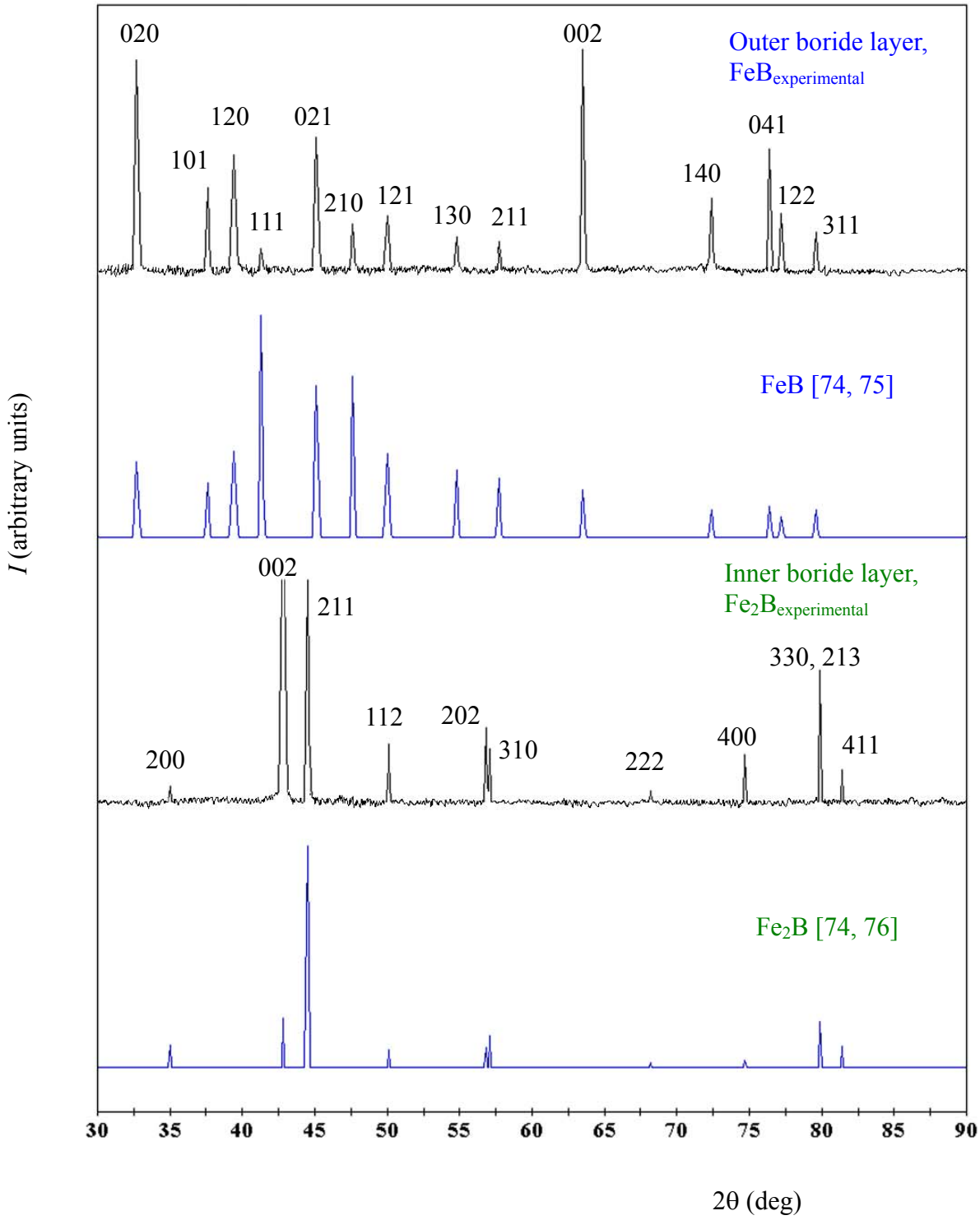

Fig. 3.2. Comparison of literature X-ray diffraction patterns for FeB and Fe_2B phases [74–76] with those obtained experimentally for boride layers formed at the Fe–15% Cr alloy-boron interface after thermochemical boriding at 950 ^{o}C for 21600 s (6 h). The experimental pattern of the outer boride layer was taken from Section 0, while that of the inner boride layer approximately from Section III, see Fig. 3.1a.

Table 3.1. Comparison of literature X-ray data for the FeB phase with our experimental patterns (angle 2θ, spacing *d* and peak intensity *I*) for the outer boride layer (Section 0, see Fig. 3.1a) formed at the 5% Cr alloy-boron interface at 950 °C and a reaction time of 21600 s (6 h)

Literature X-ray data for the FeB phase [74, 75]			Experimental X-ray patterns of the outer boride layer (Section 0, Fig. 3.1a)		
HKL	*d* (nm)	*I* (a.u.)	2θ (deg)	*d* (nm)	*I* (a.u.)
110	0.3259	143	27.4	0.3255	133
020	0.2744	335	32.6	0.2746	190
101	0.2383	239	37.8	0.2380	275
120	0.2272	382	39.7	0.2271	460
111	0.2186	1000	41.3	0.2186	1000
021, 200	0.2008	682	45.2	0.2007	685
210	0.1900	721	47.9	0.1899	910
121	0.1800	375	50.7	0.1800	400
130	0.1667	301	55.0	0.1670	393
211	0.1597	264	57.7	0.1597	330
002	0.1474	209	63.3	0.1469	76
140	0.1303	118	72.8	0.1299	141
041	0.1244	137	76.6	0.1244	125
122	01237	89	77.3	0.1234	40
311	0.1198	120	79.9	0.1200	130

Table 3.2. Comparison of literature X-ray data for the Fe_2B phase with our experimental patterns (angle 2θ, spacing *d* and peak intensity *I*) for the inner boride layer (Section III, see Fig. 3.1a) formed at the Fe–5% Cr alloy-boron interface at 950 ^oC and a reaction time of 21600 s (6 h)

Literature X-ray data for the Fe_2B phase [74, 76]			Experimental X-ray patterns of the inner boride layer (Section III, Fig. 3.1a)		
HKL	*d* (nm)	*I* (a.u.)	2θ (deg)	*d* (nm)	*I* (a.u.)
200	0.2555	100	35.0	0.2564	50
002	0.2125	222	42.6	0.2122	2650
211	0.2013	1000	45.1	0.2010	1000
112	0.1831	80	49.9	0.1828	30
202	0.1634	89	56.3	0.1634	59
310	0.1616	143	57.0	0.1616	60
222	0.1376	20	68.2	0.1375	20
400	0.1278	30	74.4	0.1276	48
123	0.1204	208	79.5	0.1205	210
411	0.1189	97	80.8	0.1190	45

Table 3.3. Comparison of literature X-ray data for the FeB phase with our experimental patterns (angle 2θ, spacing *d* and peak intensity *I*) for the outer boride layer (Section 0, see Fig. 3.1b) formed at the 30% Cr alloy-boron interface at 950 ^{o}C and a reaction time of 28800 s (8 h)

Literature X-ray data for the FeB phase [74, 75]			Experimental X-ray patterns of the outer boride layer (Section 0, Fig. 3.1b)		
HKL	*d* (nm)	*I* (a.u.)	2θ (deg)	*d* (nm)	*I* (a.u.)
110	0.3259	143	27.4	0.3255	24
020	0.2744	335	32.5	0.2749	698
101	0.2383	239	37.3	0.2410	145
120	0.2272	382	39.6	0.2276	28
111	0.2186	1000	41.3	0.2186	32
021, 200	0.2008	682	45.2	0.2006	121
210	0.1900	721	47.8	0.1903	28
121	0.1800	375	50.2	0.1801	32
130	0.1667	301	55.0	0.1670	32
211	0.1597	264	58.0	0.1591	40
002	0.1474	209	63.4	0.1467	1000
140	0.1303	118	72.0	0.1311	60
041	0.1244	137	76.3	0.1248	85
122	01237	89	77.2	0.1238	73
311	0.1198	120	80.2	0.1197	28

Table 3.4. Comparison of literature X-ray data for the Fe_2B phase with our experimental patterns (angle 2θ, spacing *d* and peak intensity *I*) for the inner boride layer (Section III, see Fig. 3.1b) formed at the Fe–30% Cr alloy-boron interface at 950 °C and a reaction time of 28800 s (8 h)

Literature X-ray data for the Fe_2B phase [74, 76]			Experimental X-ray patterns of the inner boride layer (Section III, Fig. 3.1b)		
HKL	*d* (nm)	*I* (a.u.)	2θ (deg)	*d* (nm)	*I* (a.u.)
200	0.2555	100	35.1	0.2557	140
002	0.2125	222	42.8	0.2113	1200
211	0.2013	1000	45.0	0.2014	1000
112	0.1831	80	50.0	0.1824	220
202	0.1634	89	56.5	0.1628	320
310	0.1616	143	57.0	0.1615	200
222	0.1376	20	68.3	0.1373	160
400	0.1278	30	74.2	0.1278	120
123	0.1204	208	79.3	0.1208	280
411	0.1189	97	80.8	0.1189	180

Table 3.5. Comparison of literature X-ray data for the FeB phase with our experimental patterns (angle 2θ, spacing *d* and peak intensity *I*) for the outer boride layer (Section 0, see Fig. 3.1b) formed at the 25% Cr steel-boron interface at 950 ^{o}C and a reaction time of 21600 s (6 h)

Literature X-ray data for the FeB phase [74, 75]			Experimental X-ray patterns of the outer boride layer (Section 0, Fig. 3.1a)		
HKL	*d* (nm)	*I* (a.u.)	2θ (deg)	*d* (nm)	*I* (a.u.)
110	0.3259	143	27.3	0.3258	44
020	0.2744	335	32.6	0.2746	1000
101	0.2383	239	37.7	0.2386	87
120	0.2272	382	39.6	0.2276	52
111	0.2186	1000	41.4	0.2181	157
021, 200	0.2008	682	45.1	0.2010	226
210	0.1900	721	47.7	0.1907	61
121	0.1800	375	50.2	0.1817	70
130	0.1667	301	54.8	0.1675	96
211	0.1597	264	57.5	0.1603	78
002	0.1474	209	63.3	0.1469	895
140	0.1303	118	72.4	0.1305	70
041	0.1244	137	76.3	0.1248	230
122	01237	89	77.3	0.1238	45
311	0.1198	120	80.4	0.1194	65

Table 3.6. Comparison of literature X-ray data for the Fe_2B phase with our experimental patterns (angle 2θ, spacing *d* and peak intensity *I*) for the inner boride layer (Section III, see Fig. 3.1b) formed at the 25% Cr steel-boron interface at 950 ^oC and a reaction time of 21600 s (6 h)

Literature X-ray data for the Fe_2B phase [74, 76]			Experimental X-ray patterns of the inner boride layer (Section III, Fig. 3.1b)		
HKL	*d* (nm)	*I* (a.u.)	2θ (deg)	*d* (nm)	*I* (a.u.)
200	0.2555	100	35.2	0.2549	320
002	0.2125	222	42.8	0.2113	240
211	0.2013	1000	44.9	0.2018	1000
112	0.1831	80	49.6	0.1838	315
202	0.1634	89	56.5	0.1631	320
310	0.1616	143	57.1	0.1613	480
222	0.1376	20	68.3	0.1373	80
400	0.1278	30	74.4	0.1275	480
123	0.1204	208	79.5	0.1205	410
411	0.1189	97	80.4	0.1194	200

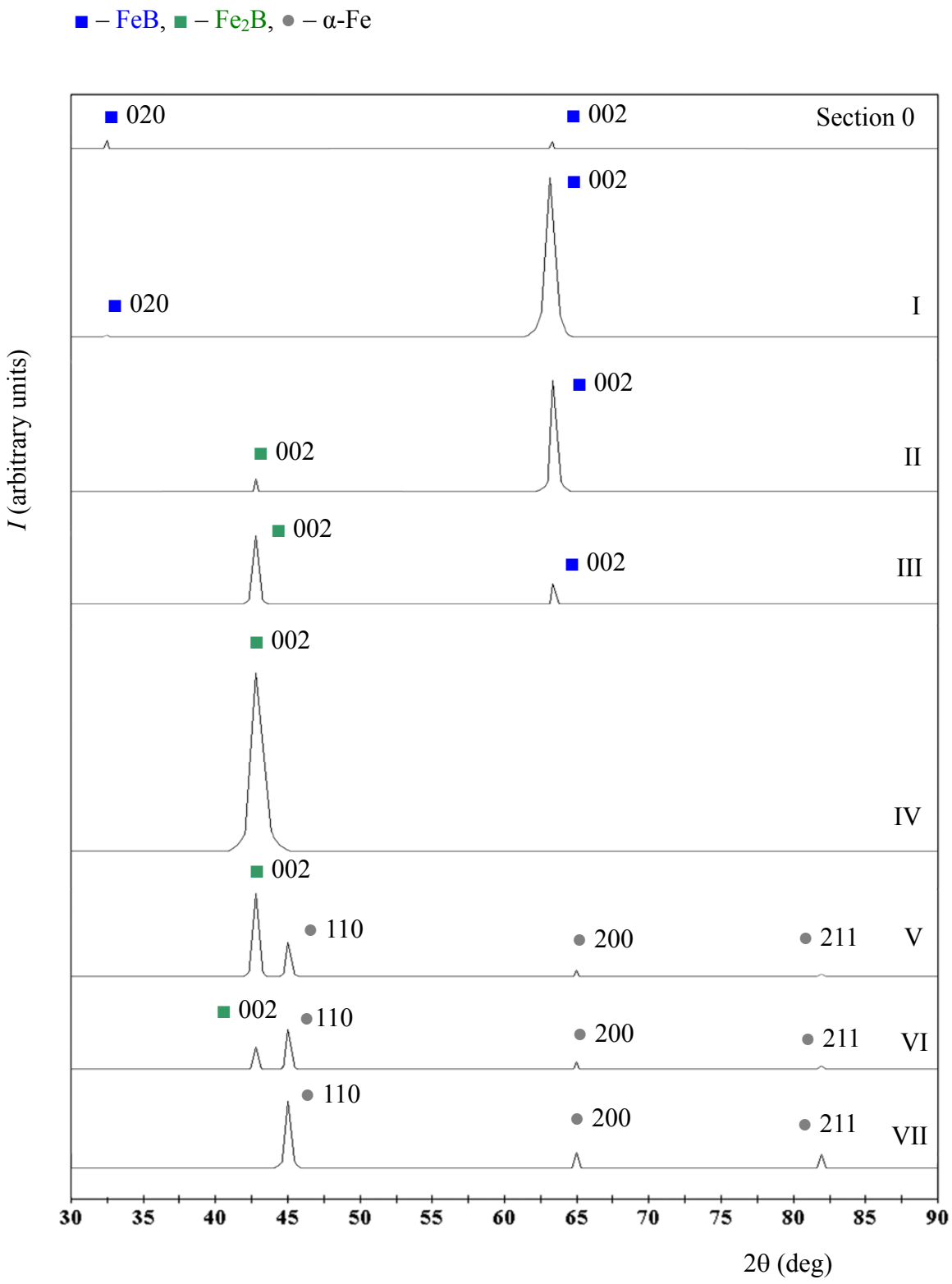

Fig. 3.3. Most intensive reflections of X-ray diffraction patterns taken from different plan-view sections of a Fe–15% Cr alloy sample borided at 950 °C for 21600 s (6 h), see also Figs 3.1 and 3.2, and Table 3.7.

Table 3.7. X-ray diffraction data showing preferential directions of growth for the FeB and Fe_2B phases formed at the interface of a Fe–15% Cr alloy and boron after boriding at a temperature of 950 °C for 21600 s (6 h), see also Fig. 3.3.

Phase	*HKL*	*d* (nm)	Peak intensity (arbitrary units)							
			0#	I	II	III	IV	V	VI	VII
FeB	020	0.275	150	17	9					
	002	0.148	128	2500	1750	332				
Fe_2B	002	0.212			215	1080	2800	1300	350	
α-Fe	110	0.201						538	625	1050
	200	0.143						103	120	250
	211	0.117						42	55	219

Serial numbers of appropriate sections of a borided tablet sample by a plane parallel to its flat surface (Section 0, I and so on, deeper into the sample bulk, see Fig. 3.1).

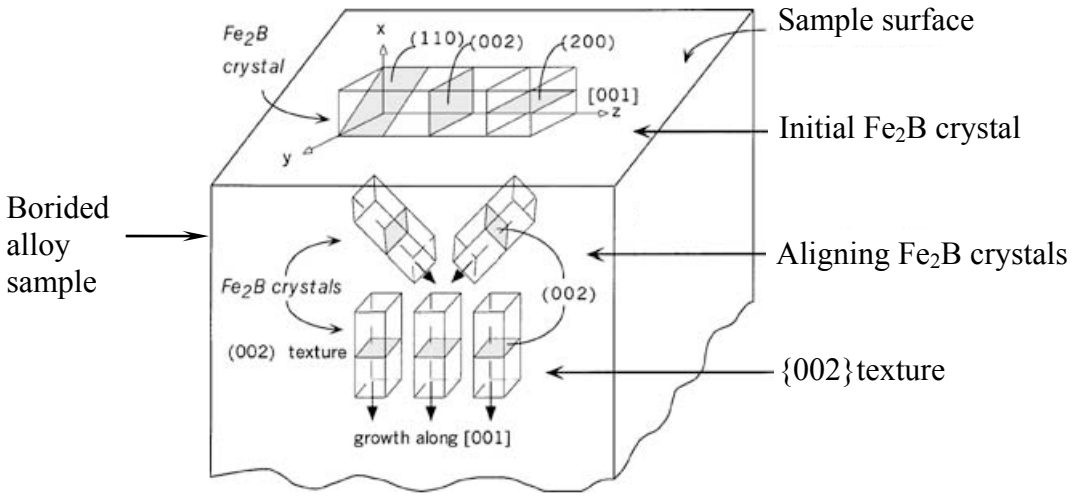

Fig. 3.4. Schematic illustration of aligning the Fe_2B crystals with the formation of texture of the inner boride layer [1, 22].

3.3. Chemical composition of boride layers

3.3.1. One-phase layers

X-ray investigations were followed by EPMA measurements to find out the chemical composition of an appropriate boride layer in its different sections from one interface to another. As seen in Fig. 3.1a, Section 0 of a borided Fe–5% Cr sample corresponds to the FeB phase. Iron, chromium and boron contents of this and other phases, found by EPMA measurements on X-ray diffraction samples, are provided in Table 3.8.

Sections I and II cross both the FeB and Fe_2B phases, with the amount of the FeB phase in Section I (Fig. 3.5a) being larger than that in Section II (Fig. 3.5b). Only the Fe_2B phase is present in Section III (Fig. 3.5c). The microstructure of Sections IV consists of Fe_2B and the alloy base <Fe> insignificantly depleted in chromium compared to its content in the alloy, while that of section V is the alloy base <Fe> of nominal composition 95% Fe–5% Cr.

The solubility of chromium in the FeB and Fe_2B phases formed during thermochemical boriding of Fe–5% Cr alloy samples is rather high (Table 3.8). Actually, it does not differ considerably from its content in the alloy base. The average content of the components in the outer boride layer is 16.3% (50.0 at.%) boron, 79.5% (47.3 at.%) iron and 4.2% (2.7 at.%) chromium that corresponds to the stoichiometry of a solid solution based on the FeB phase.

Chemical composition of the inner boride layer is 8.9% (33.4 at.%) boron, 86.6% (63.1 at.%) iron and 4.5% (3.5 at.%) chromium. These values are in fair agreement with the stoichiometry of a solid solution based on the Fe_2B phase. The Fe_2B layer bordering the alloy base immediately contains a somewhat greater amount of chromium than the more distant FeB layer.

Since both phases FeB and Fe_2B dissolve considerable amounts of chromium, their chemical formulae should be more exactly expressed as (Fe,Cr)B and $(Fe,Cr)_2B$, respectively. Simplified designations FeB and Fe_2B will nonetheless be used for brevity, in particular in writing of chemical and mathematical equations.

In the case of a Fe–10% Cr alloy, the average chromium content was found to be 6 ± 1 at.% in the (Fe,Cr)B layer and 7 ± 2 at.% in the $(Fe,Cr)_2B$ layer. No other essential differences between appropriate boride layers formed on the surface of Fe–5% Cr and Fe–10% Cr alloy samples were revealed either metallographically or by X-ray diffraction or by EPMA.

As seen in Fig. 3.6, with a Fe–15% Cr alloy the microstructure of the transition zone between the reactants is somewhat different from that with Fe–5% Cr and Fe–10% Cr alloys. Sections 0 and I of a borided Fe–15% Cr sample corresponds to the FeB phase (Fig. 3.6). Sections II (Figs 3.6 and 3.7) and III cross both the FeB and Fe_2B phases, with the FeB phase dominating in Section II and Fe_2B phase prevailing in Section III. Section IV only corresponds to the Fe_2B phase (Fig. 3.6). The microstructure of Sections V (Figs 3.6 and 3.8) and VI (Figs 3.6 and 3.9) consists mostly of the alloy base of somewhat changed composition compared to the nominal one with inclusions of crystals of the Fe_2B and occasionally Cr_2B phase. Section VII is entirely the alloy base Fe–Cr of nominal composition 85% Fe–15% Cr.

Table 3.8. Iron, chromium and boron contents of reacting phases, found by EPMA measurements on borided Fe–5% Cr alloy samples after their X-ray diffraction investigations, see also Figs 3.1a and 3.5.

Section in Fig. 3.1a	Region	Content (mass%/at.%)			Phase
		Fe	Cr	B	
0	One-phase	79.5/47.3	4.2/2.7	16.3/50.0	(Fe,Cr)B
I	Darker in Figs 3.1a and 3.5a	80.0/48.1	4.1/2.6	15.9/49.3	(Fe,Cr)B
	Brighter in Figs 3.1a and 3.5a	86.1/62.3	4.8/3.8	9.1/33.9	$(Fe,Cr)_2B$
II	Darker in Figs 3.1a and 3.5b	79.0/46.5	4.3/2.7	16.7/50.8	(Fe,Cr)B
	Brighter in Figs 3.1a and 3.5b	87.0/63.7	4.4/3.4	8.7/32.8	$(Fe,Cr)_2B$
III	One-phase	86.6/63.1	4.5/3.5	8.9/33.4	$(Fe,Cr)_2B$
IV	Darker in Fig. 3.1a	87.1/63.7	4.2/3.3	8.7/33.0	$(Fe,Cr)_2B$
	Brighter in Fig. 3.1a	95.1/94.8	4.9/5.2	0.0/0.0	Fe–Cr
V	One-phase	95.0/94.6	5.0/5.4	0.0/0.0	Fe–Cr

Iron, chromium and boron contents of the phases available in the transition zone between a Fe–15% Cr alloy and boron are provided in Table 3.9. The average chromium content is 8 ± 1 at.% in the (Fe,Cr)B layer and 12 ± 2 at.% in the $(Fe,Cr)_2B$ layer.

Comparison of micrographs of metallographic cross-sections shown in Figs 3.1a and 3.6-3.9 indicates that, in addition to two FeB and Fe_2B boride layers typical of all three Fe–5% Cr, Fe–10% Cr and Fe–15% Cr alloys, thin long crystals are formed near the Fe_2B layer in the case of a Fe–15% Cr alloy. These are enriched in chromium (Fig. 3.10) and penetrate deep into the alloy base. The width of the area occupied by them is comparable with the thickness of boride layers. Like the latter, it increases with passing time.

As seen in Figs 3.11 and 3.12, distribution of the components Fe, Cr and B in the transition zone between the reactants is rather irregular, especially for boron. Most probably, this is due to non-equilibrium conditions of layer formation. Therefore, a scan line crosses crystals of different compositions. The irregularity of distribution of the components within reacting phases is much more profound with a Fe–15% Cr alloy than with Fe–5% Cr and Fe–10% Cr alloys.

Note that no homogeneity ranges of the FeB and Fe_2B phases have been revealed by EPMA measurements across boride layers with all three alloys investigated. As exemplified with a Fe–15% Cr alloy in Table 3.10, the content of Fe, Cr or B is practically the same at any place within any boride layer, whereas in the case of existence of a noticeable homogeneity range it would gradually change from one interface to another.

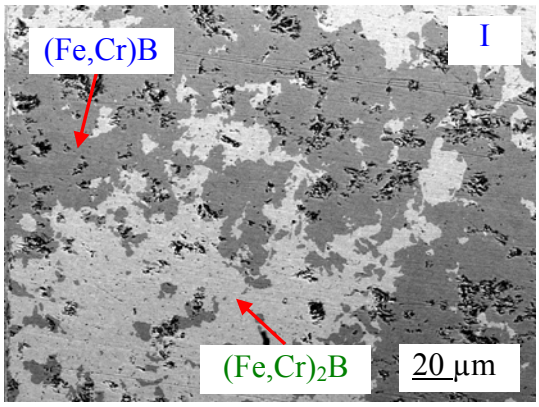

(a)

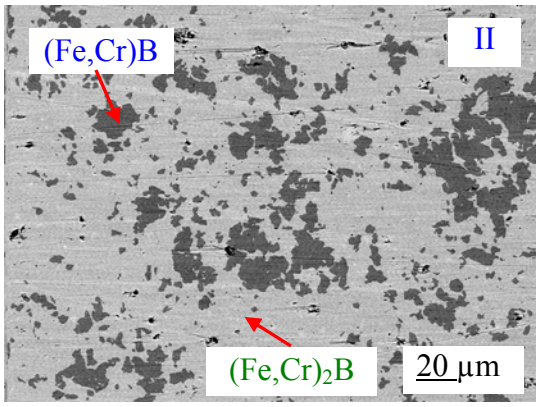

(b)

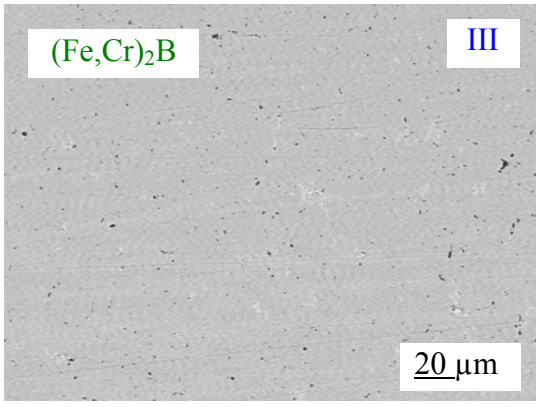

(c)

Fig. 3.5. Microstructure of a Fe–5% Cr alloy sample borided at 950 °C for 21600 s (6 h) in Section (a) I, (b) II and (c) III, see Fig. 3.1a.

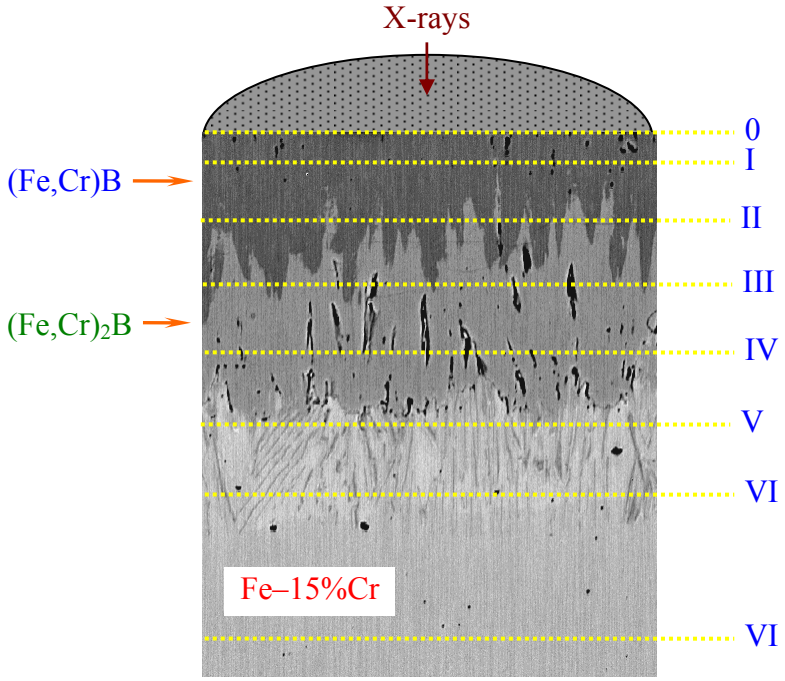

Fig. 3.6. Microstructure and scheme of X-ray diffraction investigations of a borided Fe–15% Cr alloy sample. Boriding conditions: 950 ^{o}C, 21600 s (6 h). Distance between successive sections of the sample (from top deeper inside its bulk): 10 μm (0-I), 30 μm (I-II), 30 μm (II-III), 30 μm (III-IV), 30 μm (IV-V), 30 μm (V-VI) and 50 μm (VI-VII).

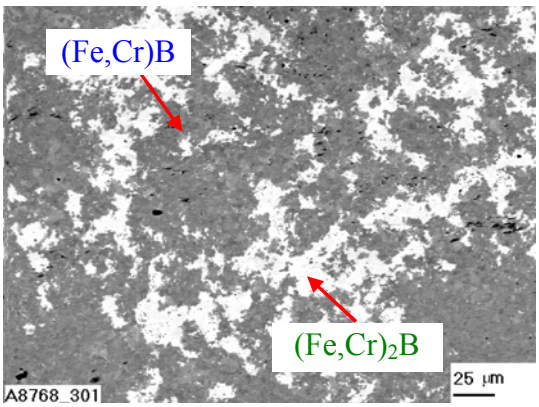

×300

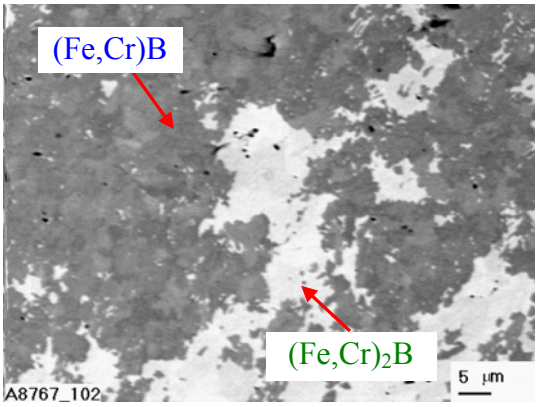

×1000

Fig. 3.7. A plan-view micrograph corresponding to Section II in Fig. 3.6 of a borided Fe–15% Cr alloy sample at magnifications ×300 and ×1000. The darker phase is FeB, while the brighter phase is Fe_2B. Black spots are holes.

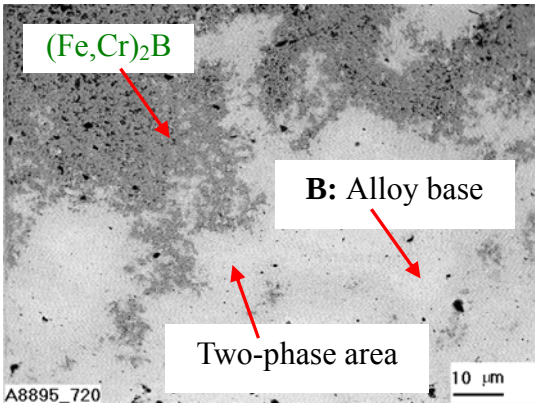

×72

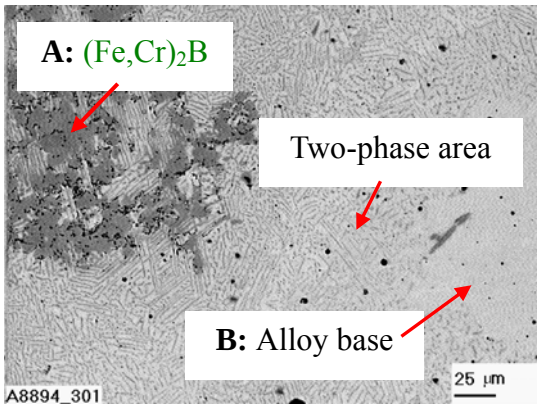

×300

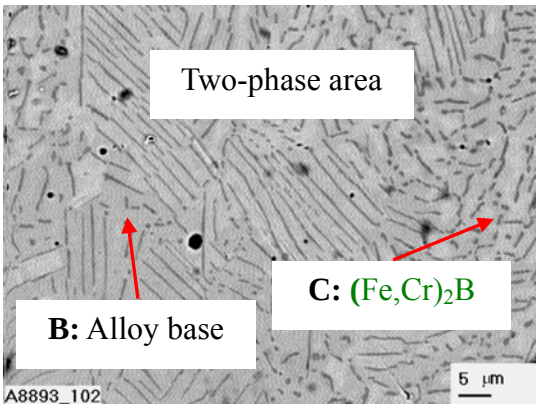

×1000

Fig. 3.8. A plan-view micrograph corresponding to Section V in Fig. 3.6 of a borided Fe–15% Cr alloy sample at magnifications ×72, ×300 and ×1000.

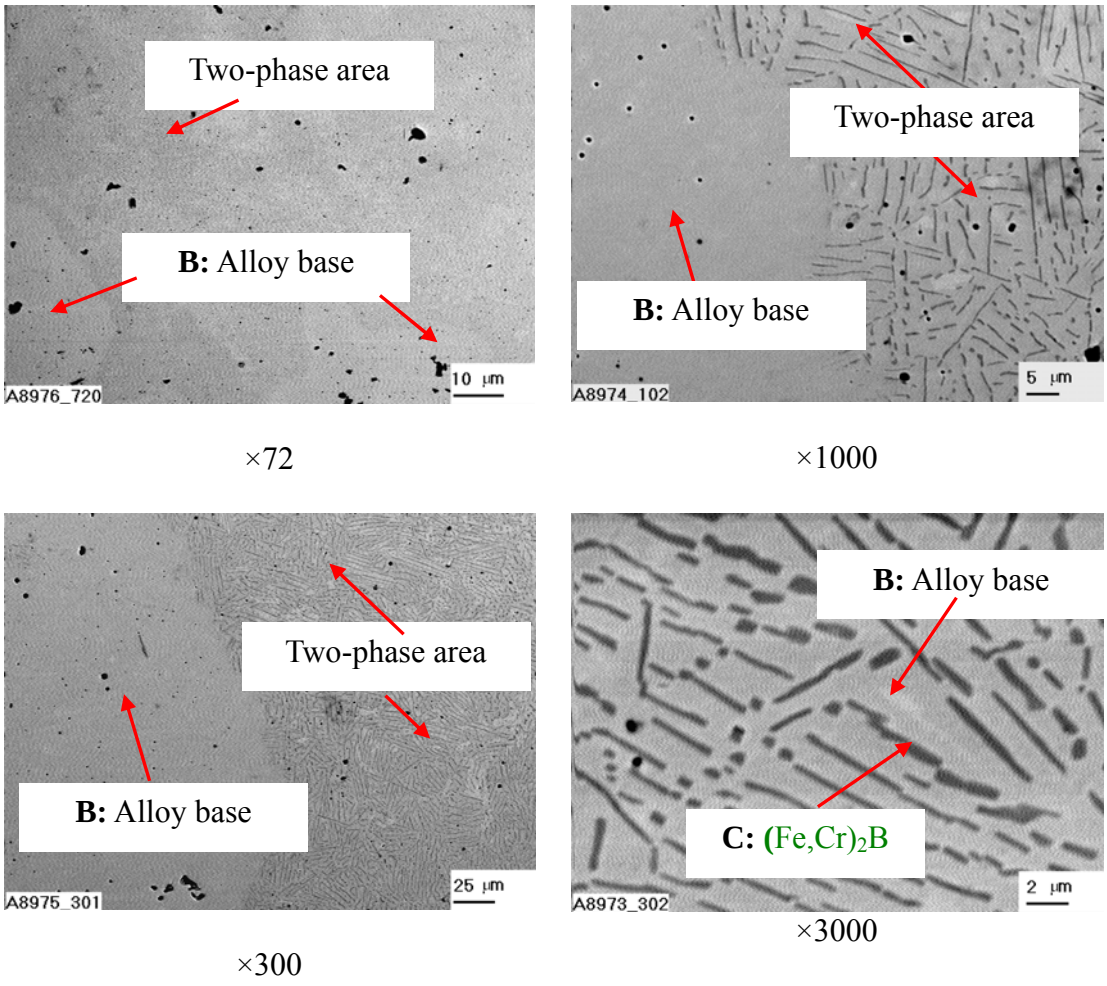

Fig. 3.9. A plan-view micrograph corresponding to Section VI in Fig. 3.6 of a borided Fe–15% Cr alloy sample at magnifications ×72, ×300, ×1000 and ×3000.

Table 3.9. Iron, chromium and boron contents of reacting phases, found by EPMA measurements on borided Fe–15% Cr alloy samples after their X-ray diffraction investigations, see also Figs 3.6-3.9.

Section in Fig. 3.6	Region	Content (mass%/at.%)			Phase
		Fe	Cr	B	
I	One-phase	71.7/42.6	12.1/7.7	16.2/49.7	(Fe,Cr)B
II	Darker in Fig. 3.7	70.7/41.7	12.8/8.1	16.5/50.2	(Fe,Cr)B
	Brighter in Fig. 3.7	77.8/56.4	13.3/10.3	8.9/33.3	$(Fe,Cr)_2B$
IV	One-phase	76.9/55.9	14.3/11.1	8.8/33.0	$(Fe,Cr)_2B$
V	**A** in Fig. 3.8	78.8/57.9	12.8/10.1	8.4/32.0	$(Fe,Cr)_2B$
	B in Fig. 3.8	88.1/87.3	11.9/12.7	0.0/0.0	Fe–Cr
	C in Fig. 3.8	46.9/35.9	44.3/31.6	8.8/32.5	$(Fe,Cr)_2B$
VI	**B** in Fig. 3.9	87.4/85.9	12.4/13.1	0.0/0.0	Fe–Cr
	C in Fig. 3.9	54.5/38.6	36.3/27.7	9.2/33.7	$(Fe,Cr)_2B$
VII	One-phase	85.2/84.3	14.8/15.7	0.0/0.0	Fe–Cr

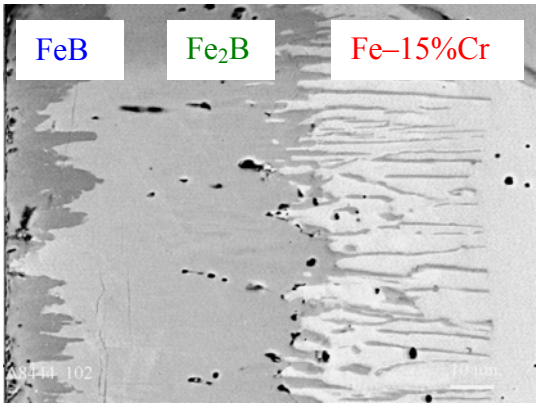

BEI

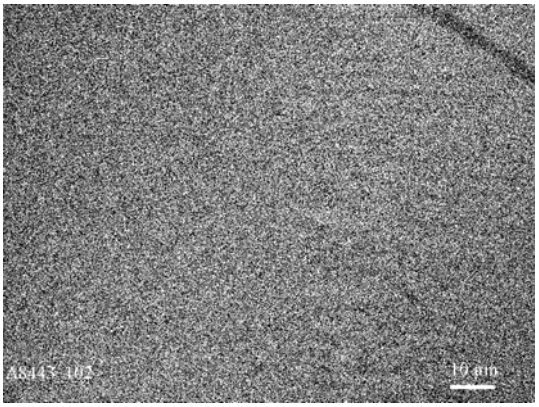

X-ray Fe Kα

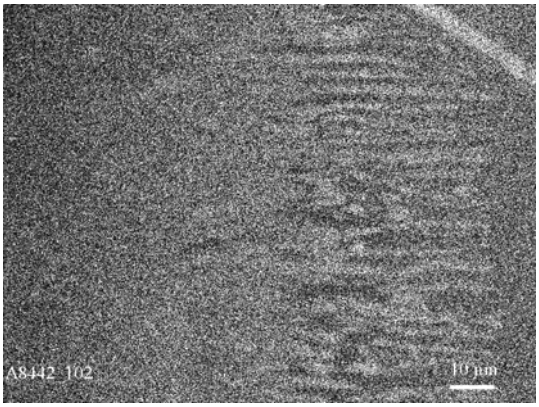

X-ray Cr Kα

Fig. 3.10. Cross-sectional backscattered electron image (BEI) of the transition zone of a Fe–15% Cr alloy sample borided at 950 ^{o}C for 10800 s (3h), and X-ray maps for iron and chromium. The brighter the region, the higher is the content of an appropriate element (Fe or Cr). Long thing crystals near the Fe_2B layer are seen to be somewhat enriched in chromium.

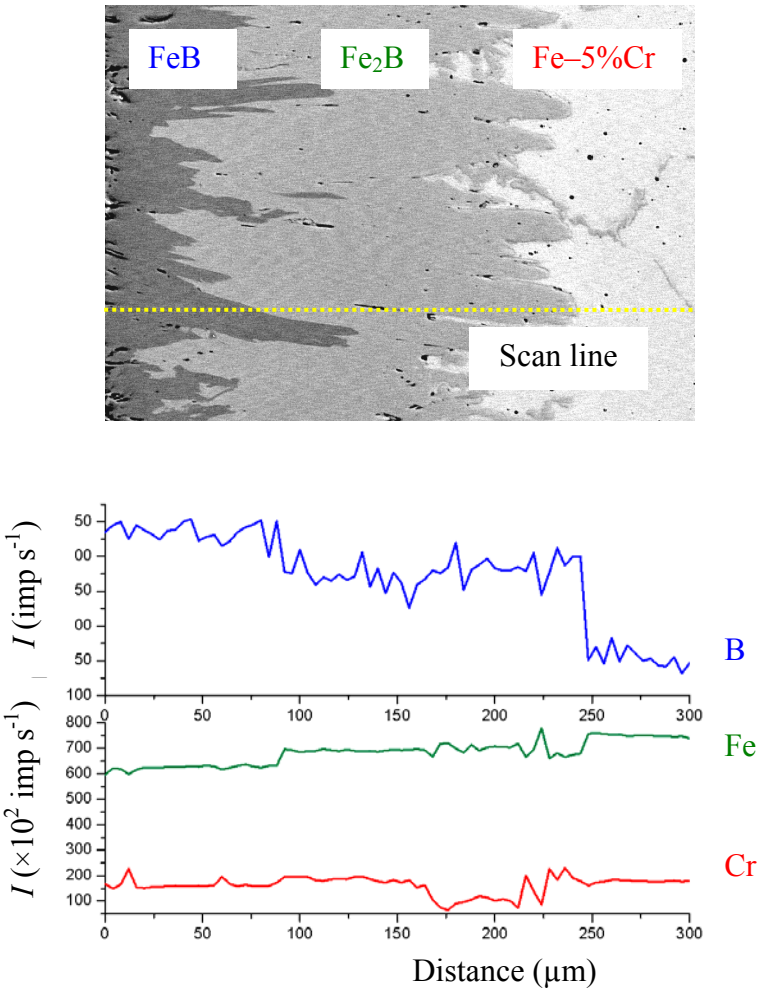

Fig. 3.11. Microstructure of the transition zone between a Fe–5% Cr alloy and boron, and concentration profiles of boron, iron and chromium. Boriding conditions: temperature 950 ^{o}C, reaction time 21600 s (6 h).

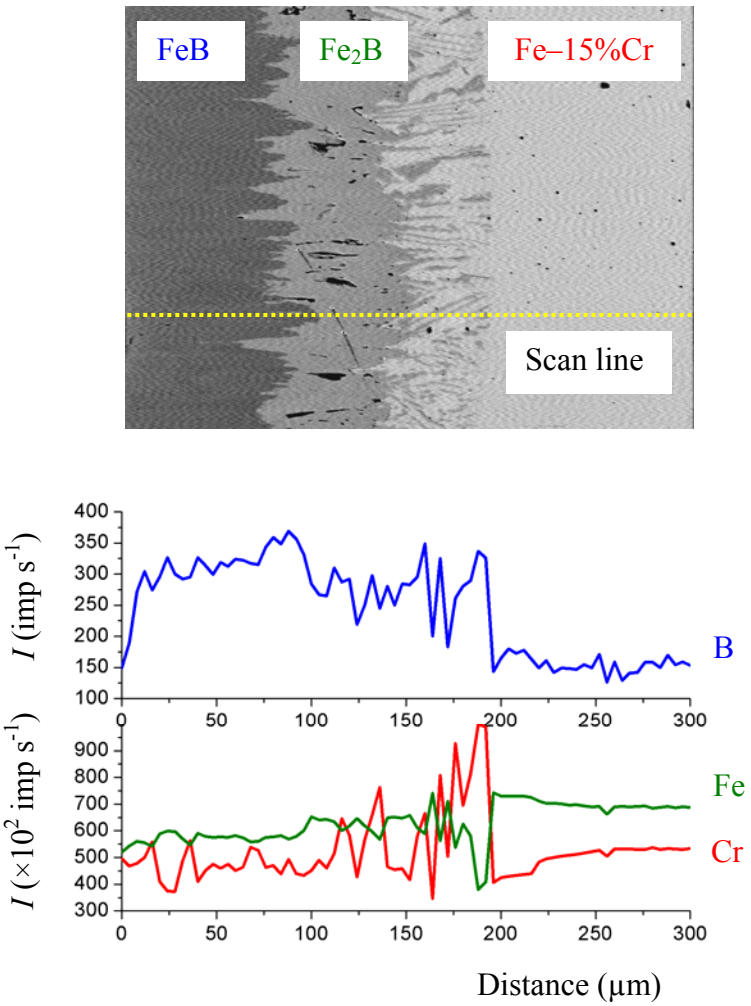

Fig. 3.12. Microstructure of the transition zone between a Fe–15% Cr alloy and boron, and concentration profiles of boron, iron and chromium. Boriding conditions: temperature 950 ^{o}C, reaction time 21600 s (6 h).

Table 3.10. EPMA data for the Fe–15% Cr alloy-boron transition zone, showing the lack of homogeneity ranges of the FeB and Fe_2B phases. The scatter of Fe, Cr and B contents within both boride layers is purely statistical. Boriding conditions: temperature 950 °C, reaction time 21600 s (6 h)

Alloy or layer	Place of measurement	Content (mass%/at.%)			Phase
		Fe	Cr	B	
	At distance l away from the alloy-boride layer interface				
Alloy Fe–Cr	*l* = –200 μm	85.3/84.4	14.7/15.6	0.0/0.0	Solid solution <Fe>
	–120	84.7/83.7	15.3/16.3	0.0/0.0	
	–60	86.1/85.2	13.9/14.8	0.0/0.0	
	–40	88.1/87.4	11.9/12.6	0.0/0.0	
	–20	86.3/85.4	13.6/14.5	0.02/0.11	
Inner boride layer	10	71.8/51.5	19.0/14.6	9.2/33.9	$(Fe,Cr)_2B$
	20	80.0/57.4	10.8/8.4	9.2/34.2	
	30	78.2/56.5	12.8/9.9	9.0/33.6	
	40	77.8/56.9	13.7/10.8	8.5/32.3	
	50	75.5/54.7	15.7/12.3	8.8/33.0	
	60	77.8/57.7	14.1/11.3	8.1/31.0	
	70	77.5/55.3	13.1/10.1	9.4/34.6	
Outer boride layer	80	71.2/42.6	12.8/8.2	16.0/49.2	(Fe,Cr)B
	90	71.3/42.0	12.2/7.8	16.5/50.2	
	100	70.5/41.6	13.0/8.2	16.5/50.2	
	110	71.7/43.0	12.5/8.0	15.9/49.0	
	120	71.6/42.3	12.0/7.6	16.4/50.1	

To show that boride layers formed in 13% Cr steel samples are similar to those formed in Fe–5% Cr, Fe–10% Cr and Fe–15% Cr alloy ones, microstructures, X-ray maps of iron and chromium, and Fe, Cr and B concentration profiles are provided for this steel in Figs 3.13-3.18. Also, iron, chromium and boron contents of reacting phases are given in Tables 3.11 and 3.12.

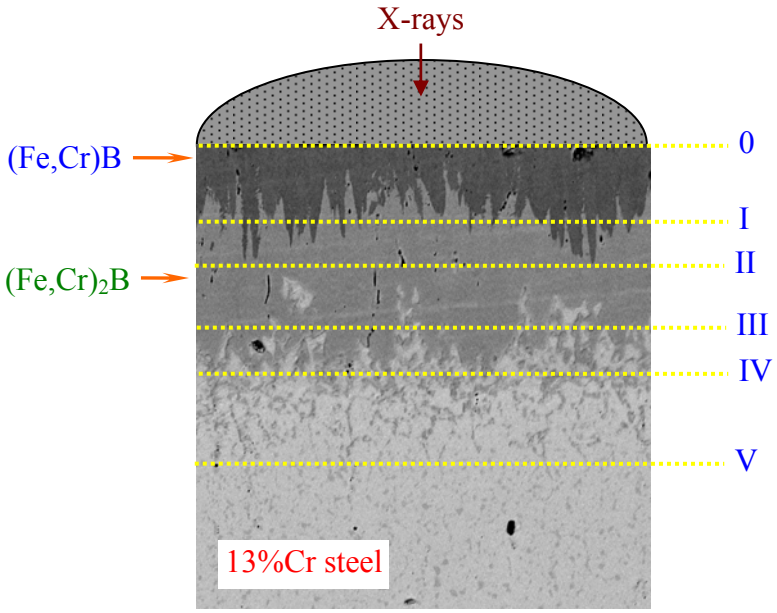

Fig. 3.13. Microstructure and scheme of X-ray diffraction investigations of a borided 13% Cr steel sample. Boriding conditions: 950 °C, 21600 s (6 h). Distance between successive sections of the sample (from top deeper inside its bulk): 40 μm (0-I), 20 μm (I-II), 30 μm (II-III), 25 μm (III-IV) and 30 μm (IV-V).

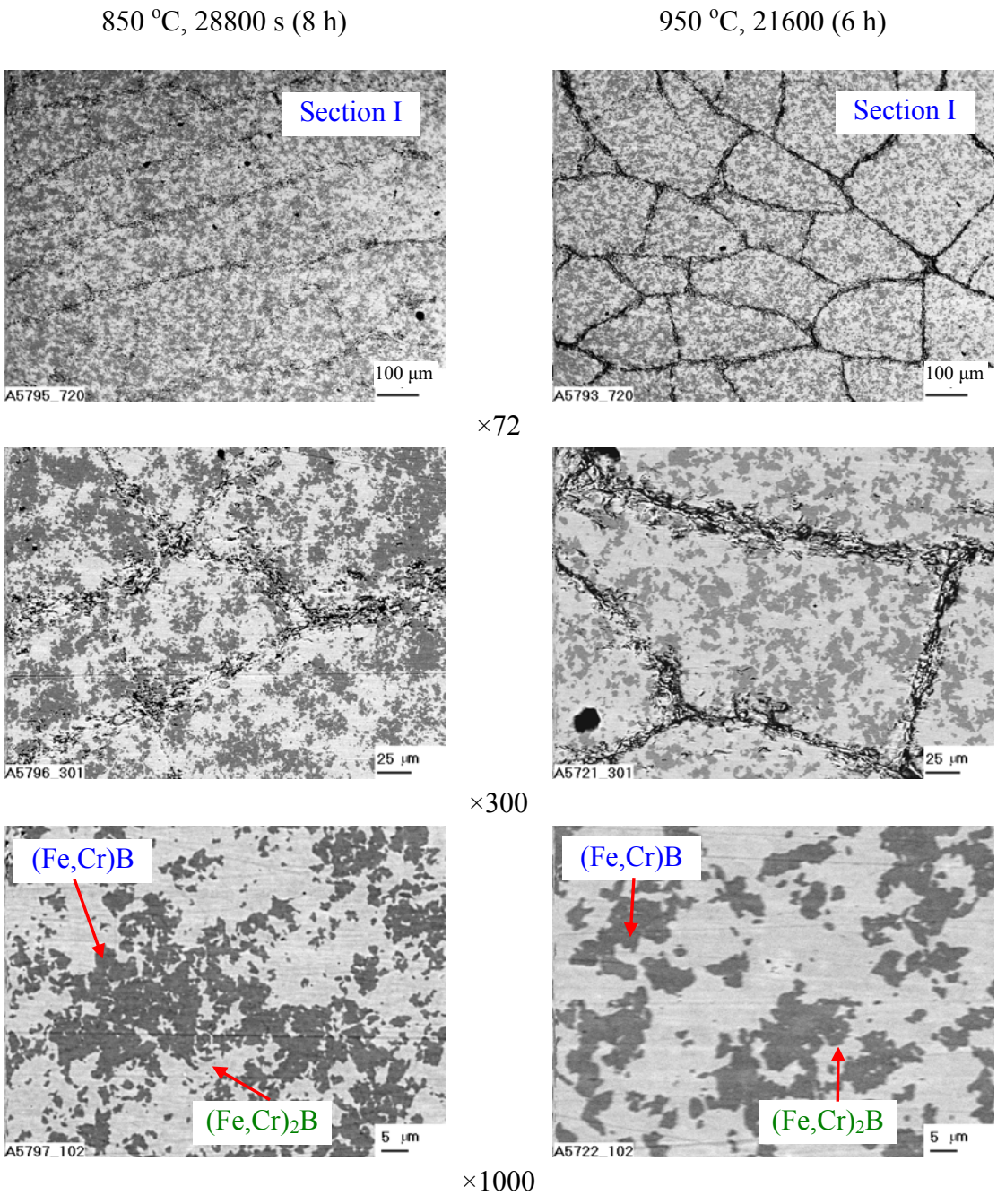

Fig. 3.14. Plan-view micrographs corresponding to Section I in Fig. 3.13 of a borided 13% Cr steel sample at magnifications ×72, ×300 and ×1000. The darker phase is (Fe,Cr)B, while the brighter phase is $(Fe,Cr)_2B$. Black spots are holes. Penetration of boron along grain boundaries, never observed with Fe–Cr alloys investigated, is worth noting.

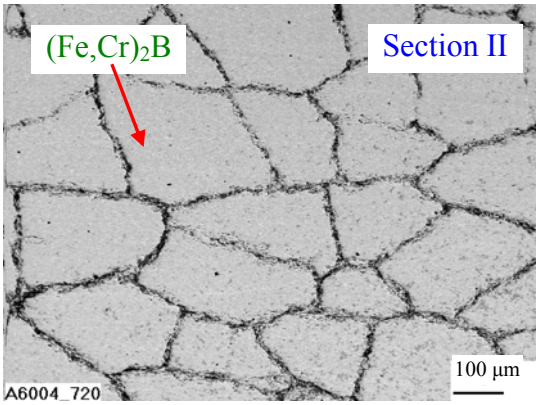

×72

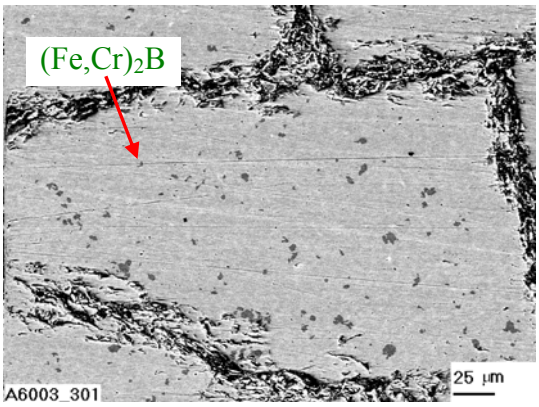

×300

Fig. 3.15. Plan-view micrographs corresponding to Section II in Fig. 3.13 of a borided 13% Cr steel sample at magnifications ×72 and ×300. The major phase is $(Fe,Cr)_2B$ (bright). Inclusions of (Fe,Cr)B (darker spots) are fine and rare. Again, penetration of boron along grain boundaries is readily seen.

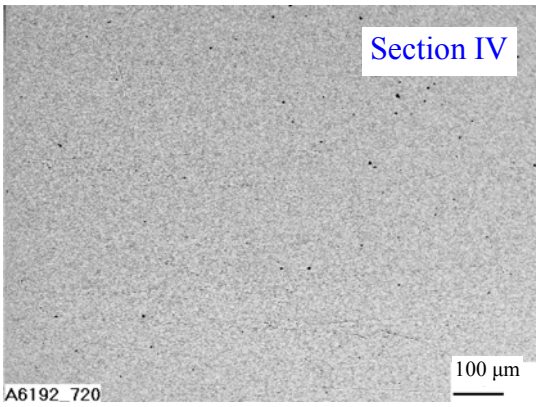

×72

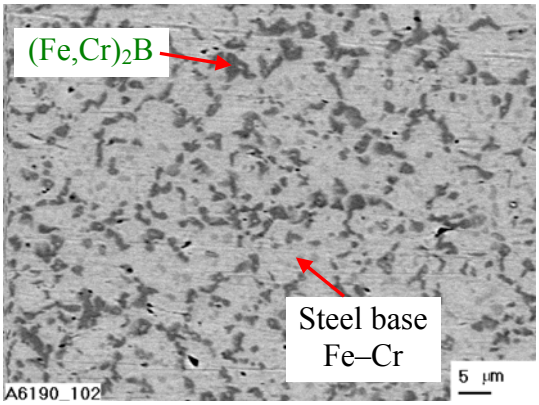

×1000

Fig. 3.16. Plan-view micrographs corresponding to Section IV in Fig. 3.13 of a borided 13% Cr steel sample at magnifications ×72 and ×1000. The darker phase is $(Fe,Cr)_2B$, while the brighter phase is the steel base. The steel base is non-homogeneous. Its grayish regions are enriched in chromium.

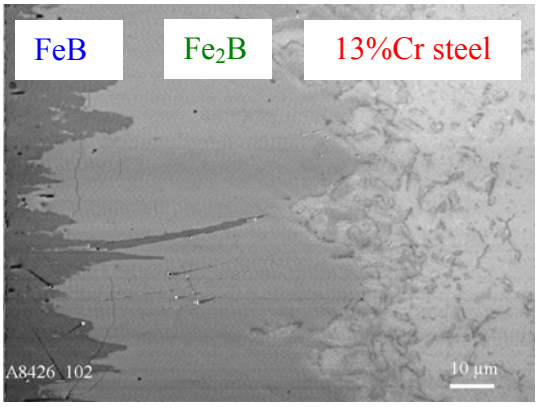

BEI

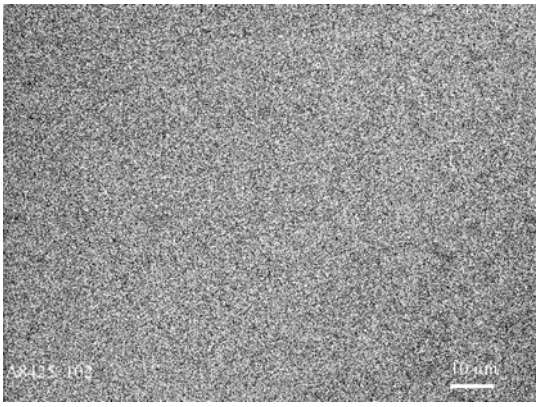

X-ray Fe Kα

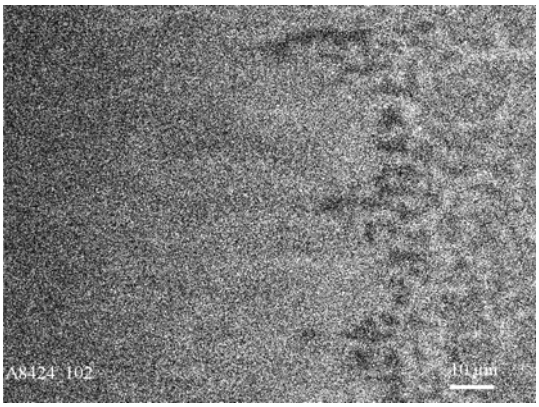

X-ray Cr Kα

Fig. 3.17. Cross-sectional backscattered electron image (BEI) of the transition zone of a 13% Cr steel sample borided at 950 ^{o}C for 14400 s (4 h), and X-ray maps for iron and chromium. The brighter the region, the higher is the content of an appropriate element (Fe or Cr). The crystals near the Fe_2B layer are seen to be somewhat enriched in chromium.

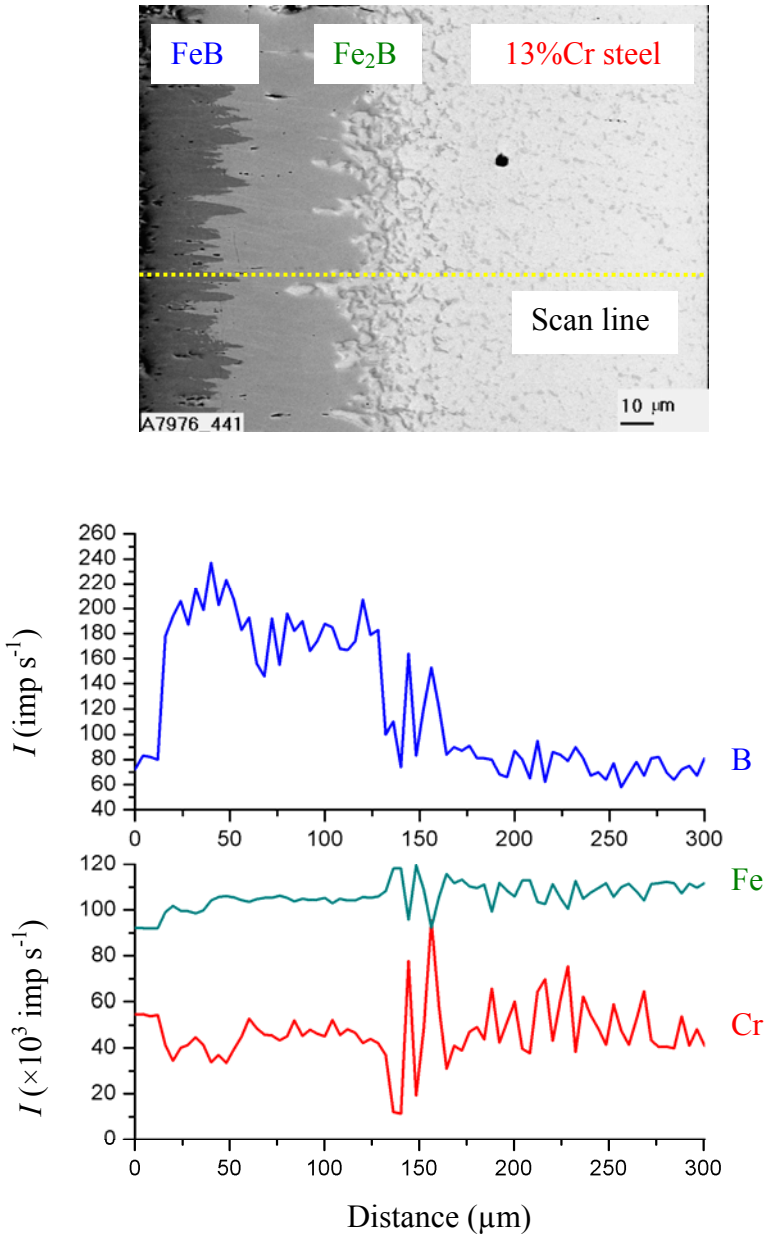

Fig. 3.18. Microstructure of the 13% Cr steel-boron transition zone, and concentration profiles of boron, iron and chromium. Boriding conditions: temperature 950 °C, reaction time 21600 s (6 h).

Table 3.11. Iron, chromium and boron contents of reacting phases, found by EPMA measurements on borided Fe–13% Cr steel samples after their X-ray diffraction investigations, see also Figs 3.13-3.16. Boriding conditions: temperature 950 °C, reaction time 21600 s (6 h).

Section	Region	Content (at.%)			Phase
		Fe	Cr	B	
I	Darker in Fig. 3.14	42.0	8.1	49.9	(Fe,Cr)B
		41.6	7.5	50.9	
		43.5	8.2	48.3	
		41.3	8.7	50.0	
		42.3	9.3	48.4	
	Brighter in Fig. 3.14	58.6	9.1	32.3	$(Fe,Cr)_2B$
		56.1	9.7	34.2	
		55.5	10.4	34.1	
		57.1	10.4	32.5	
		55.8	9.3	34.9	
II	Brighter in Fig. 3.15	53.6	11.9	34.5	$(Fe,Cr)_2B$
		54.9	10.8	33.3	
		55.0	10.9	34.1	
	Darker in Fig. 3.15	39.1	11.3	49.6	(Fe,Cr)B
		39.4	8.8	51.8	
		40.9	10.5	48.6	
IV	Brighter in Fig. 3.16	85.6	14.4	0.0	Steel base
		83.3	16.7	0.0	
		86.2	13.8	0.0	
	Darker in Fig. 3.16	34.9	29.4	35.7	$(Fe,Cr)_2B$
		43.0	27.3	29.7	
		40.3	25.3	34.3	
	Grayish in Fig. 3.16	61.7	38.3	0.0	Fe–Cr
		66.8	33.2	0.0	
		44.8	55.2	0.0	
V	Homogeneous	86.1	13.9	0.0	Steel base
		84.7	15.3	0.0	
		85.7	14.3	0.0	

Table 3.12. EPMA data for the 13% Cr steel-boron transition zone. The scatter of Fe, Cr and B contents within both boride layers is purely statistical. Boriding conditions: temperature 950 ^{o}C, reaction time 21600 s (6 h)

Steel or layer	Place of measurement	Content (at.%)			Phase
		Fe	Cr	B	
	At distance l away from the steel-boride layer interface				
Steel	l = –150 μm	86.8	13.2	0.0	Solid solution <Fe>
	–80	78.5	17.8	3.7	
	–50	87.0	13.0	0.0	
	–20	89.8	10.1	0.0	
	–10	82.7	10.7	6.6	
Inner boride layer	10	56.5	9.2	34.3	$(Fe,Cr)_2B$
	20	59.2	9.0	31.8	
	30	54.8	10.7	34.6	
	40	60.9	9.2	30.0	
	50	61.7	6.4	31.9	
Outer boride layer	60	40.9	7.4	51.7	(Fe,Cr)B
	70	43.3	8.6	48.1	
	80	42.1	7.2	50.7	
	90	43.3	8.5	48.2	

3.3.2. Two-phase layers

X-ray diffraction analysis carried out with all alloys and steels has only indicated the presence of the FeB and Fe_2B phases and the entire absence of any chromium boride in the boride layers formed. The X-ray patterns of borided samples of Fe–25% Cr and Fe–30% Cr alloys and a 25% Cr steel were similar to those of Fe–5% Cr, Fe–10% Cr and Fe–15% Cr alloys and a 13% Cr steel. Figures 3.2 and 3.19 and numerical data in Tables 3.1-3.6 show that their distinction from each other is merely the different intensity of appropriate reflections due to the formation of layer texture.

In view of the relatively high chromium content (25% or more) in Fe–25% Cr and Fe–30% Cr alloys and a 25% Cr steel, of seven known compounds CrB_4, CrB_2, Cr_2B_3, Cr_3B_4, CrB, Cr_5B_3 and Cr_2B [50], the formation of at least CrB and Cr_2B phases could be expected. Moreover, in this case the microstructure of both boride layers is readily seen visually in Fig. 3.1b to be two-phase. With each layer, it consists of distinct darker and brighter regions. More microstructures of different plan-view sections of Fe–25% Cr alloy samples, including X-ray maps for iron and chromium and Fe, Cr and B concentration profiles, are shown in Figs 3.20-3.24. Iron, chromium and boron contents of reacting phases are given in Table 3.13. Similar results are provided in Figs 3.25-3.30 and Table 3.14 for Fe–30% Cr alloy samples and in Figs 3.31-3.38 and Table 3.15 for 25% Cr steel ones.

EPMA measurements presented in Tables 3.13-3.15 indicate that iron prevails in brighter regions, while chromium is dominant in darker ones of any boride layer. Thus, the outer boride layer consists of a mixture of crystals of the (Fe,Cr)B and (Cr,Fe)B phases. With Fe–25% Cr and Fe–30% Cr alloys, these have a peculiar regular arrangement that is practically not observed in 25% Cr steel samples (see Figs 3.20, 3.26 and 3.33). Nonetheless, even most strong reflections of CrB (spacing, d = 0.2350, 0.1965 and 0.1255 nm) and Cr_2B (d = 0.2590, 0.2158 and 0.2043 nm) [77, 78] were missing from experimental X-ray patterns of boride layers formed in Fe–25% Cr and Fe–30% Cr alloy and 25% Cr steel samples.

Most probably, presence of the CrB phase in boride layers can hardly be revealed by XRD or any other method of structural analysis such as electron diffraction because under highly non-equilibrium conditions the lattice rearrangement FeB → CrB is not completed in view of time limitations. Therefore, part of iron sites of the FeB lattice, very similar to that of CrB, is merely replaced by chromium atoms, without any noticeable structural changes.

In other words, the non-equilibrium CrB phase crystallizes in the FeB lattice. Hence, being far from equilibrium, the outher boride layer appears to be single-phase structurally (crystallographically) and two-phase compositionally (chemically).

Similar considerations are also applicable to another pair Fe_2B and Cr_2B that are the constituents of the inner boride layer. Therefore, formation of the (Cr,Fe)B and $(Cr,Fe)_2B$ phases, readily seen visually in the microstructure of boride layers occurred on the surface of borided Fe–25% Cr and Fe–30% Cr alloy and 25% Cr steel samples can hardly be doubted.

With high-alloy steels, two-phase microstructure of boride layers is much less profound in view of the strong influence of other constituting elements (C, P, S, Si, Mn, *etc*.). Perhaps, just for this reason it was overlooked by previous researchers who dealt mainly with steels of complicated chemical composition.

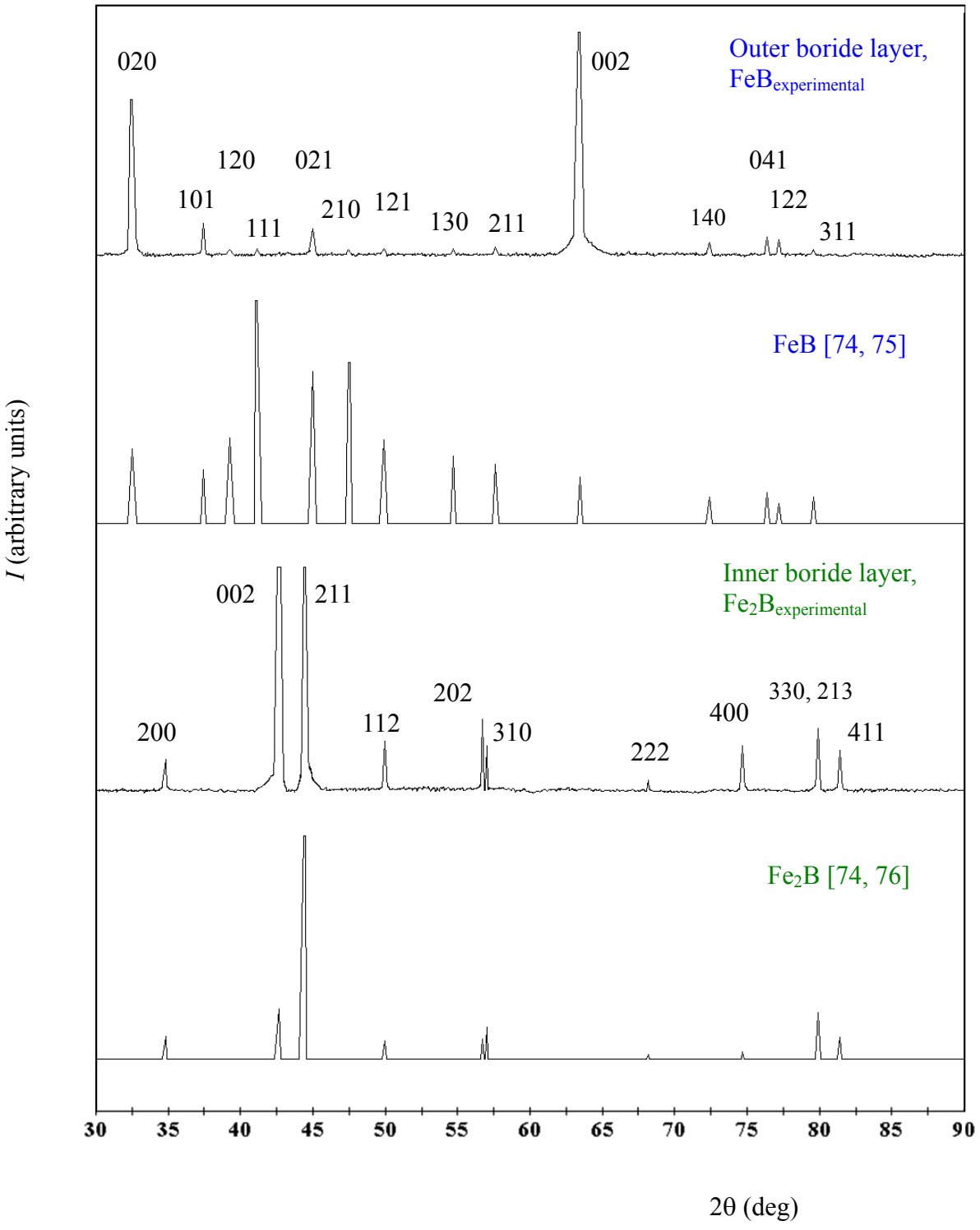

Fig. 3.19. Comparison of literature X-ray diffraction patterns for FeB and Fe_2B phases [74–76] with those obtained experimentally for boride layers formed at the Fe–30% Cr alloy-boron interface after thermochemical boriding at 950 °C for 21600 s (6 h). The experimental pattern of the outer boride layer was taken from Section 0, while that of the inner boride layer approximately from Section III, see Fig. 3.1b.

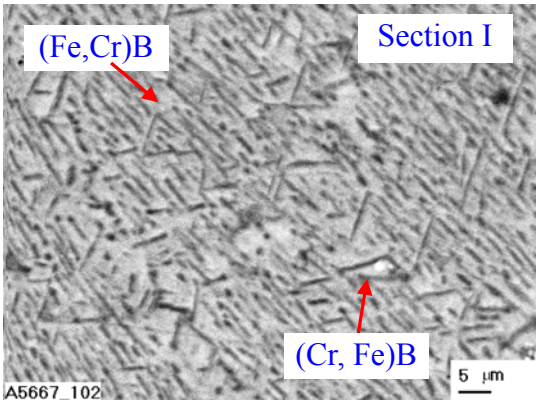

850 °C

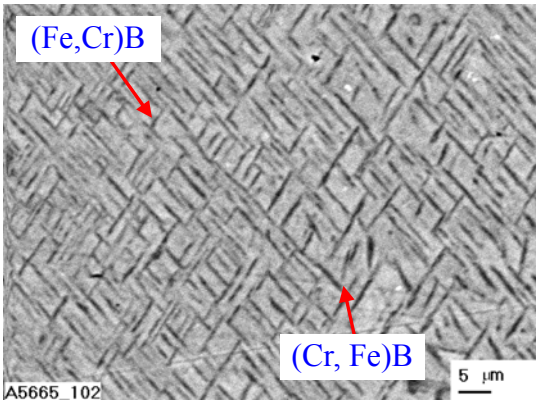

900 °C

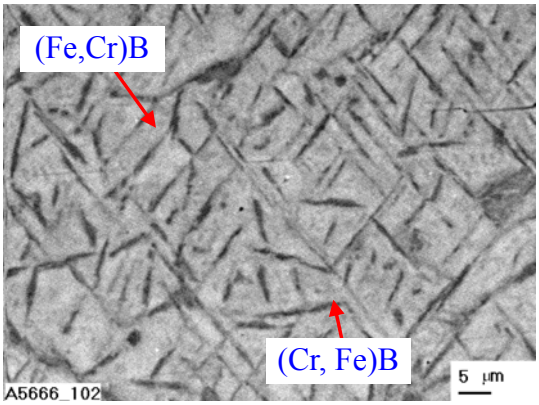

950 °C

Fig. 3.20. Plan-view micrographs corresponding to Section I in Fig. 3.1b of borided Fe–25% Cr alloy samples. Reaction time 21600 s (6 h). The brighter regions are the (Fe,Cr)B phase, while the darker regions (thin long crystals) are the (Cr,Fe)B phase (see also Table 3.11).

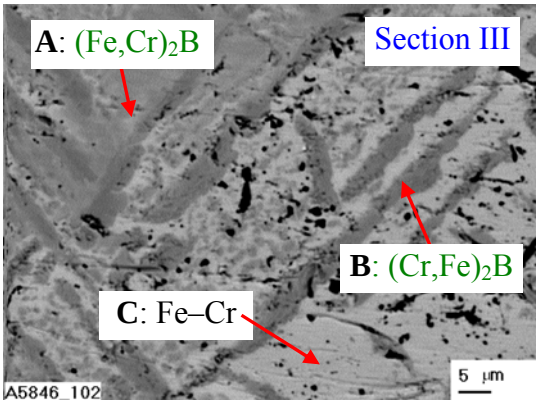

BEI

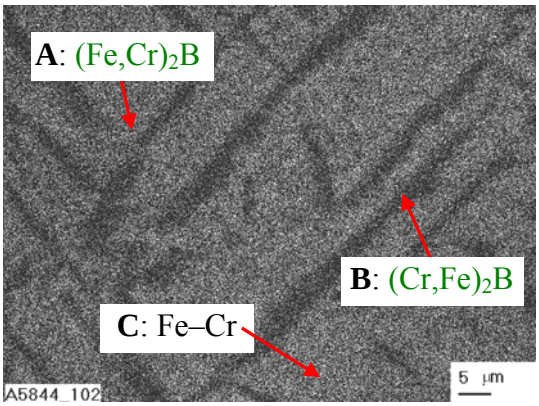

X-ray Fe Kα

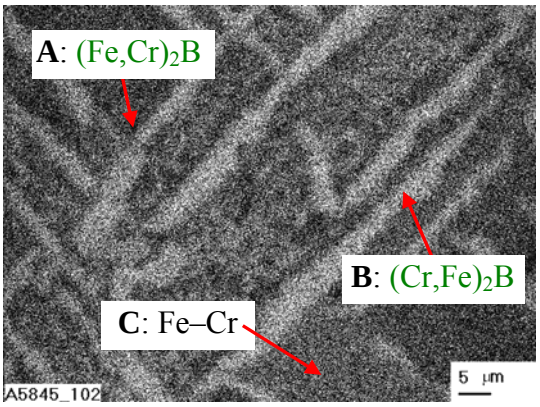

X-ray Cr Kα

Fig. 3.21. A plan-view micrograph corresponding to Section III in Fig. 3.1b of a borided Fe–25% Cr alloy sample, and X-ray maps for iron and chromium (the brighter the region, the higher is the content of an appropriate element). BEI = backscattered electron image. Boriding conditions: 950 ^{o}C, 21600 s (6 h).

Section IV

Section V

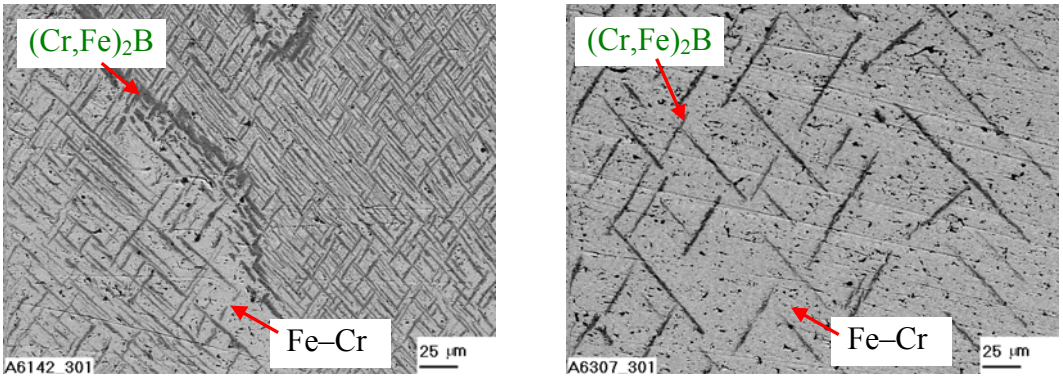

×300

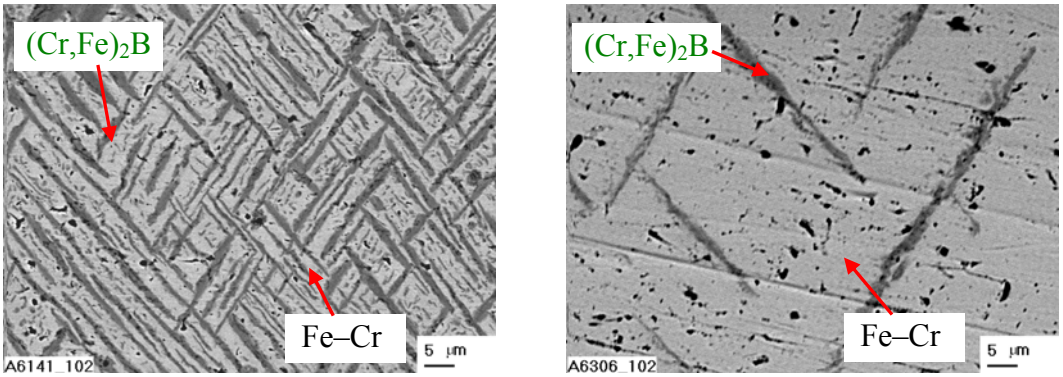

×1000

Fig. 3.22. Plan-view micrographs corresponding to Sections IV and V in Fig. 3.1b of a borided Fe–25% Cr alloy sample. Boriding conditions: 950 ^{o}C, 21600 s (6 h). The darker regions (thin long crystals) are the $(Cr,Fe)_2B$ phase, while brighter regions are the alloy base Fe–Cr. Black spots are holes and cracks. Magnification: ×300 and ×1000.

Reaction time

21600 s (6 h) 28800 s (8 h)

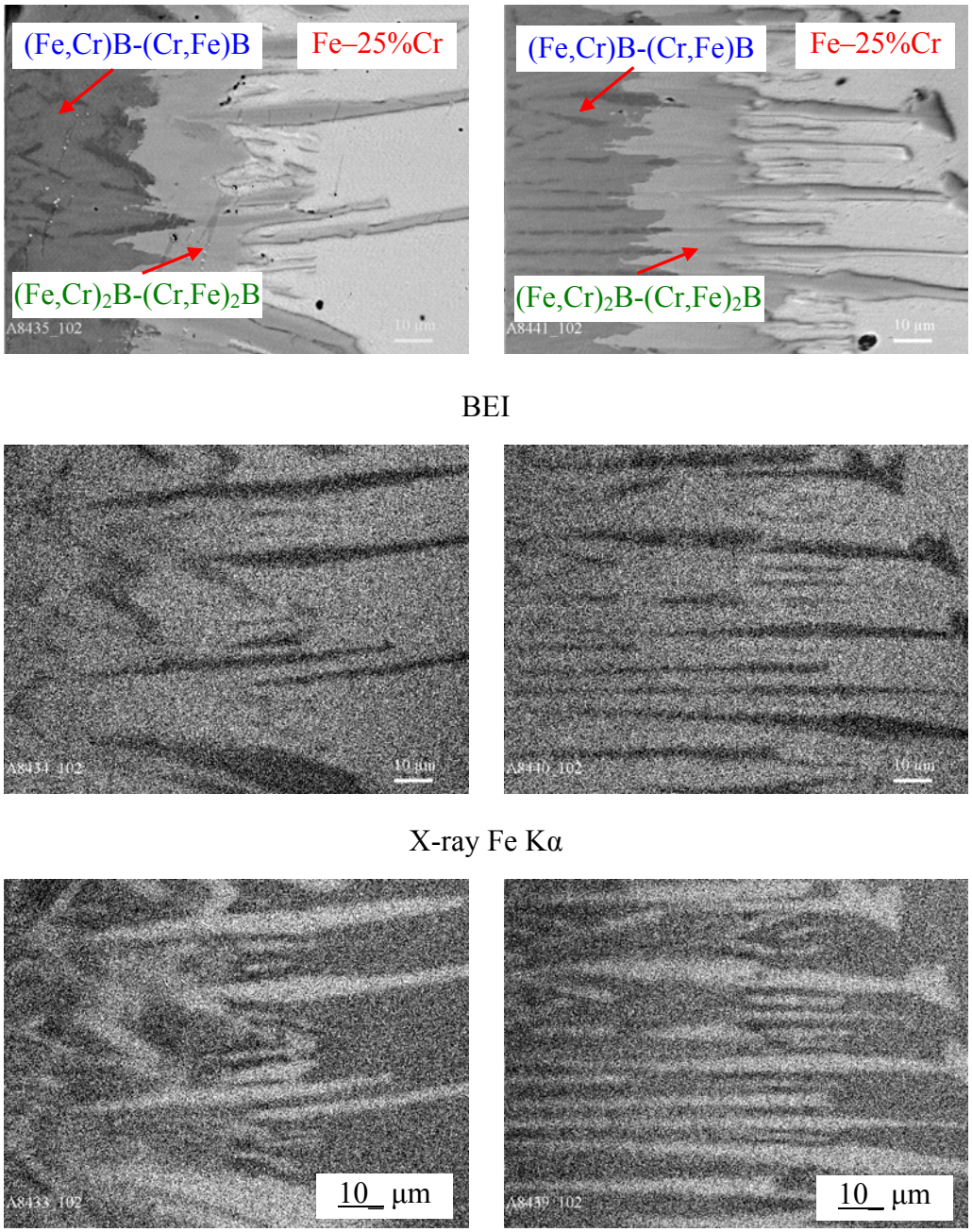

Fig. 3.23. Cross-sectional backscattered electron image (BEI) of the transition zone of a Fe–25% Cr alloy sample borided at 950 °C, and X-ray maps for iron and chromium. The brighter the region, the higher is the content of an appropriate element (Fe or Cr).

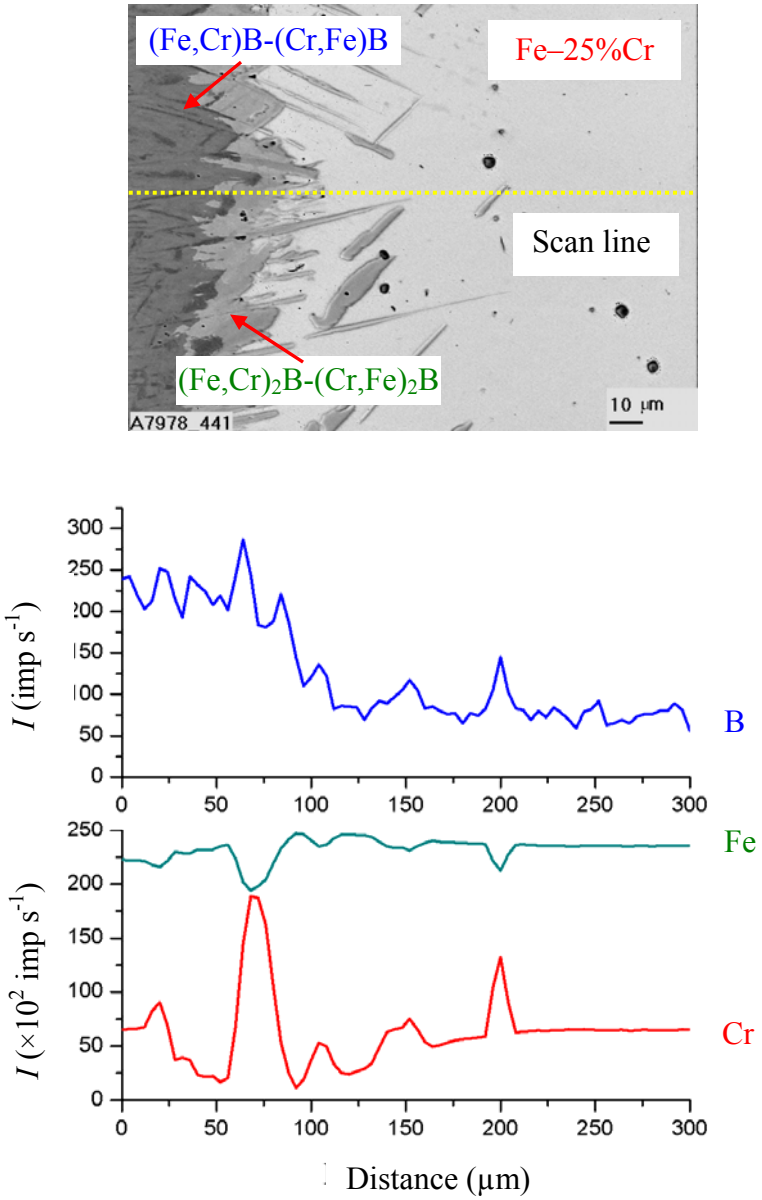

Fig. 3.24. Microstructure of the transition zone between a Fe–25% Cr alloy and boron, and concentration profiles of boron, iron and chromium. Boriding conditions: temperature 950 ^{o}C, reaction time 21600 s (6 h).

Table 3.13. Iron, chromium and boron contents of reacting phases, found by EPMA measurements on borided Fe–25% Cr alloy samples after their X-ray diffraction investigations, see also Figs 3.1b and 3.20-3.22.

Section in Fig. 3.1b	Region	Content (at.%)			Phase
		Fe	Cr	B	
I	Brighter in Fig. 3.20	25.9	23.9	50.2	(Fe,Cr)B
		29.0	22.9	48.1	
		26.9	21.1	52.0	
		29.2	19.9	50.9	
		33.1	16.2	50.7	
	Darker in Fig. 3.20	23.7	24.4	51.9	(Cr,Fe)B
		22.0	29.5	48.5	
		17.7	32.2	50.1	
		20.9	29.8	49.2	
		15.0	33.1	51.9	
III	**A** in Fig. 3.21	56.6	12.2	31.2	$(Fe,Cr)_2B$
		53.9	11.5	34.6	
		50.0	16.2	33.8	
	B in Fig. 3.21	18.4	46.8	34.8	$(Cr,Fe)_2B$
		24.2	44.1	31.7	
		19.6	46.8	33.6	
	C in Fig. 3.21	79.4	20.6	0.0	Fe–Cr
		77.5	22.5	0.0	
		81.9	18.1	0.0	
IV	Brighter in Fig. 3.22	76.1	23.9	0.0	Fe–Cr
		80.1	19.4	0.5	
		74.2	25.8	0.0	
	Darker in Fig. 3.22	18.8	49.2	32.1	$(Cr,Fe)_2B$
		19.0	47.0	34.0	
		19.6	50.7	29.7	
V	Brighter in Fig. 3.22	72.8	27.2	0.0	Fe–Cr
		72.2	27.8	0.0	
		72.5	27.5	0.0	
	Darker in Fig. 3.22	23.4	43.1	33.5	$(Cr,Fe)_2B$
		18.6	48.7	32.7	
		21.8	45.1	33.1	
VI	Homogeneous	73.9	26.1	0.0	Fe–25%Cr
		73.0	27.0	0.0	
		73.7	26.3	0.0	

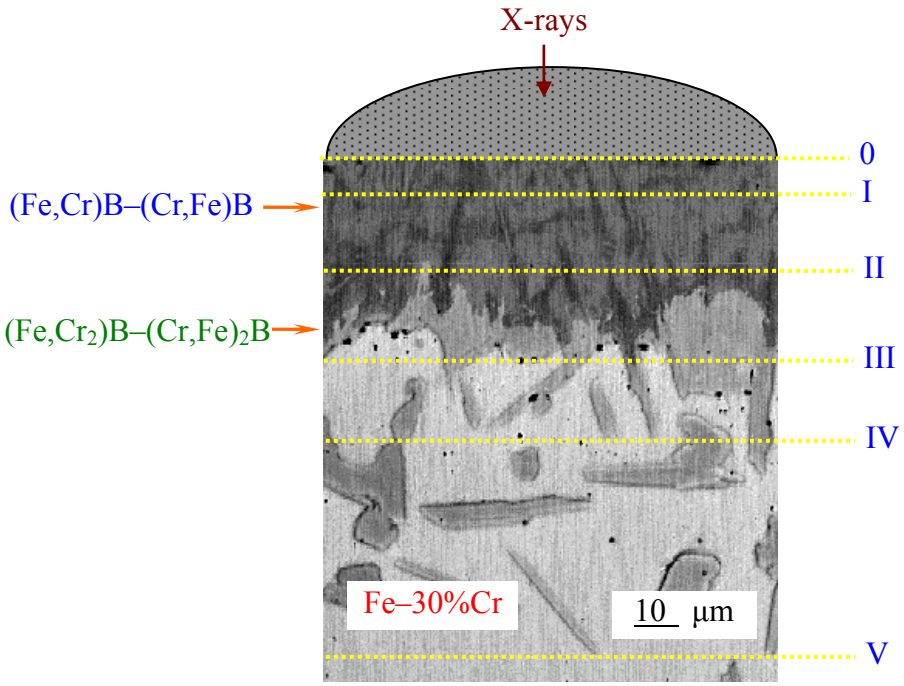

Fig. 3.25. Microstructure and scheme of X-ray diffraction investigations of a borided Fe–30% Cr alloy sample. Boriding conditions: 950 °C, 28800 s (8 h). Distance between successive sections of the sample (from top deeper inside its bulk): 10 μm (0-I), 30 μm (I-II), 30 μm (II-III), 30 μm (III-IV) and 50 μm.

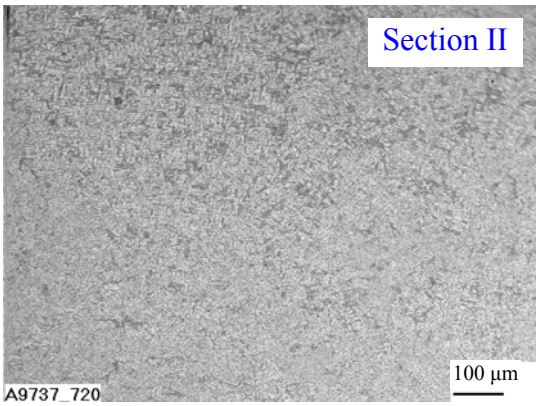

× 72

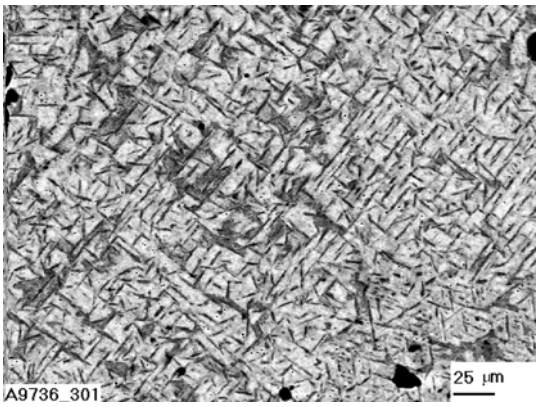

× 300

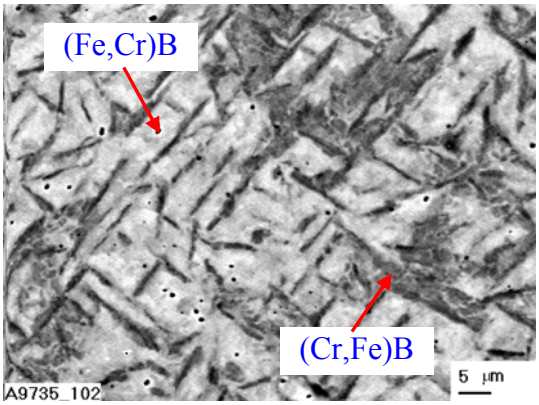

× 1000

Fig. 3.26. A plan-view micrograph corresponding to Section II in Fig. 3.25 of a borided Fe–30% Cr alloy sample at magnifications ×72, ×300 and ×1000. This section crosses the outher boride layer and provides clear evidence for its two-phase structure. The brighter regions are the (Fe,Cr)B phase, while the darker regions are the (Cr,Fe)B phase (see also Table 3.14). Boriding conditions: 950 ^{o}C, 28800 s (8 h).

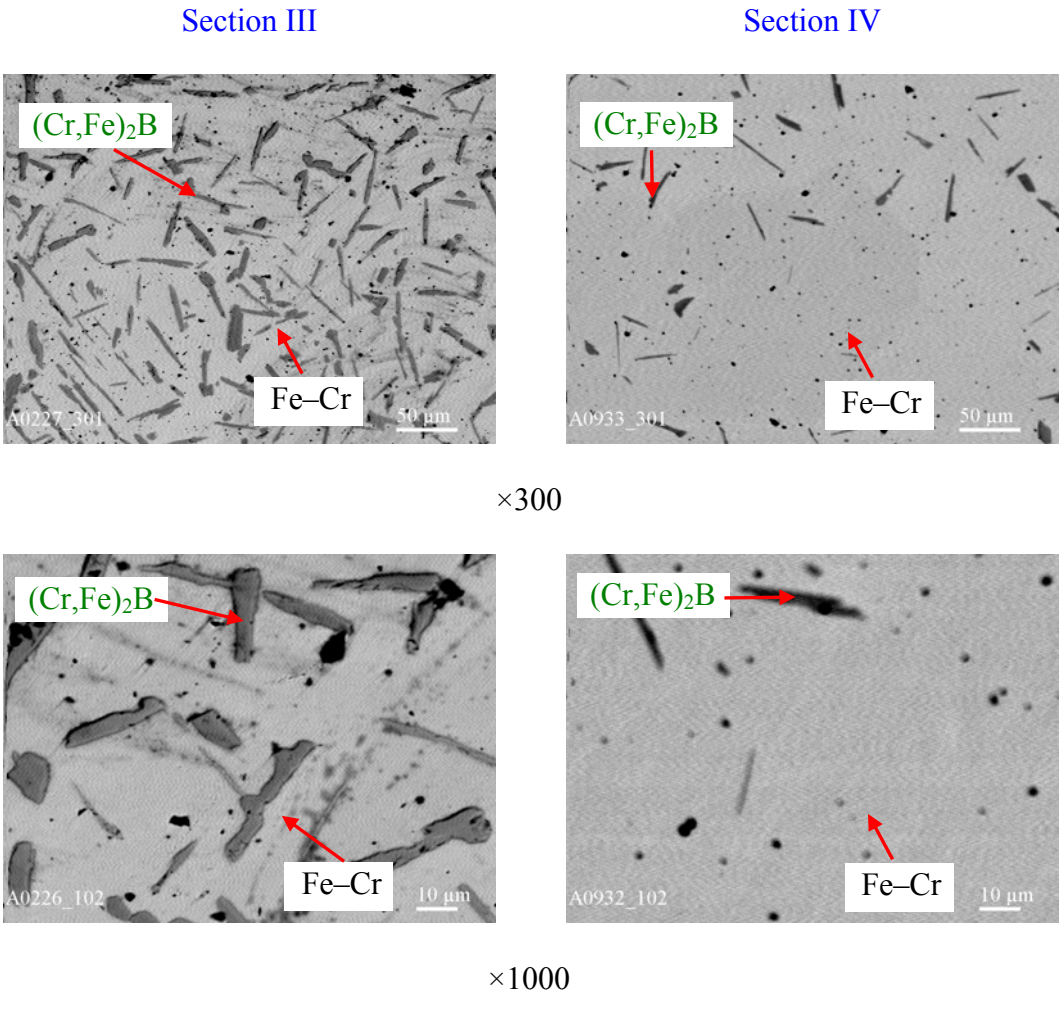

Fig. 3.27. Plan-view micrographs corresponding to Sections III and IV in Fig. 3.25 of a borided Fe–30% Cr alloy sample at magnifications ×300 and ×1000. Boriding conditions: 950 ^{o}C, 28800 s (8 h). The darker regions (thin long crystals) are the $(Cr,Fe)_2B$ phase, while brighter regions are the alloy base Fe–Cr. Black spots are holes and cracks.

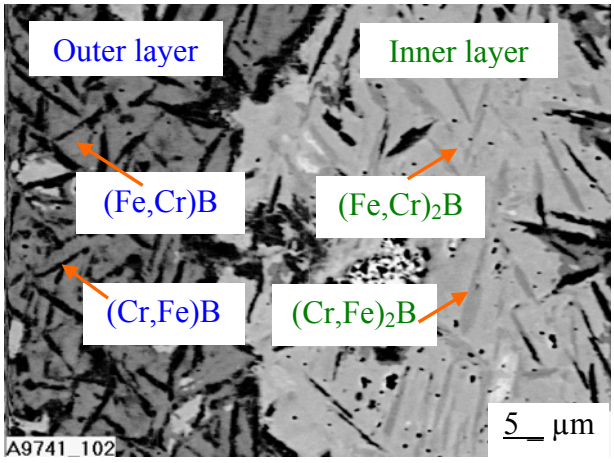

Fig. 3.28. Plan-view micrograph (BEI) corresponding to the second section of a Fe–30% Cr alloy sample borided at 850°C for 43200 s (12 h). This section crosses both boride layers and clearly shows their two-phase structure. The dark area is the outer boride layer. Its brighter regions are the (Fe,Cr)B phase, while the darker regions are the (Cr,Fe)B phase. The bright area is the inner boride layer. Its brighter regions are the $(Fe,Cr)_2B$ phase, while the darker regions are the $(Cr,Fe)_2B$ phase.

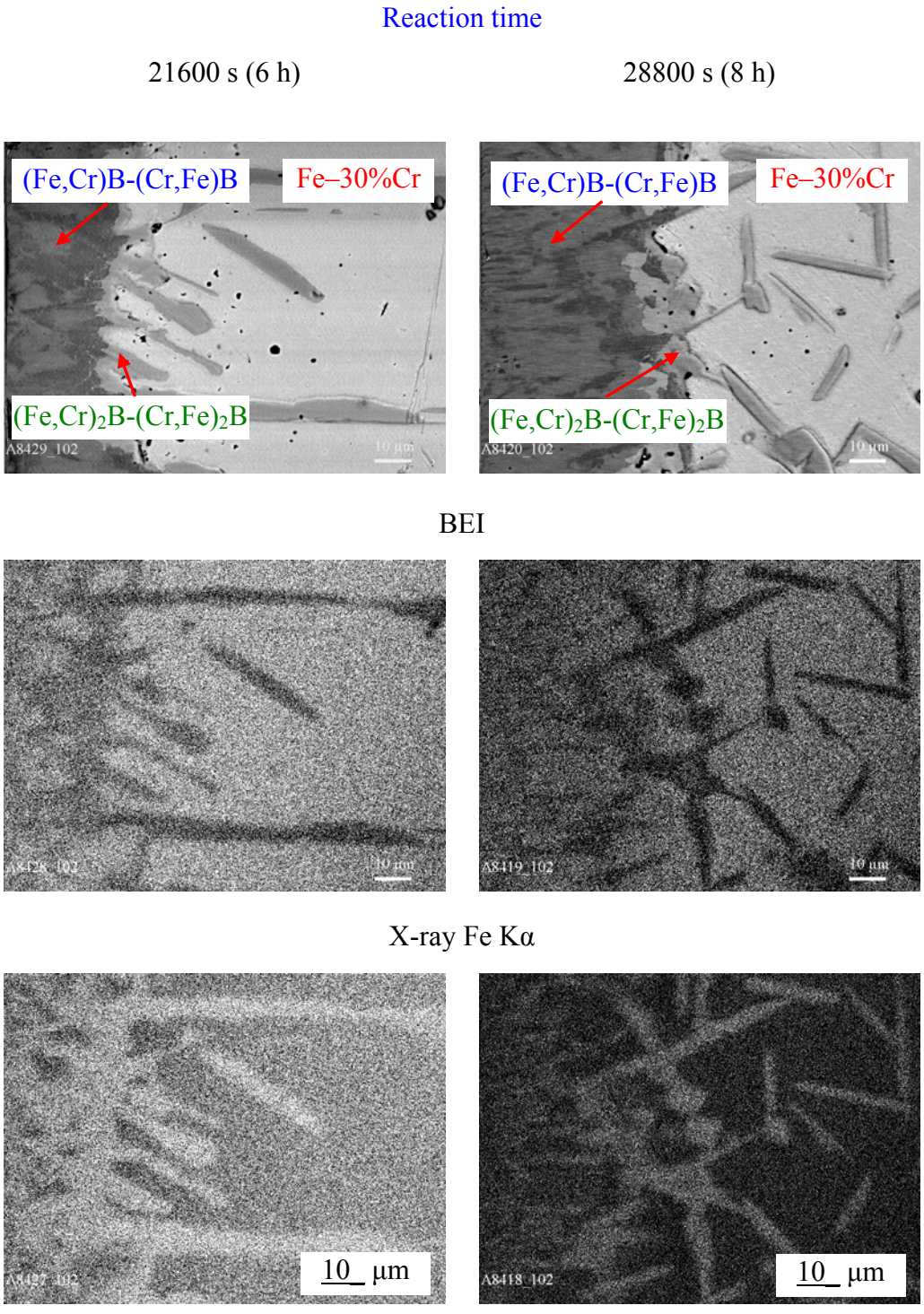

Fig. 3.29. Cross-sectional backscattered electron image (BEI) of the transition zone of a Fe–30% Cr alloy sample borided at 950 °C, and X-ray maps for iron and chromium. The brighter the region, the higher is the content of an appropriate element (Fe or Cr).

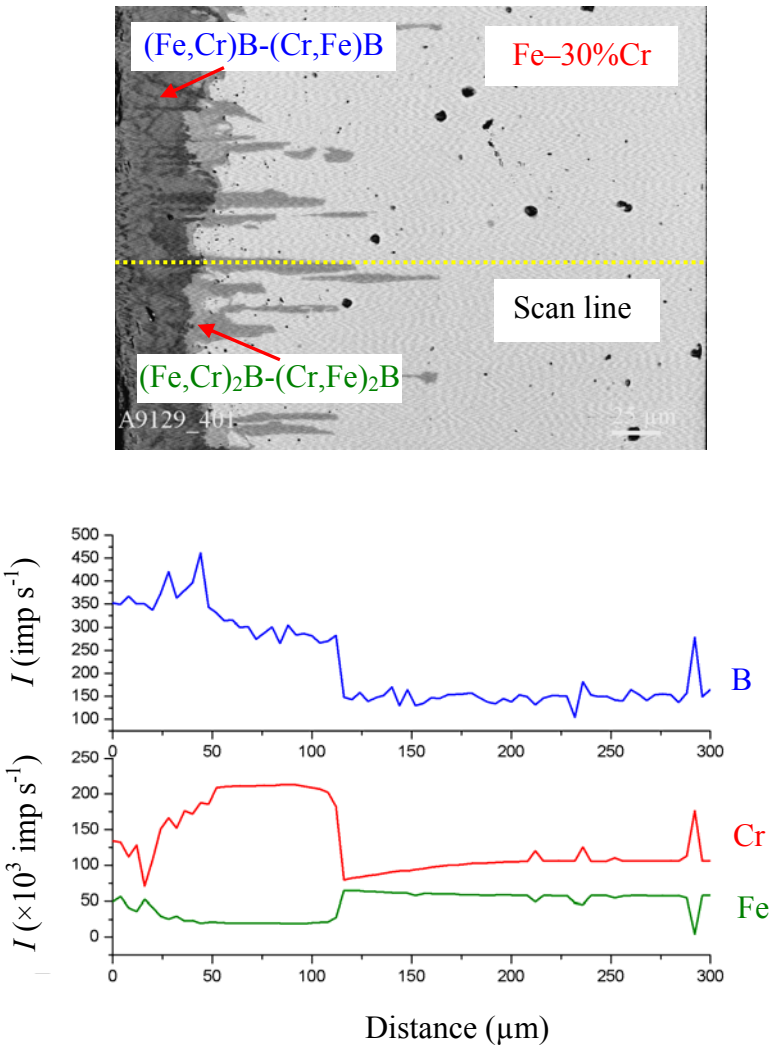

Fig. 3.30. Microstructure of the transition zone between a Fe–30% Cr alloy and boron, and concentration profiles of boron, iron and chromium. Boriding conditions: temperature 950 ^{o}C, reaction time 21600 s (6 h).

Table 3.14. Average iron, chromium and boron contents of reacting phases, found by EPMA measurements on borided Fe–30% Cr alloy samples after their X-ray diffraction investigations, see also Figs 3.25-28.

Section in Fig. 3.25	Region	Content (mass%/at.%)			Phase
		Fe	Cr	B	
I	Brighter (see Fig. 3.25)	60.8/35.6	22.7/14.3	16.5/50.1	(Fe,Cr)B
	Darker (see Fig. 3.25)	34.4/21.4	48.8/28.3	16.8/50.3	(Cr,Fe)B
II	Brighter in Fig. 3.26	72.0/43.1	12.1/7.8	15.9/49.1	(Fe,Cr)B
	Darker in Fig. 3.26	21.9/12.6	61.6/38.2	16.5/49.2	(Cr,Fe)B
II	Brighter of the outer boride layer in Fig. 3.28	65.4/38.4	18.0/11.4	16.5/50.2	(Fe,Cr)B
	Darker of the outer boride layer in Fig. 3.28	39.8/23.5	44.3/28.1	15.9/48.4	(Cr,Fe)B
	Brighter of the inner boride layer in Fig. 3.28	76.9/55.7	14.2/11.1	8.9/33.2	$(Fe,Cr)_2B$
	Darker of the inner boride layer in Fig. 3.28	28.1/19.7	62.8/47.3	9.1/33.0	$(Cr,Fe)_2B$
III	Brighter in Fig. 3.27	79.7/78.5	20.3/21.5	0.0/0.0	Fe–Cr
	Darker in Fig. 3.27	24.6/17.2	66.1/49.5	9.3/33.3	$(Cr,Fe)_2B$
IV	Brighter in Fig. 3.27	72.5/71.1	27.5/28.9	0.0/0.0	Fe–Cr
	Darker in Fig. 3.27	15.1/22.0	68.3/50.3	9.8/34.6	$(Cr,Fe)_2B$
V	Homogeneous	69.9/68.3	30.1/31.7	0.0/0.0	Fe–Cr

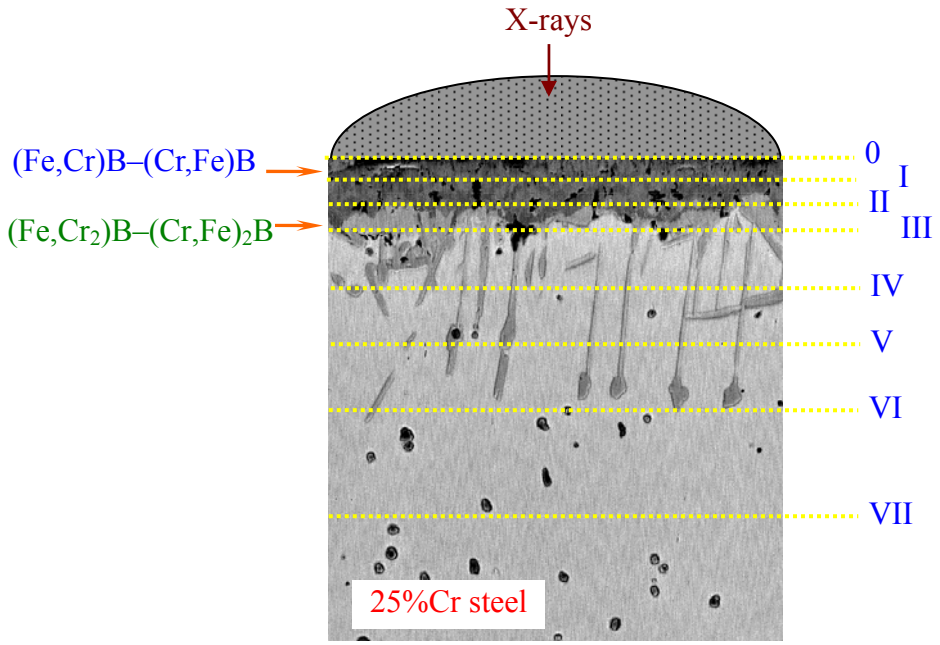

Fig. 3.31. Microstructure and scheme of X-ray diffraction investigations of a borided 25% Cr steel sample. Boriding conditions: 950 ^{o}C, 21600 s (6 h). Distance between successive sections of the sample (from top deeper inside its bulk): 10 μm (0-I), 10 μm (I-II), 10 μm (II-III), 20 μm (III-IV), 20 μ (IV-V), 20 μ (V-VI) and 30 μ (VI-VII).

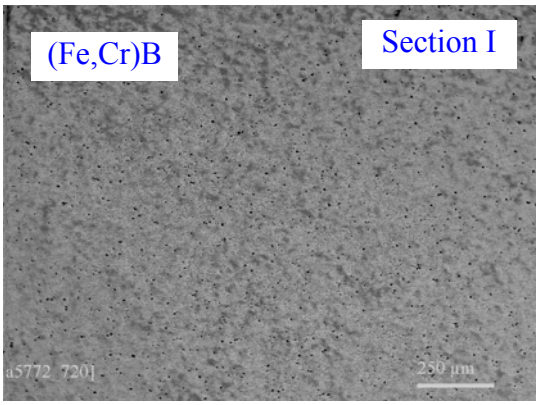

×72

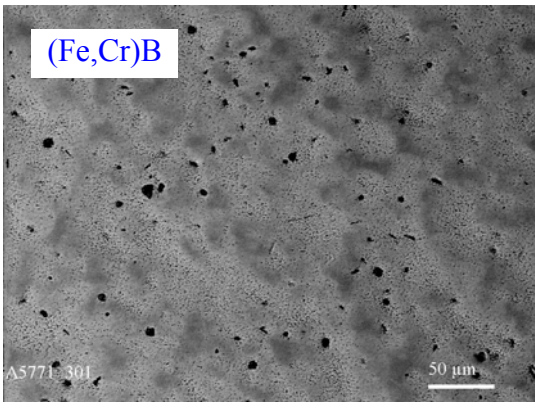

×300

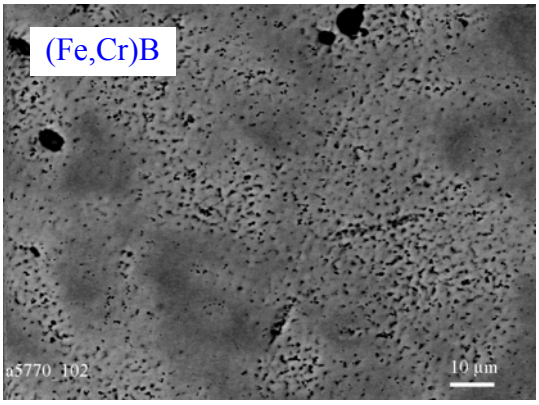

×1000

Fig. 3.32. A plan-view micrograph corresponding to Section I in Fig. 3.31 of a borided 25% Cr steel sample at magnifications ×72, ×300 and ×1000. The major phase is (Fe,Cr)B. The chromium content of its brighter regions is 7-12 at.%, while that of the darker regions is up to 20 at.%. It is the beginning of formation of the two-phase structure of the outer boride layer. Fine black spots are probably iron and chromium carbides and borocarbides, while large black spots are holes. Boriding conditions: 950 ^{o}C, 21600 s (6 h).

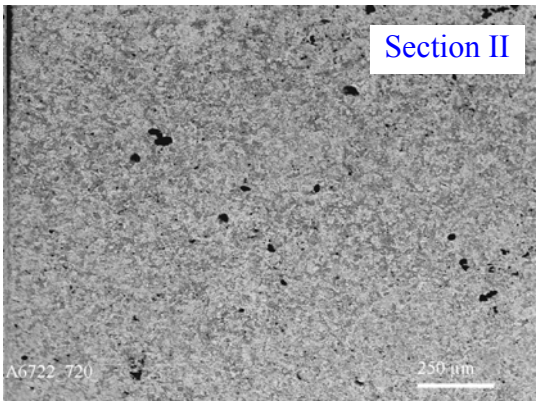

×72

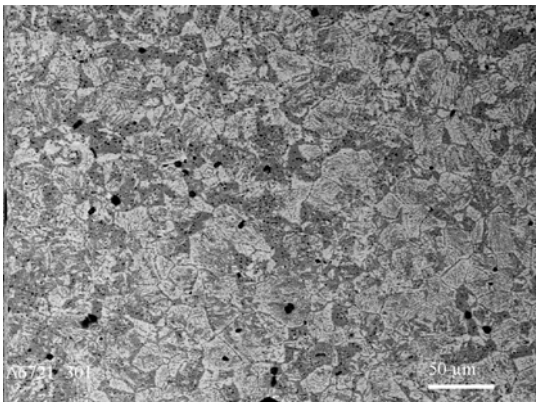

×300

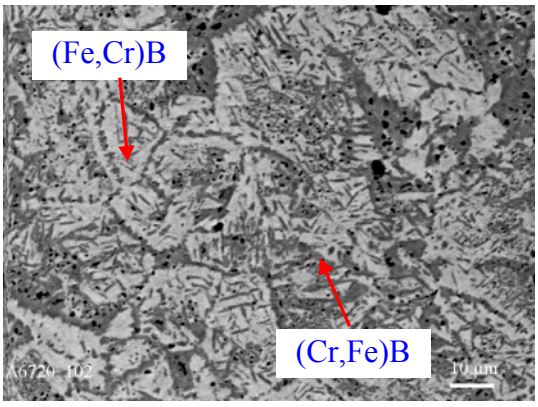

×1000

Fig. 3.33. A plan-view micrograph corresponding to Section II in Fig. 3.31 of a borided 25% Cr steel sample at magnifications ×72, ×300 and ×1000. The brighter phase is (Fe,Cr)B, while the darker phase is (Cr,Fe)B. Though much less profound than with Fe–25% Cr and Fe–30% Cr alloys (see Figs 3.20 and 3.26), two-phase structure of the outer boride layer has already formed. Boriding conditions: 950 ^{o}C, 21600 s (6 h).

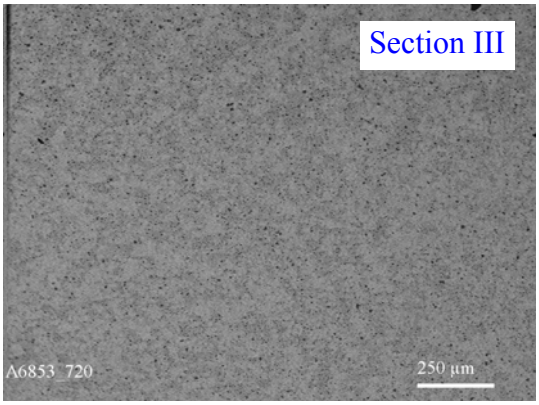

×72

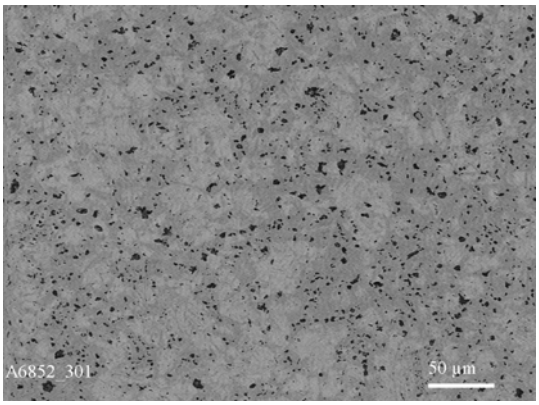

×300

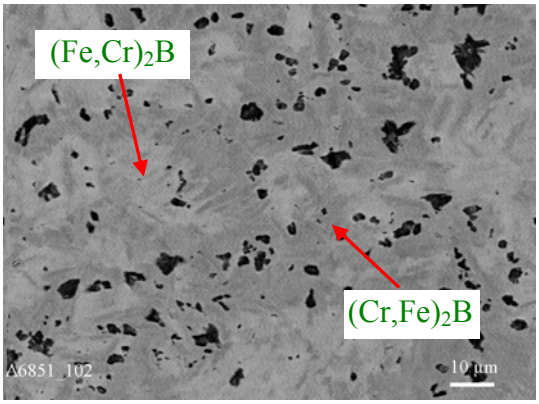

×1000

Fig. 3.34. A plan-view micrograph corresponding to Section III in Fig. 3.31 of a borided 25% Cr steel sample at magnifications ×72, ×300, and ×1000. This section crosses the inner boride layer. Its structure is seen to be two-phase. The brighter phase is $(Fe,Cr)_2B$, while the darker phase is $(Cr,Fe)_2B$. Black spots are probably iron and chromium carbides and borocarbides or holes. Boriding conditions: 950 ^{o}C, 21600 s (6 h).

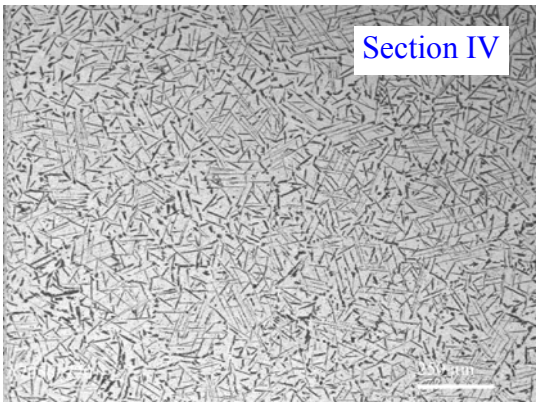

×72

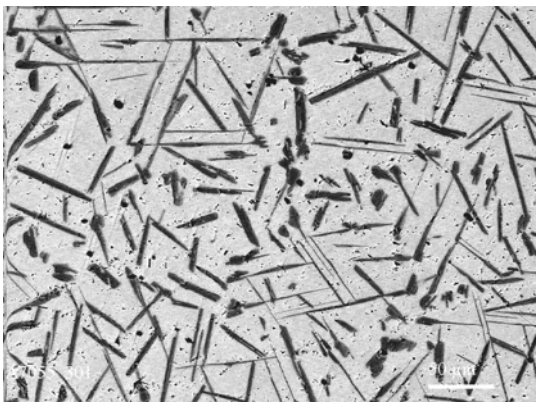

×300

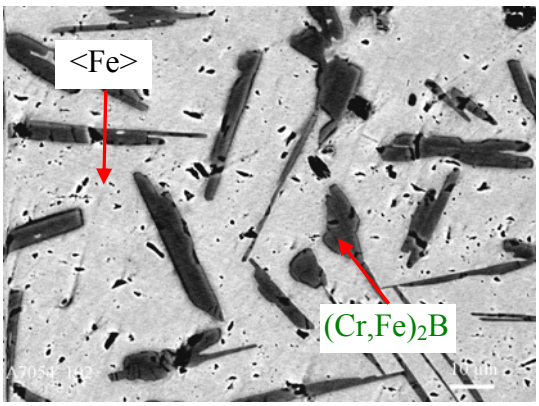

×1000

Fig. 3.35. A plan-view micrograph corresponding to Section IV in Fig. 3.31 of a borided 25% Cr steel sample at magnifications ×72, ×300, and ×1000. The constituent phases are the steel base (a solid solution of iron and chromium <Fe>) (bright) and $(Cr,Fe)_2B$ (dark crystals). Boriding conditions: 950 ^{o}C, 21600 s (6 h).

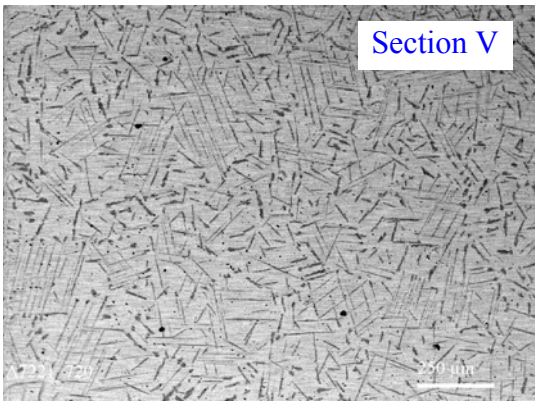

×72

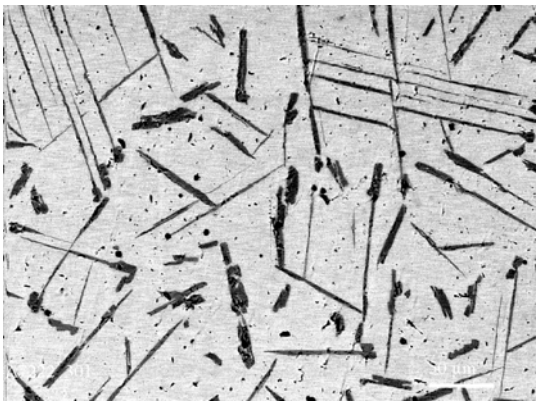

×300

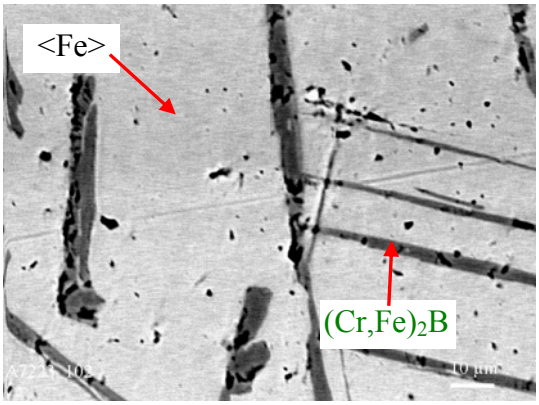

×1000

Fig. 3.36. A plan-view micrograph corresponding to Section V in Fig. 3.31 of a borided 25% Cr steel sample at magnifications ×72, ×300, and ×1000. The constituent phases are the steel base (a solid solution of iron and chromium <Fe>) (bright) and $(Cr,Fe)_2B$ (dark crystals). The $(Cr,Fe)_2B$ crystals are less numerous than in Section IV. Boriding conditions: 950 ^{o}C, 21600 s (6 h).

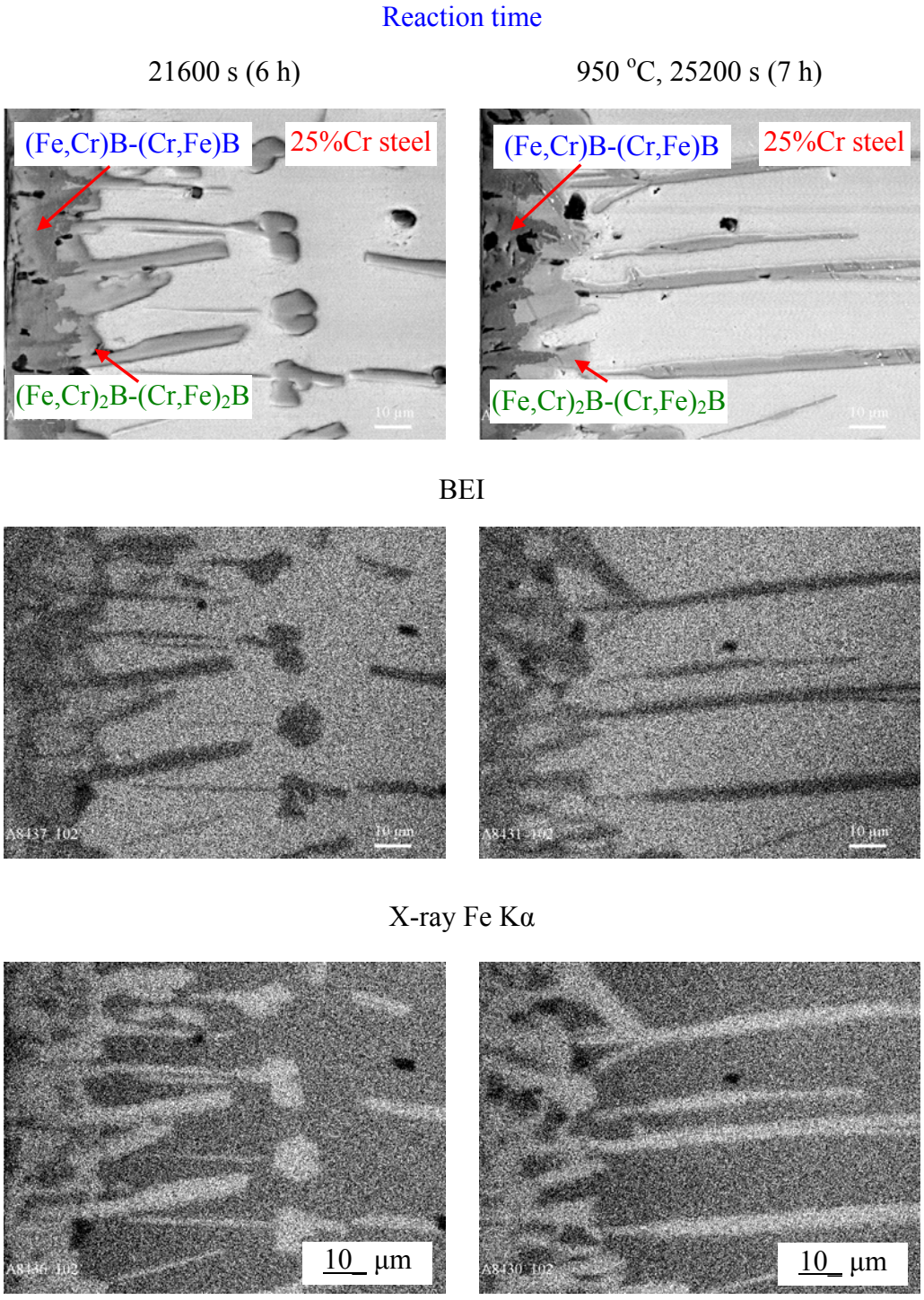

Fig. 3.37. Cross-sectional backscattered electron image (BEI) of the transition zone of a 25% Cr steel sample borided at 950 °C, and X-ray maps for iron and chromium. The brighter the region, the higher is the content of an appropriate element (Fe or Cr).

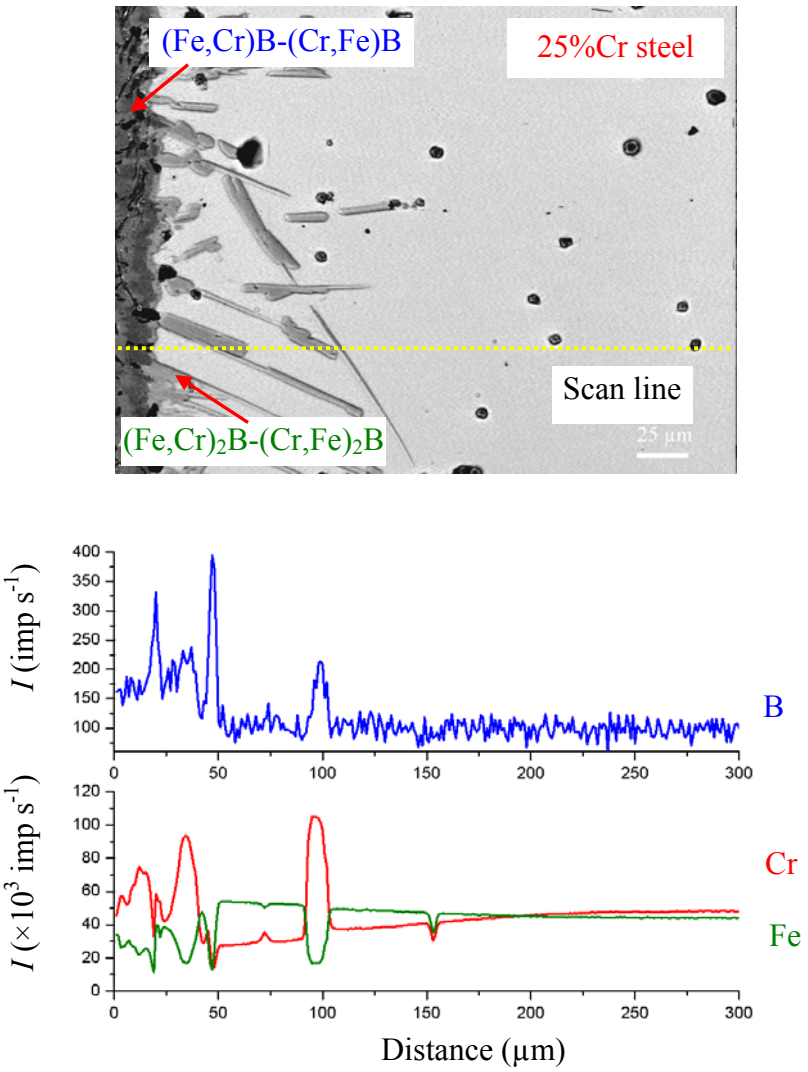

Fig. 3.38. Microstructure of the 25% Cr steel-boron transition zone, and concentration profiles of boron, iron and chromium. Boriding conditions: temperature 950 °C, reaction time 21600 s (6 h).

Table 3.15. Average iron, chromium and boron contents of reacting phases, found by EPMA measurements on borided 25% Cr steel samples after their X-ray diffraction investigations, see also Figs 3.31-3.36.

Section in Fig. 3.31	Region	Content (mass %/at.%)			Phase
		Fe	Cr	B	
I	Brighter of the outer boride layer in Fig. 3.32	71.4/42.2	12.2/7.7	16.4/50.1	(Fe,Cr)B
	Darker of the outer boride layer in Fig. 3.32	53.8/31.8	30.2/19.1	16.1/49.1	(Fe,Cr)B
II	Brighter of the outer boride layer in Fig. 3.33	54.3/31.6	28.9/18.1	16.8/50.3	(Fe,Cr)B
	Darker of the outer boride layer in Fig. 3.33	21.9/12.6	61.6/38.2	16.5/49.2	(Cr,Fe)B
III	Brighter of the inner boride layer in Fig. 3.34	68.1/48.6	22.6/17.3	9.3/34.1	$(Fe,Cr)_2B$
	Darker of the inner boride layer in Fig. 3.34	24.6/17.4	66.8/51.0	8.6/31.6	$(Cr,Fe)_2B$
IV	Brighter in Fig. 3.35	84.1/83.2	15.9/16.8	0.0/0.0	<Fe>
	Darker in Fig. 3.35	27.0/18.8	63.8/48.0	9.2/33.2	$(Cr,Fe)_2B$
V	Brighter in Fig. 3.36	81.3/80.2	18.7/19.8	0.0/0.0	<Fe>
	Darker in Fig. 3.36	24.6/17.4	66.8/51.0	8.6/31.6	$(Cr,Fe)_2B$
VI	Homogeneous	80.7/79.6	19.3/20.4	0.0/0.0	<Fe>

3.3.3. Types of microstructure of boride layers

To summarize, comparative analysis of the microstructure of boride layers formed in samples of all alloys and steels investigated provides evidence for the existence of its two types as illustrated in Fig. 3.39. The first type (Type I) is exhibited by Fe–5% Cr, Fe–10% Cr and Fe–15% Cr alloys and a 13% Cr steel. In this microstructure, each of two boride layers consists of a homogeneous phase either (Fe,Cr)B or $(Fe,Cr)_2B$, Fig. 3.39b and d. The second type (Type II) is characteristic of Fe–25% Cr and Fe–30% Cr alloys and a 25% Cr steel. In this microstructure, each of two boride layers is two-phase, with the outer layer consisting of the (Fe,Cr)B and (Cr,Fe)B phases (Fig. 3.39b' and d') and the inner consisting of the $(Fe,Cr)_2B$ and $(Cr,Fe)_2B$ phases. As seen in Fig. 3.39b', the microstructure of the second type has a distinguishable regular arrangement that is much less profound for a 25% Cr steel (Fig. 3.39d') than for Fe–25% Cr and Fe–30% Cr alloys.

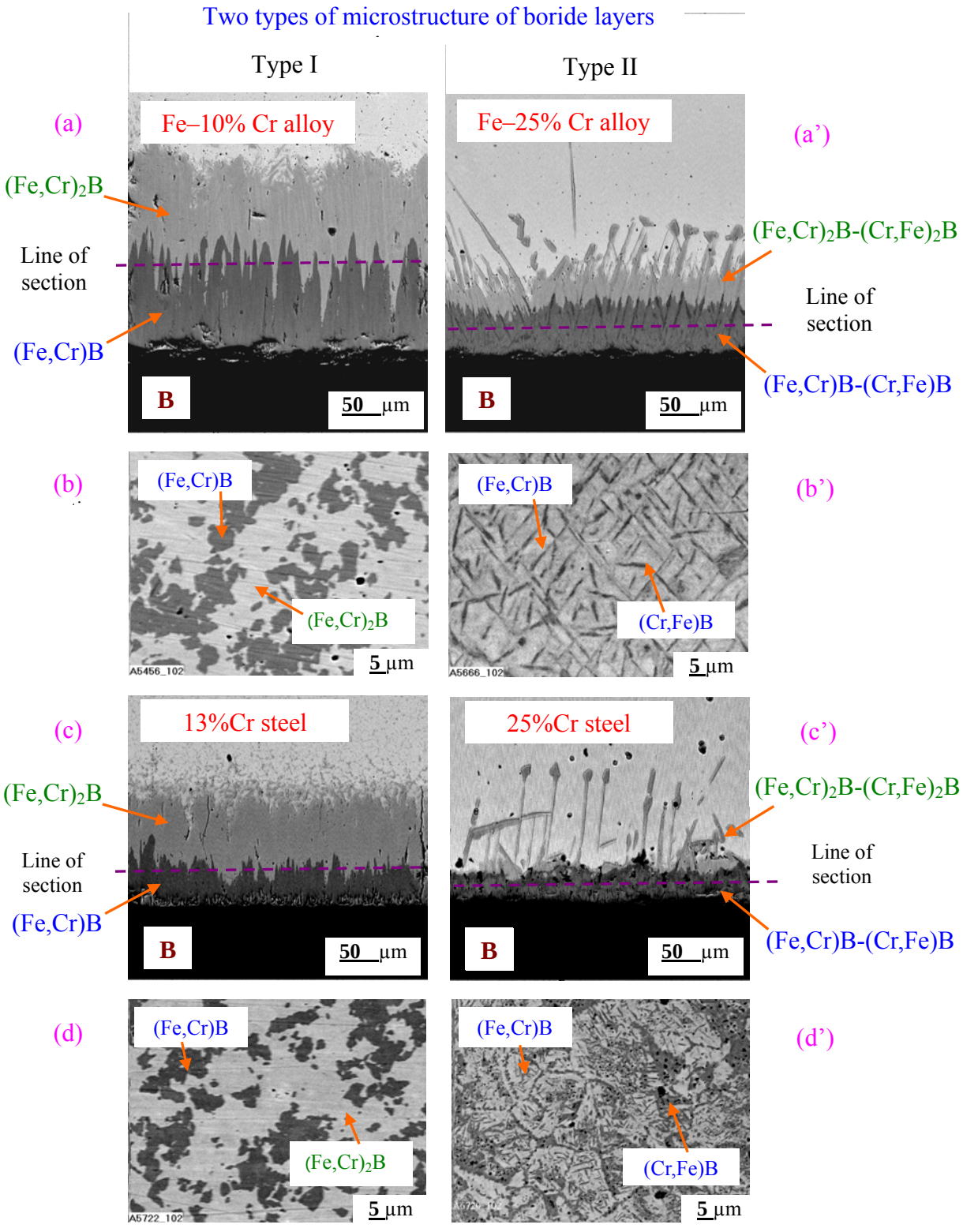

Fig. 3.39. Backscattered electron images (BEI) of the transition zone between reacting phases illustrating two types of microstructure of boride layers, and those of their plan-view sections shown by a line of section. Boriding conditions: 950°C, 21600 s (6 h).

4. Mechanism of formation of boride layers

4.1. Sequence of layer occurrence

Figure 4.1 provides clear evidence that in the case of a Fe–5% Cr alloy the FeB and Fe_2B layers occur sequentially, with the Fe_2B layer being the first to form. This single boride layer grows up to a reaction time of at least 14400 s (4 h). The next continuous FeB layer is only formed at a reaction time of 21600 s (6 h) when the thickness of the Fe_2B layer exceeds, depending on the temperature of thermochemical boriding, 100-180 μm.

After a reaction time of 3600 s (1 h) at 950 °C, the FeB layer is seen in Fig. 4.2 to be still missing from the Fe–10% Cr alloy-boron interface, even though the Fe_2B layer has already reached a thickness of around 70 μm. Simultaneous formation of the FeB and Fe_2B layers at this temperature is observed at a reaction time of 7200 s (2 h) or more. In the temperature range of 850–950 °C, a reaction time of 3600 s (1 h) was found to be sufficient for both boride layers to form on the surface of samples of other alloys and steels investigated (Figs 4.3-4.7). Under similar temperature-time conditions, their thickness tends to decrease with increasing chromium content of Fe–Cr alloys and steels, the difference, for example, with a Fe–5% Cr alloy and a 25% Cr steel being up to 5 times.

4.2. Chemical reactions at layer interfaces

Initially, the first-formed Fe_2B layer can readily grow at the Fe-B interface by *direct* chemical reaction between the surface iron and boron atoms (Fig. 4.8)

$$2\,Fe_{surf} + B_{surf} = Fe_2B \qquad (4.1)$$

as long as these are in immediate contact with each other.

To simplify the designations and further analytical treatment of kinetic data, iron and chromium will be considered as a single chemical element (Fe). In view of the close similarity of their physico-chemical properties, this simplification does not appear to cause any misleading results.

It is clear, however, that the formation of the Fe_2B layer, even one crystal-lattice thick, separates the reactants from one another, thereby making the further progress of the direct chemical reaction between the surface iron and boron atoms impossible. Subsequently, growth of the Fe_2B layer can only take place at the expense of counter-diffusion of iron and boron atoms across its bulk and further two *partial* chemical reactions

$$2\,Fe_{dif} + B_{surf} = Fe_2B \qquad (4.2_1)$$

and

$$B_{dif} + 2\,Fe_{surf} = Fe_2B, \qquad (4.2_2)$$

proceeding at the B–Fe_2B and Fe_2B–Fe interfaces, respectively, as shown in Fig. 4.9.

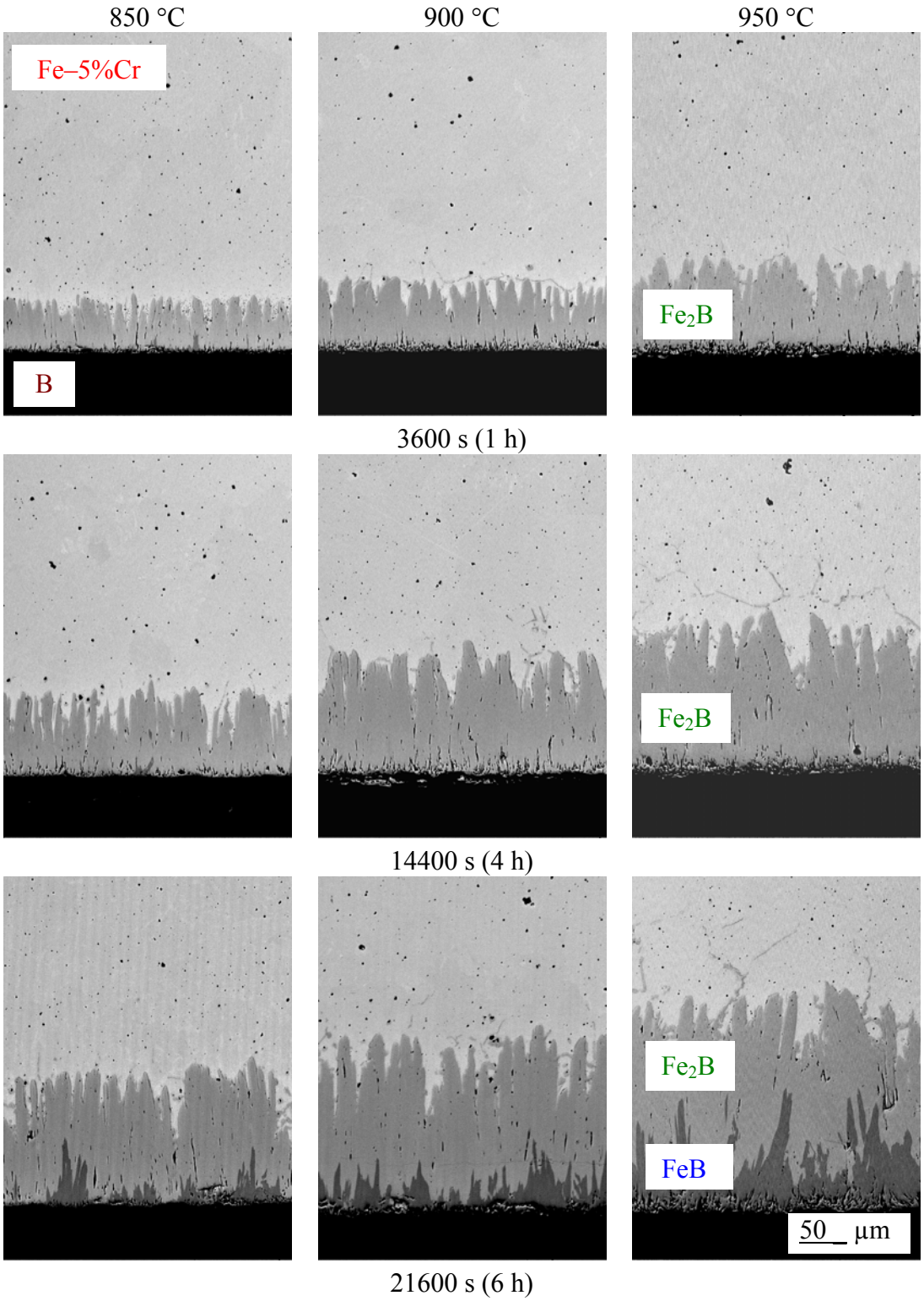

Fig. 4.1. Backscattered electron images (BEI) of the transition zone between a Fe–5% Cr alloy and boron. The Fe_2B layer is seen to be the first to occur and grow in a time range of 3600-14400 s (1-4 h). The next FeB layer is only formed when the thickness of the first-occurred Fe_2B layer becomes more than 100–180 µm.

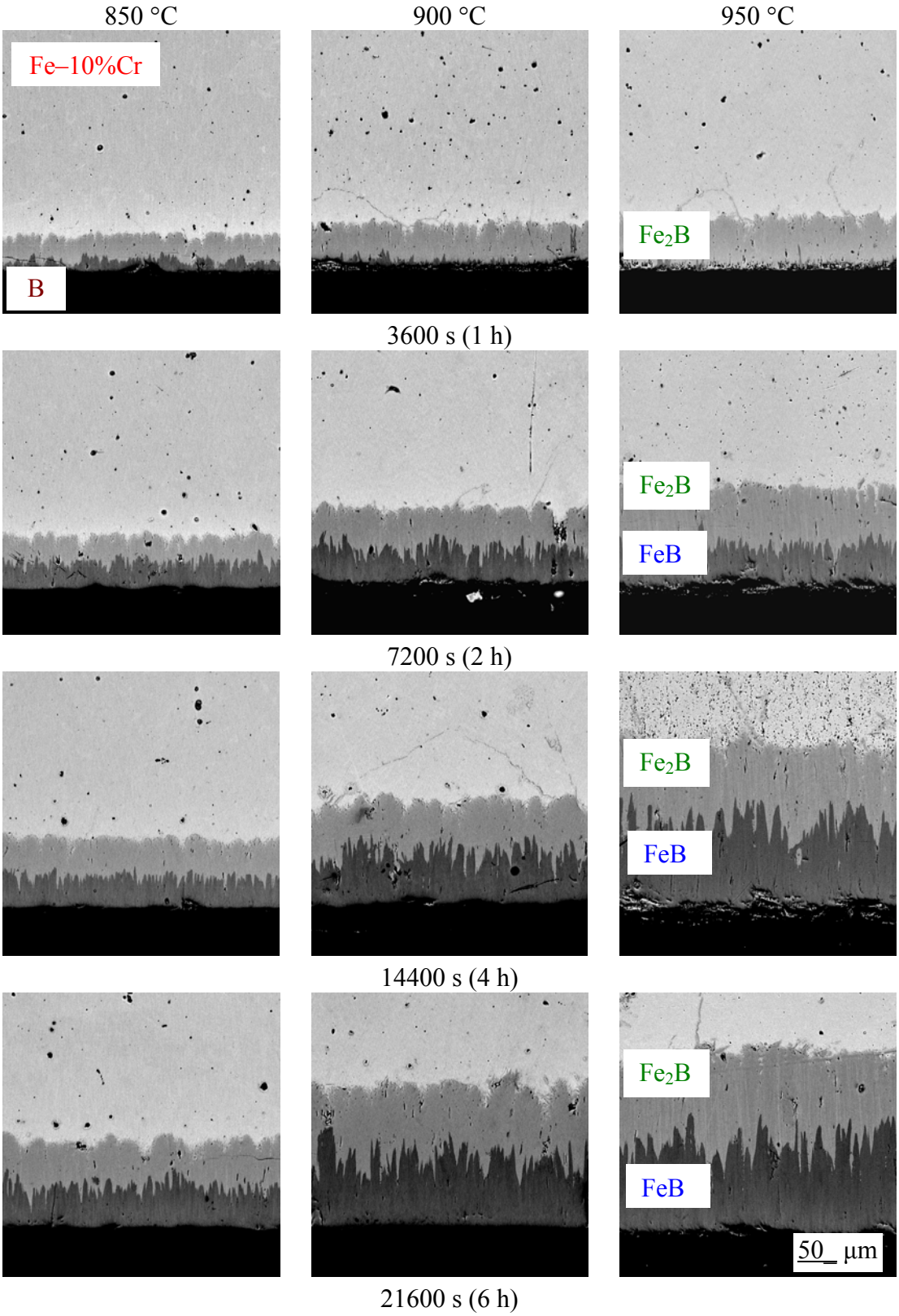

Fig. 4.2. Backscattered electron images (BEI) of the transition zone between a Fe–10% Cr alloy and boron. The FeB layer is missing at 950 °C and a reaction time of 3600 s (1 h).

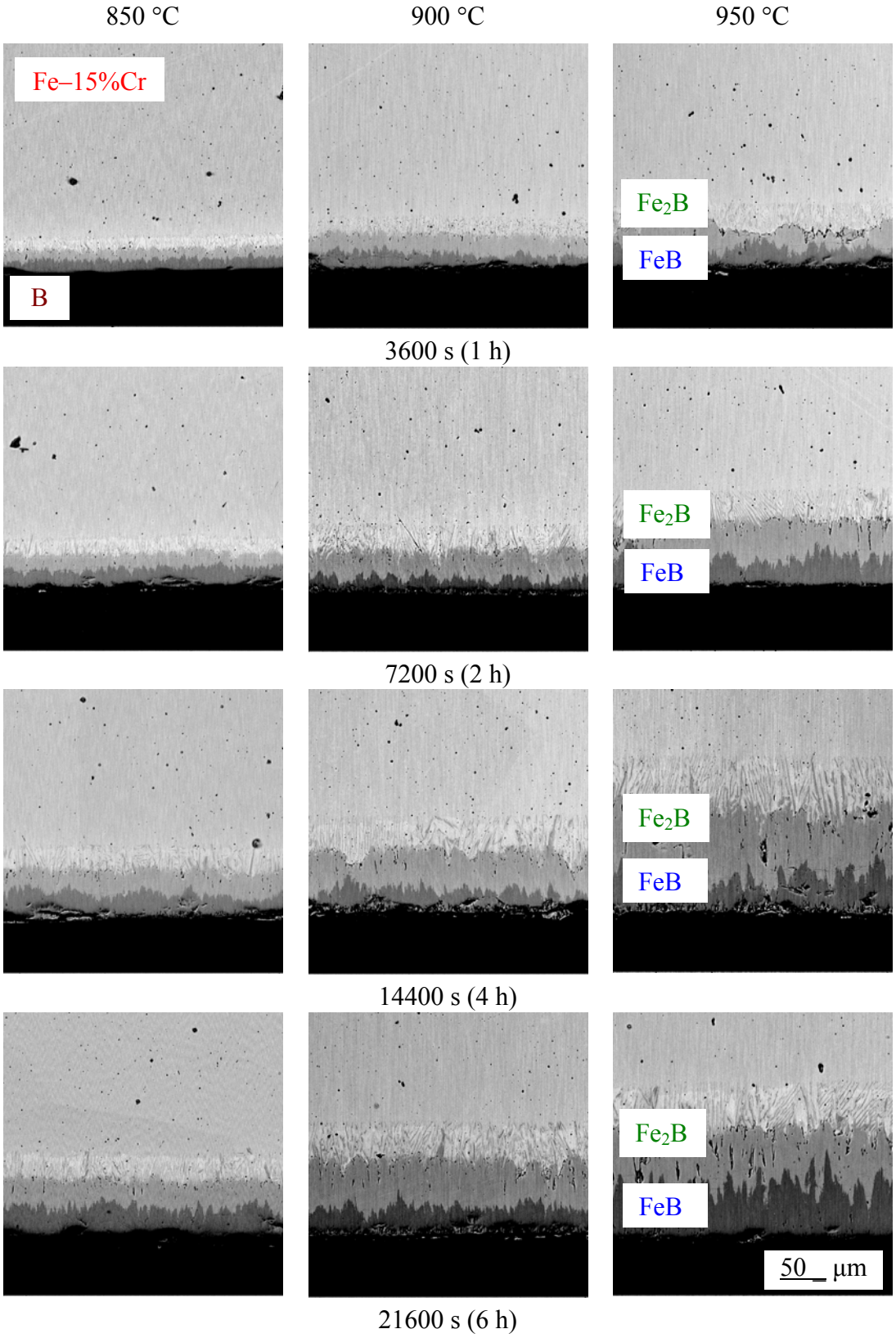

Fig. 4.3. Backscattered electron images (BEI) of the transition zone between a Fe–15% Cr alloy and boron.

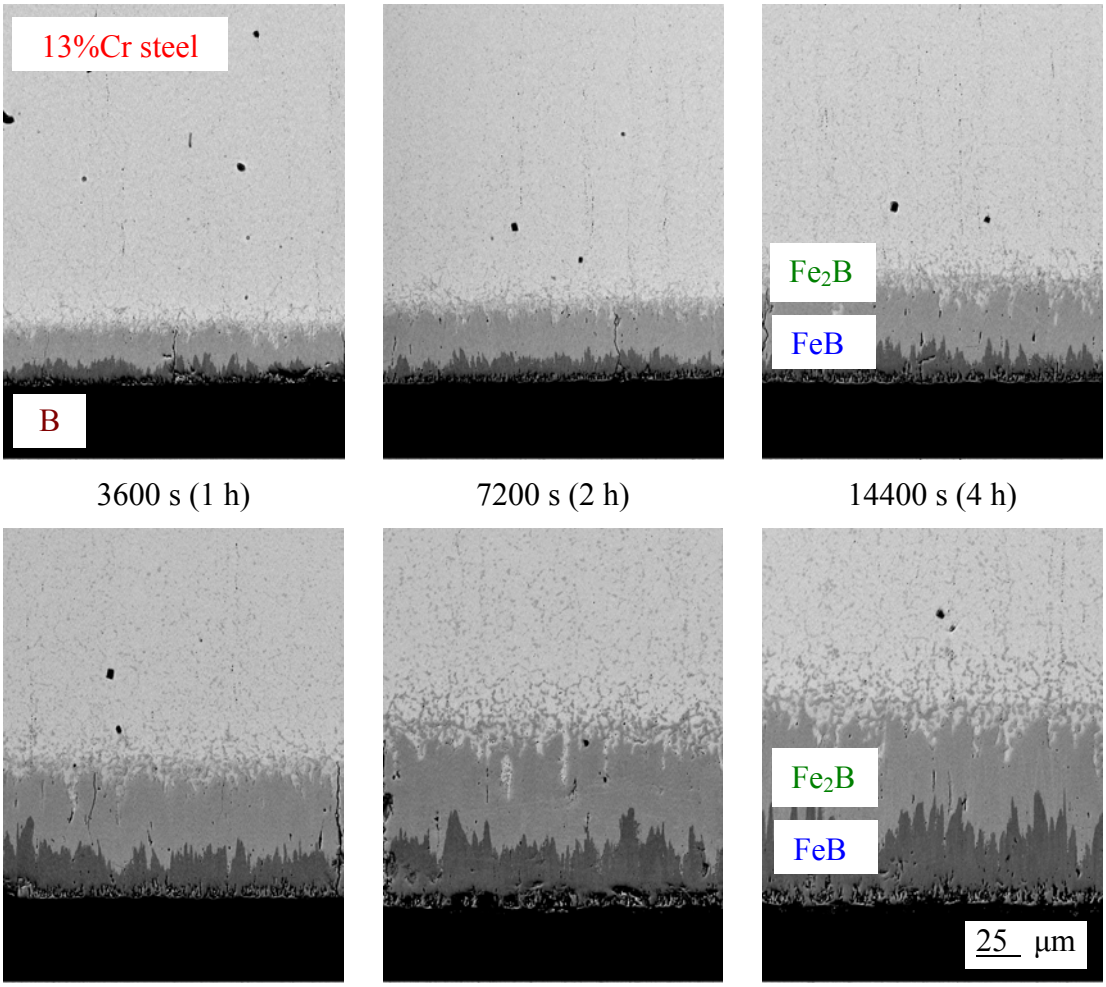

Fig. 4.4. Backscattered electron images (BEI) of the transition zone between a 13% Cr steel and boron.

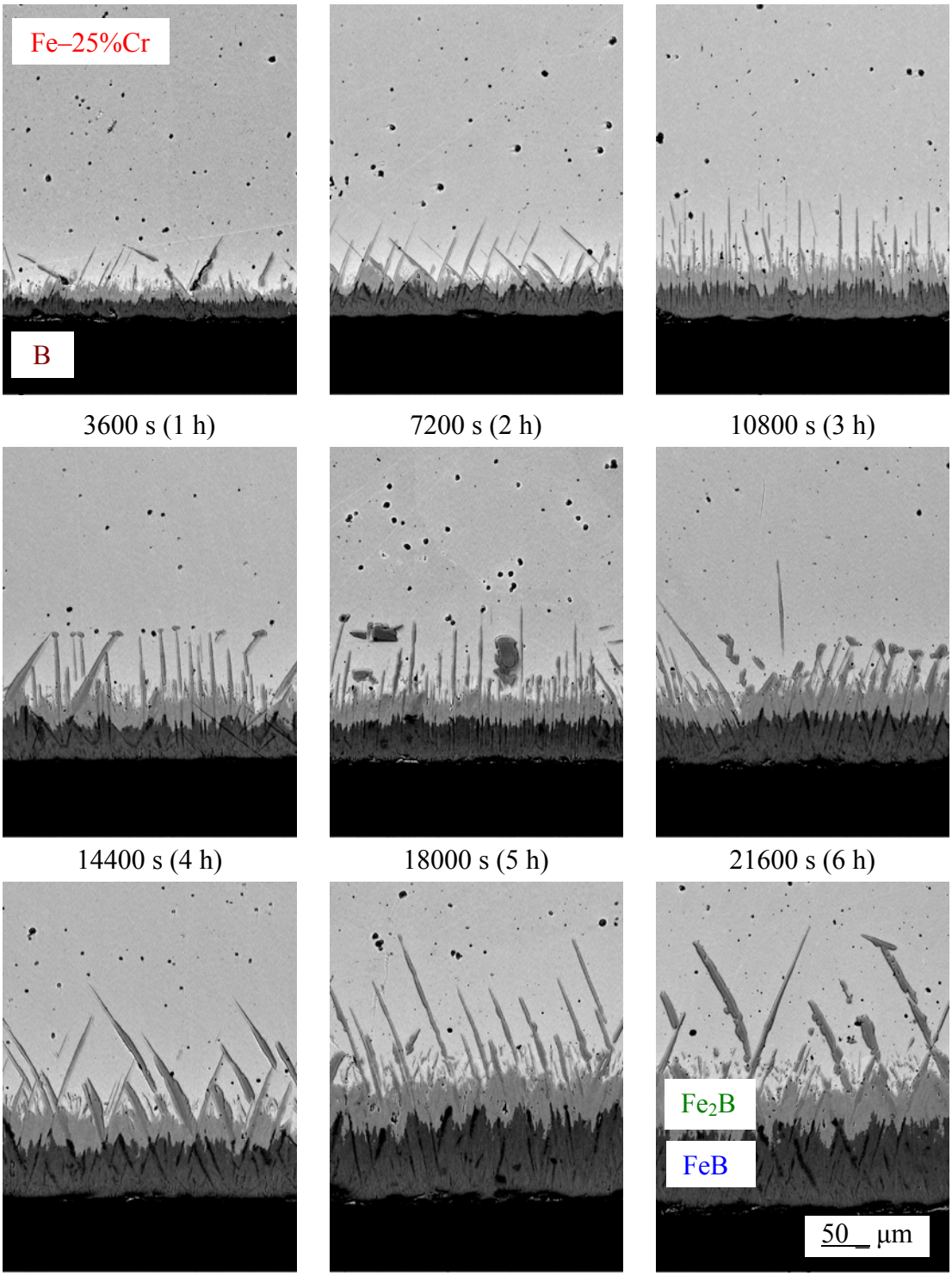

Fig. 4.5. Backscattered electron images (BEI) of the transition zone between a Fe–25% Cr alloy and boron after thermochemical boriding at 950 °C.

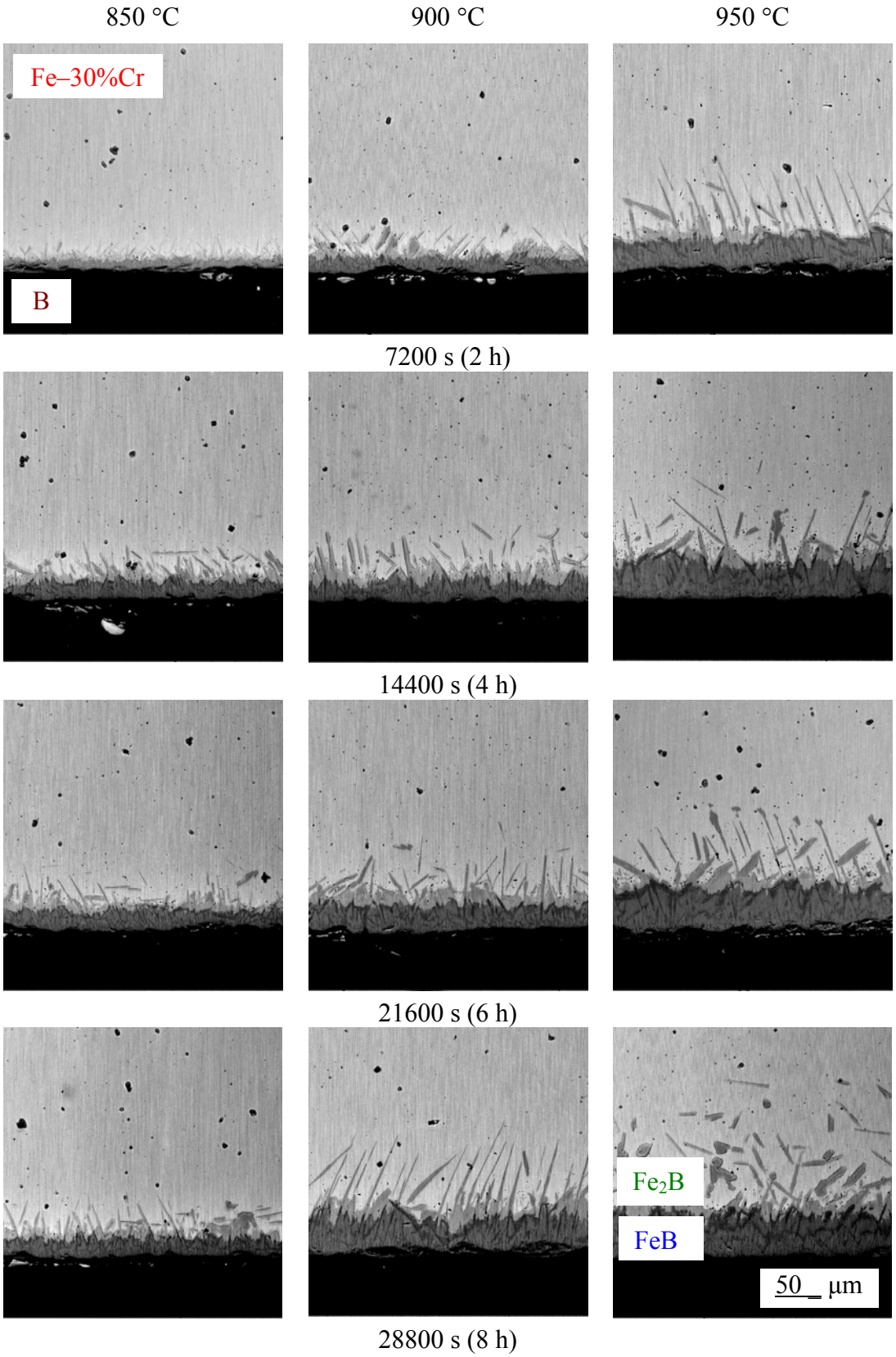

Fig. 4.6. Backscattered electron images (BEI) of the transition zone between a Fe–30% Cr alloy and boron.

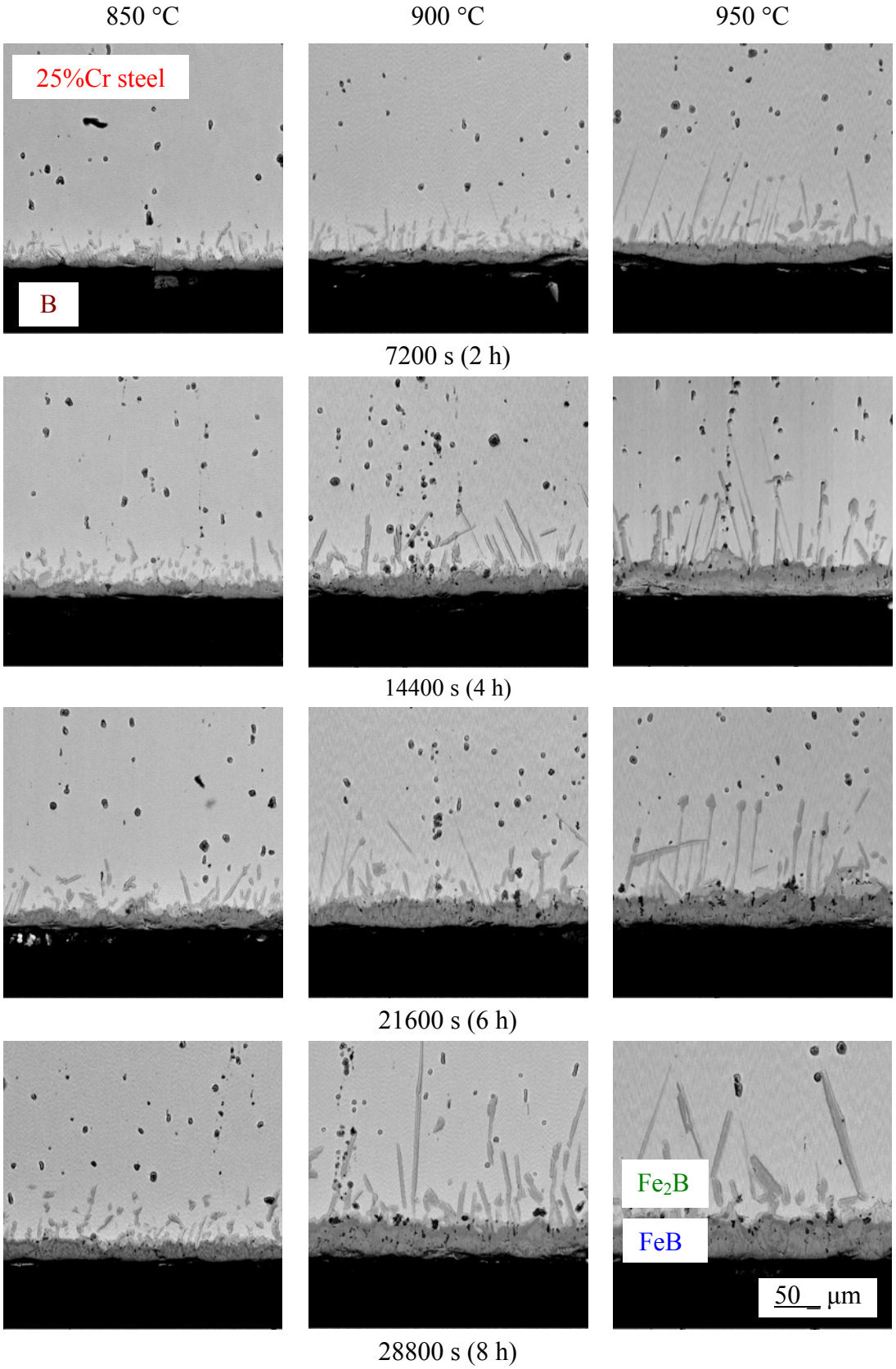

Fig. 4.7. Backscattered electron images (BEI) of the transition zone between a 25% Cr steel and boron.

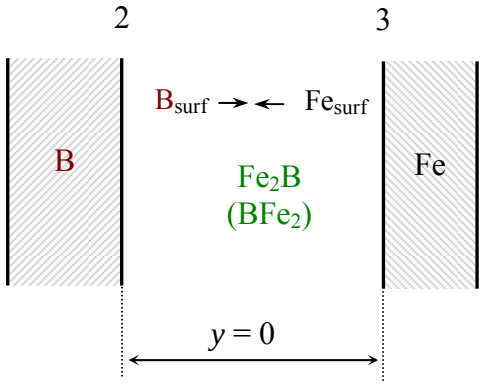

Fig. 4.8. Schematic diagram to illustrate the beginning of formation of the Fe_2B layer by direct chemical reaction between the surface iron and boron atoms. Initially, the reactants B and Fe are in immediate contact with each other ($y = 0$).

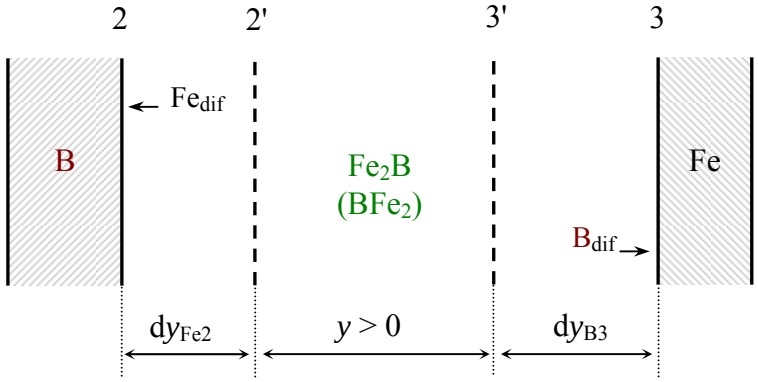

Fig. 4.9. Schematic diagram illustrating the growth process of the Fe_2B layer by partial chemical reactions between the diffusing iron atoms and surface boron atoms at interface 2 and between the diffusing boron atoms and surface iron atoms at interface 3. At $y > 0$, the reactants B and Fe prove to be separated from one another by the growing Fe_2B layer.

These reactions cause an increase in thickness of the Fe_2B layer during a time dt by dy_{Fe2} at the former interface and by dy_{B3} at the latter. Note that no reaction can take place between the diffusing iron and boron atoms in the bulk of the growing Fe_2B layer. Any chemical transformations (reactions as such following the diffusion of reacting elements Fe and B) proceed entirely at the layer interfaces where the reaction product Fe_2B is accumulating (for more detail about the mechanism of solid-state formation of compound layers, see [46-49]).

After the continuous layers of both iron borides have formed, their subsequent growth under conditions of reaction (chemical) control, when the rate of diffusion of reacting atoms across their bulks exceeds the rate of interfacial (chemical) transformations, is due to *four partial* chemical reactions (Fig. 4.10)

Layer	Interface	Reaction	
FeB	1	$Fe_{dif} + B_{surf} = FeB,$	(4.3_1)
	2	$B_{dif} + Fe_2B = 2FeB,$	(4.3_2)
Fe_2B	2	$Fe_{dif} + FeB = Fe_2B,$	(4.4_1)
	3	$B_{dif} + Fe_{surf} = Fe_2B.$	(4.4_2)

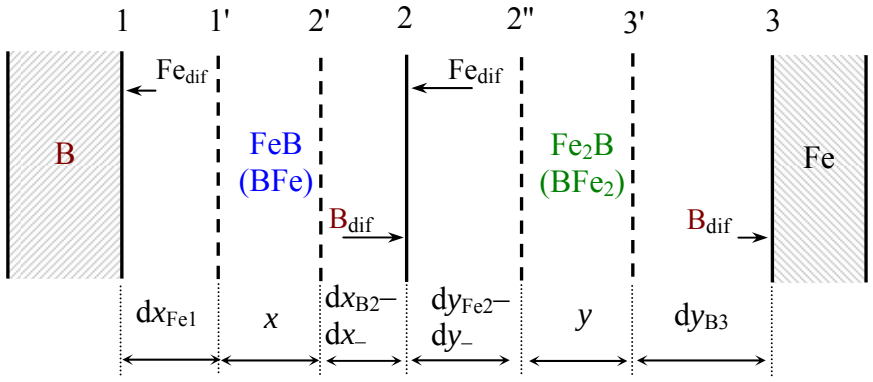

Fig. 4.10. Schematic diagram illustrating the growth process of the FeB and Fe_2B layers under conditions of reaction (chemical) control. Arrows of different length are employed to indicate the decrease in amount of diffusing atoms, available at a particular interface, with increasing distance from an appropriate initial substance (B or Fe).

Both components (Fe and B) are supposed to be capable of diffusing in both layers. As a result of these reactions, the thickness of the FeB layer increases during a time dt by dx_{Fe1} at interface 1 and by dx_{B2} at interface 2, while that of the Fe_2B layer increases during the same time by dy_{Fe2} at interface 2 and by dy_{B3} at interface 3. Simultaneously, the thicknesses of the FeB and Fe_2B layers decrease at their common interface 2 due to the mutual consumption in reactions (4.3_2) and (4.4_1). This decrease is dx_- for the FeB layer and dy_- for the Fe_2B layer.

Arrows of different length are employed in Fig. 4.10 to indicate the decrease in amount of diffusing atoms, available at a particular interface, with increasing distance from a given initial substance (boron or iron). It is obvious that only those boron atoms which have not entered into partial chemical reaction (4.3_2) at interface 2 can diffuse further to interface 3 and enter there into partial chemical reaction (4.4_2). Similarly, only those iron atoms which have not entered into partial chemical reaction (4.4_1) at interface 2 can diffuse further to interface 1 and enter there into partial chemical reaction (4.3_1).

Obviously, thickening of the FeB and Fe_2B layers with passing time eventually results in a change of the regime of their growth from reaction controlled to diffusion controlled, when the rate of interfacial transformations (reactions) becomes first equal to, at a certain *critical* layer thickness, and then greater than, at layer thicknesses exceeding this critical value, the rate of diffusion of appropriate reacting atoms to the reaction sites (interfaces) (for more detail, see [46-49]). After the FeB layer has reached its critical thickness $x_{1/2}^{(\mathrm{Boron})}$ with regard to boron, the Fe_2B layer loses the source of boron atoms and therefore stops growing at the expense of diffusion of this component. Note that the only source of boron atoms for both boride layers to grow is the initial boron phase (boron powder).

Again, after the Fe_2B layer has reached its critical thickness $y_{1/2}^{(\mathrm{Iron})}$ with regard to iron, the FeB layer loses the source of iron atoms and therefore stops growing at the expense of diffusion of this component. It must be clear that the only source of iron atoms for both layers to grow is the initial iron-containing phase (Fe–Cr alloy or steel).

Hence, under conditions of diffusion control the FeB and Fe_2B layers are only able to grow at their common interface 2, as shown in Fig. 4.11. The FeB layer grows at the expense of diffusion of boron atoms across its bulk and their subsequent reaction with the Fe_2B compound. The Fe_2B layer grows at the expense of diffusion of iron atoms across its bulk and their subsequent reaction with the FeB compound. Thus, both boride layers grow at interface 2 by pushing each other in opposite directions.

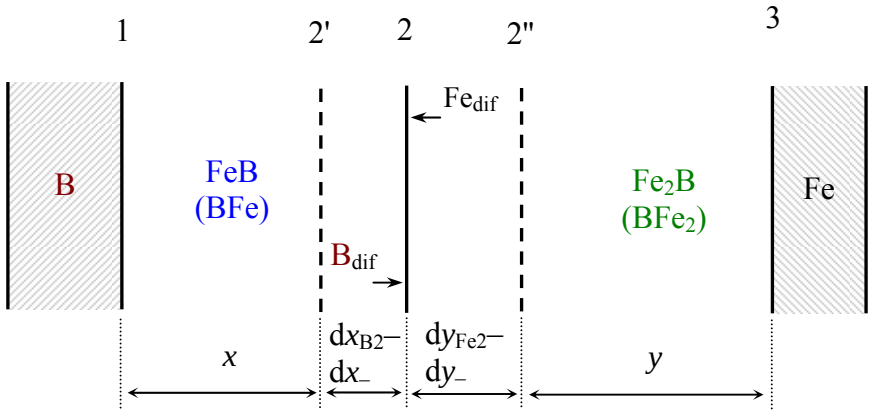

Fig. 4.11. Schematic diagram illustrating the growth process of the FeB and Fe_2B layers under conditions of diffusion control. Both layers only thicken at their common interface 2. No partial chemical reactions can take place at interfaces 1 and 3 due to the lack of appropriate diffusing atoms (Fe at interface 1 and B at interface 3).

Even though the FeB and Fe_2B layers are often considered to grow entirely at the expense of diffusion of the single component boron across their bulks, it is hardly possible with compact layers having no macroscopic defects and therefore growing by the volume-diffusion mechanism. During diffusional growth, by definition, diffusion across the layer bulks is the rate-determining step, the interfacial partial chemical reactions being very fast. It means that all the boron atoms reaching interface 2 react with Fe_2B to form FeB at that

interface. Since under conditions of diffusion control the ability of interface 2 to combine those atoms exceeds their diffusional transport across the FeB layer (slow diffusion followed by fast reaction), none of them can diffuse further to interface 3 and react with Fe to form Fe_2B according to reaction (4.4_2): $B_{dif} + 2Fe = Fe_2B$. This reaction can only take place either under conditions of reaction control when the flux of boron atoms from the initial B-containing phase is sufficient for both boride layers to grow or if the FeB layer is non-protective, due to the presence of cracks, fissures and other macroscopic defects, while boriding is carried out from a vapour or liquid phase.

If boride layers are permeable to a vapour or liquid phase, direct chemical reactions between initial substances prove to be possible. Grain-boundary diffusion can also make a considerable contribution to the layer-growth process. If a few growth mechanisms are operative simultaneously, a complicated and hardly tractable microstructure of boride layers can readily be formed.

From a chemical viewpoint, it must thus be clear that the diffusionally growing compact FeB layer itself can by no means be a source of boron atoms for the Fe_2B layer to grow. It only serves as a transport media for these atoms. Suppose that two FeB molecules decompose at interface 2 to yield one molecule of Fe_2B and one diffusing boron atom: $2FeB = Fe_2B + B_{dif}$. However, this boron atom will be unable to diffuse from interface 2 to interface 3 because under conditions of diffusion control the Fe_2B surface is undersaturated with boron atoms and therefore the just-released atom is immediately combined at interface 2 according to the reaction $B_{dif} + Fe_2B = 2FeB$. The net result of those reactions is zero.

In contrast, under conditions of reaction control the Fe_2B surface bordering the FeB layer is oversaturated with boron atoms and therefore part of them (not combined into the FeB phase at interface 2) can readily diffuse further to interface 3 and react with the iron atoms to form Fe_2B. As the source of boron atoms for both layers to grow is the boriding phase (boron powder), it is clear that sooner or later the flux of boron atoms, diminishing as the FeB layer thickens, becomes only sufficient for the FeB layer itself to grow, whereas the faraway Fe_2B layer must stop growing. Note that in the absence of the boriding phase or if the contact of the FeB layer with it is lost, reaction $2FeB = Fe_2B + B_{dif}$ can readily proceed, resulting in degradation of the existing FeB layer and enhanced growth of the Fe_2B layer at the expense of diffusion of the released boron atoms.

Similarly, under conditions of diffusion control all the iron atoms diffusing across the Fe_2B layer are combined into Fe_2B by their reaction with FeB at interface 2. Hence, iron atoms cannot take part in the formation of the faraway FeB layer at interface 1.

This conclusion is usually overlooked, if the process of formation of compound layers is treated without writing the equations of chemical reactions proceeding at layer interfaces. In fact, at the diffusional stage of layer formation each of two compound layers without any macroscopic defects can grow only at the expense of diffusion of the atoms from a neighbouring initial phase. When one of the initial phases is exhausted, then the compound layer adjacent to this phase becomes a new initial phase. This is the only way (by successive consumption of initial substances) for binary systems without a noticeable solubility in the solid state, like Fe–B, to attain equilibrium.

5. Layer-growth kinetics

5.1. Parabolic growth of boride layers

Growth kinetics of chemical compound layers are conventionally treated from a diffusional viewpoint giving parabolic equations of the type $x^2 = 2k_1t$, where x is the layer thickness, k_1 is the layer growth-rate constant and t is the time (see, for example, [44-49]. In the case of rather thick layers (1 μm or more), such equations produce a quite satisfactory fit to the experimental data, as exemplified with boride layers FeB and Fe_2B in Tables 5.1 and 5.2 where the layer thicknesses (Table 5.1) and the average values of the layer growth-rate constant (Table 5.2) are presented for a Fe–5% Cr alloy.

The temperature dependence of the layer growth-rate constants is mostly described by a relation of the Arrhenius type

$$K = K_0 \exp(-E/RT),$$

where K stands for any layer growth-rate constant, K_0 is the pre-exponential factor, E is the activation energy, R is the gas constant (8.314 J mol^{-1} K^{-1}) and T is the absolute temperature.

A plot of ln k_1 against T^{-1} for the Fe_2B layer in the time range 3600-14400 s (1-4 h) when the FeB layer is still missing between boron and the Fe_2B layer is shown in Fig. 5.1. The least-squares fit method yields the following equation

$$k_1^{(Fe_2B)} = 7.00\times10^{-6} \exp(-135.0 \text{ kJ mol}^{-1}/RT) \text{ m}^2 \text{ s}^{-1}.$$

It should be emphasized, however, that purely diffusional considerations and parabolic equations are generally insufficient to understand and explain a variety of known experimental observations. The main amongst those are as follows.

(1) Initial layer growth is known to be linear and not parabolic.

(2) In multiphase binary systems, formation of compound layers is more often sequential than simultaneous, whereas from a diffusional viewpoint they all must occur and then grow parabolically with passing time.

(3) Existence of a rather wide range of homogeneity is a necessary condition in derivation of parabolic equations but many, if not the vast majority of, chemical compounds have no homogeneity range. Nonetheless, their layers grow at a rate, sometimes even far exceeding that of the layers of compounds with a wide homogeneity range.

(4) According to diffusional considerations, any compound layer of a multiphase binary system, once formed, cannot subsequently disappear, whereas experiments provide evidence that in artificially prepared reaction couples some of them can either grow or shrink or even disappear entirely, depending on the ratio of their initial thickness.

These and other inconsistencies of the diffusional approach to the consideration of layer-growth kinetics are readily overcome in the framework of the physico-chemical one [46-49]). Unlike the former, the latter takes account both of *the rate of diffusion* across the bulks of growing compound layers and *the rate of subsequent chemical transformations* at layer interfaces. Thus, any solid-state chemical reaction resulting in layer formation is supposed to take place in two consecutive steps and not in one step. The first step (diffusion) is a necessary but insufficient one for any compound layer to occur and grow. It must necessarily be followed by the second step of purely chemical transformations.

Table 5.1. Thickness and growth-rate constants k_1 of the FeB and Fe_2B layers formed at the Fe–5% Cr alloy-boron interface. Values of k_1 are provided for the total thickness of both layers and also for each of them separately.

Temperature (°C)	Time ($\times 10^2$ s)	Layer thickness ($\times 10^{-6}$ m)			k_1 ($\times 10^{-13}$ m^2 s^{-1}) from the equation $x^2 = 2k_1t$		
		total	FeB	Fe_2B	total	FeB	Fe_2B
850	36	50	-	50	3.5	-	3.5
	72	74	-	74	3.8	-	3.8
	144	100	-	100	3.5	-	3.5
	216	156	30	126	0.563	0.0208	0.368
	288	187	40	147	0.607	0.0278	0.375
900	36	71	-	71	7.0	-	7.0
	72	100	-	100	7.2	-	7.2
	144	140	-	140	6.8	-	6.8
	216	205	45	160	0.973	0.047	0.593
	288	227	54	173	0.894	0.050	0.520
950	36	91	-	91	11.5	-	11.5
	72	130	-	130	11.7	-	11.7
	144	184	-	184	11.8	-	11.8
	216	227	60	167	1.193	0.083	0.646
	288	254	74	180	1.120	0.095	0.563

Table 5.2. Average values of the growth-rate constants of the FeB and Fe_2B layers formed at the Fe–5% Cr alloy-boron interface. These are provided for the total thickness of both layers and also for each of them separately.

Temperature (°C)	Time range ($\times 10^2$ s)	k_1 ($\times 10^{-13}$ m^2 s^{-1})		
		total	FeB	Fe_2B
850	36–144	3.6	-	3.6
	216–288	0.585	0.0243	0.372
900	36–144	7.0	-	7.0
	216–288	0.934	0.049	0.557
950	36–144	11.7	-	11.7
	216–288	1.157	0.089	0.605

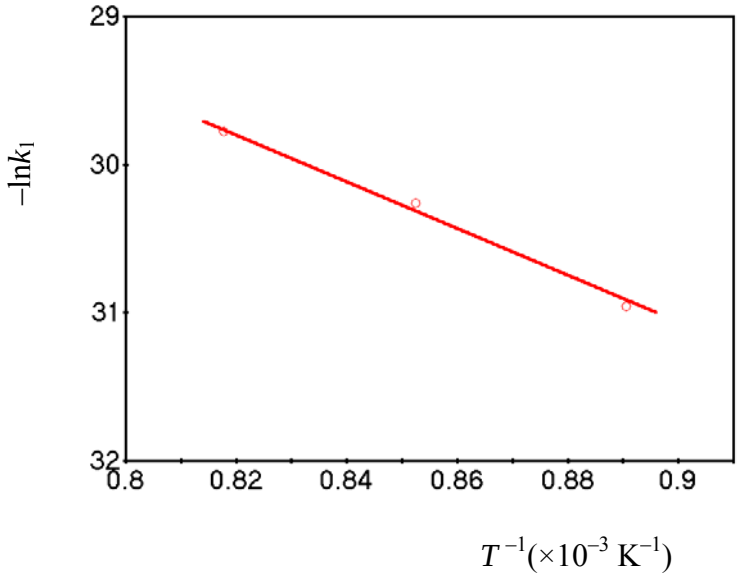

Fig. 5.1. Temperature dependence of the growth-rate constant of the Fe_2B layer in the time range 3600-14400 s (1-4 h) in the absence of the FeB layer from the Fe–5% Cr alloy-boron interface.

5.2. General system of two differential equations describing layer-growth rates

Growth kinetics of the FeB and Fe_2B layers at the interface of a Fe–Cr alloy or steel and boron at the expense of diffusion of both components can generally be described by a system of two non-linear differential equations (for its derivation, see [46-49])

$$\frac{dx}{dt} = \frac{k_{0Fe1}}{1+\frac{k_{0Fe1}x}{k_{1Fe1}}} + \frac{k_{0B2}}{1+\frac{k_{0B2}x}{k_{1B2}}} - \frac{rg}{p}\,\frac{k_{0Fe2}}{1+\frac{k_{0Fe2}y}{k_{1Fe2}}}, \qquad (5.1_1)$$

$$\frac{dy}{dt} = \frac{k_{0Fe2}}{1+\frac{k_{0Fe2}y}{k_{1Fe2}}} + \frac{k_{0B3}}{1+\frac{k_{0B3}y}{k_{1B3}}} - \frac{q}{sg}\,\frac{k_{0B2}}{1+\frac{k_{0B2}x}{k_{1B2}}}. \qquad (5.1_2)$$

where x is the outer FeB layer thickness; y is the inner Fe_2B layer thickness; k_{0Fe1} and k_{0B2} are the chemical growth-rate constants of the FeB layer at the expense of diffusion of iron and boron atoms, respectively; k_{1Fe1} and k_{1B2} are the diffusional (physical) growth-rate constants of the FeB layer at the expense of diffusion of iron and boron atoms, respectively; k_{0Fe2} and k_{0B3} the chemical growth-rate constants of the Fe_2B layer at the expense of diffusion of iron and boron atoms, respectively; k_{1Fe2} and k_{1B3} are the diffusional (physical) growth-rate constants of the Fe_2B layer at the expense of diffusion of iron and boron atoms, respectively; g is the ratio of the molar volumes of the FeB and Fe_2B compounds; $p = q = r = 1$ and $s = 2$ (factors from the chemical formulae of FeB (written as BFe) and Fe_2B (BFe_2)).

The value of g is determined from the density of the compounds FeB (BFe) $\rho_1 = 6.70 \times 10^3$ kg m^{-3} and Fe_2B (BFe_2) $\rho_2 = 7.34 \times 10^3$ kg m^{-3} [1] and their molecular mass $M_1 = 66.65$ g mol^{-1} and $M_2 = 122.49$ g mol^{-1}: $g = M_1\rho_2/M_2\rho_1 = 0.60$.

5.2.1. Initial reaction controlled stage of layer growth

Initially, growth kinetics of compound layers is seen from the system of equations (5.1) to be linear because at low t the terms of the type k_0x/k_1 and k_0y/k_1 can be neglected in comparison with unity and therefore this system is simplified to

$$\frac{dx}{dt} = k_{0Fe1} + k_{0B2} - \frac{rg}{p}\,k_{0Fe2}, \qquad (5.2_1)$$

$$\frac{dy}{dt} = k_{0Fe2} + k_{0B3} - \frac{q}{sg}\,k_{0B2}. \qquad (5.2_2)$$

System of equations (5.2) describes the *reaction controlled stage* of growth of boride layers when the rates of diffusion of iron and boron atoms across layer bulks are so high that their effect on the overall rates of formation of the layers is negligible in comparison with that of the rates of subsequent chemical transformations taking place at phase interfaces. This is that case in which the purely chemical processes are rate-determining (chemical control), for there is a great excess of diffusing atoms of both kinds for both layers to grow.

It does not mean, however, that under such circumstances the FeB and Fe_2B layers will necessarily occur and grow at the alloy (steel)-boron interface simultaneously. Clearly, their simultaneous occurrence is only possible, if the derivatives dx/dt and dy/dt in equations (5.1) and (5.2) are positive dx/dt > 0 and dy/dt > 0, and consequently the inequalities $k_{0Fe1} + k_{0B2} > (rg/p)k_{0Fe2}$ and $k_{0Fe2} + k_{0B3} > (q/sg)k_{0B2}$ are satisfied. In such a case, both boride layers will grow simultaneously from the very beginning of interaction of initial substances according to a linear law

$$x = (k_{0Fe1} + k_{0B2} - \frac{rg}{p} k_{0Fe2})t, \qquad (5.3_1)$$

$$y = (k_{0Fe2} + k_{0B3} - \frac{q}{sg} k_{0B2})t. \qquad (5.3_2)$$

Note that their growth rates are the highest possible under given (constant) temperature-pressure conditions. Linear stage of growth of boride layers has not yet been explored properly due probably to the necessity of carrying out thorough experiments with very thin films.

5.2.2. Sequential layer formation

If the condition

$$k_{0Fe1} + k_{0B2} < (rg/p)k_{0Fe2} \qquad (5.4)$$

is satisfied, the FeB layer cannot form at all (dx/dt < 0). Therefore, only the Fe_2B layer will be observed to grow at the interface of reacting phases, as is the case with Fe–5% Cr alloy (see Fig. 4.1).

It should be emphasized that even if the FeB layer were in an artificially prepared sample Fe–Fe_2B–FeB–B, its thickness would decrease, and it might eventually disappear completely. The FeB layer is *kinetically* (not thermodynamically) *unstable* since the decrease in its thickness due to the consumption during growth of the Fe_2B layer by reaction (4.4_1) exceeds the increase due to reactions (4.3_1) and (4.3_2).

From the system of equations (5.1), it is easy to see that the sequential formation of boride layers (dx/dt < 0, dy/dt > 0 or dx/dt > 0, dy/dt < 0) is more probable than simultaneous (dx/dt > 0 and dy/dt > 0), the ratio of probabilities being 2 : 1. Besides, this system indicates a necessary condition for the occurrence of the next layer, if their formation happened to be not simultaneous. Since the Fe_2B layer is the first to occur, the FeB layer can only start to form when dx/dt > 0 and hence

$$k_{0Fe1} + k_{0B2} \geq \frac{rg}{p} \frac{k_{0Fe2}}{1 + \frac{k_{0Fe2} y_{min}}{k_{1Fe2}}}, \qquad (5.5)$$

where y_{min} is a smallest (*minimal*) thickness of the Fe_2B layer necessary for the FeB layer to occur and grow. Chemically, it merely means that at this thickness of the Fe_2B layer, the rate of consumption of the FeB layer during growth of the Fe_2B layer by reaction (4.4_1) becomes first equal and then less than the rate of its growth due to reactions (4.3_1) and (4.3_2).

5.2.3. Effect of homogeneity ranges and inherent vacancies on layer-growth kinetics

Note that the existing kinetic descriptions of diffusional growth of boride layers (see, for example, [24, 25, 35, 79, 80]) are tacitly or explicitly based on an assumption of the existence of a rather wide range of homogeneity *HR* of appropriate borides, iron borides in particular. However, as follows from the available data on the phase equilibria in the binary system Fe–B [7-10] and the ternary system Fe–Cr–B [50], iron borides FeB and Fe_2B have no noticeable homogeneity range. Our experiments with Fe–Cr alloys and steels provide an additional proof for the validity of these observations.

Also, the concentration profiles of the elements within the growing layers are assumed to be close to linear (see, for example, Fig. 1 in [25]). In such a case, the parabolic layer growth-rate constant k_1 proves to be proportional to the diffusion coefficient D of a given component and the difference Δc in its concentration (content) at the interfaces of a growing compound layer: $k_1 \sim D\,\Delta c$. The latter is conventionally considered to be equal to the width of the homogeneity range *HR* of an appropriate compound: $\Delta c = HR$. If it were so, however, then the layers of compounds without any range of homogeneity would not grow at all that contradicts available experimental data.

Again, for compounds with a narrow range of homogeneity these descriptions yield the unrealistically high values of the diffusion coefficients because in the limit it means dividing by zero and hence $D \to \infty$, as $\Delta c \to 0$. From a physical viewpoint, such values are hardly possible.

In fact, however, the layer of any compound grows at the expense of stoichiometry of that compound and not at the expense of its range of homogeneity. The value of Δc is the difference in concentration of vacancies at layer interfaces (see [46-49]). It is necessary to distinguish between the newly-formed and native (equilibrium) vacancies. The newly-formed vacancies arise in the course of partial chemical reactions proceeding at layer interfaces. These are thus reaction-induced vacancies which do not exist in a given equilibrated compound. The native (inherent), mainly thermal, vacancies are present in the compound initially (in the equilibrium state), their amount being quite negligible by comparison, except perhaps at temperatures close to its melting point.

The concentration of newly-formed vacancies of a given component in a growing compound layer at its interface where a product-forming partial chemical reaction takes place is regarded to be numerically equal (with the opposite sign) to the content of this component in the compound, while that at another (non-reacting) interface zero (ideal case in which no native vacancies are available in the compound). Then, $k_1 = D$ if $\Delta c = HR = 0$.

Hence, the parabolic growth-rate constant k_1 is identified with the diffusion coefficient D of a given component in the lattice of a chemical compound. If $HR \neq 0$, $k_1 \approx D$, with the difference between k_1 and D decreasing, as *HR* tends to zero. In other words, the closer the compound to its stoichiometric composition, the more nearly k_1 approaches D. Thus, the two

assumptions made allow a self-consistent approach, excluding dividing by zero and yielding physically reasonable values of the diffusion coefficient D, to be developed.

It can be concluded that the effect of a homogeneity range on the layer-growth rate is relatively insignificant and by no means decisive. Moreover, it is negative. Its value may roughly be estimated quantitatively as $HR : c_{total}$, c_{total} being the content (concentration) of a given component in a chemical compound. If $HR = 0$, this effect is also zero. If $HR = 1\%$ and $c_{total} = 50\%$, its (negative) value is 2%. Note that in more exact calculations the values of HR and c_{total} must be expressed in mol m^3 and not in mass or atomic percent.

It must also be emphasized that, contrary to wide-spread and nonetheless misleading views (examples are too numerous to cite here, appropriate references can readily be found in [46-49]), the role of native point defects, such as vacancies of a given component, in the reaction-diffusion process of formation of any chemical compound, like boriding, carburizing, nitriding, metallization and others, is opposite to their role in the process of self-diffusion of that component in the compound taken as a separate phase. In the absence of complicating factors, the *higher* the amount of native vacancies, the *higher* is the rate of self-diffusion of the component in the separate phase. Contrary to this, the *higher* the amount of native vacancies, the *less* is the rate of growth of the compound layer in any reaction couple at the expense of diffusion of that component, *i.e*. the *less* is a value of the diffusional constant k_1.

From a chemical viewpoint, this conclusion appears to be quite understandable because unoccupied (empty) sites (vacancies) present initially can hardly take part in chemical reactions yielding material products. It is just available atoms, ions, molecules or radicals and not native vacancies that are responsible for the progress of any interfacial chemical reaction. The formation of any reaction product is a result of their joint efforts.

In the case of the reaction-diffusion process, it does not seem substantiated to make a relatively small amount of missing atoms, say one atom in every hundred atoms, responsible for its course and to consider a much greater amount of available atoms (99) as an inert mass. The actual role of this single missing atom can roughly be estimated as 100% with the plus sign in the self-diffusion process and as 1% with the minus sign in the reaction-diffusion one.

Thus, the layer of any chemical compound must generally be considered to grow at the expense of stoichiometry of that compound. Boride layers are no exception. For any compound layer to occur between initial substances capable of reacting chemically, it does not matter, whether or not a given compound has any range of homogeneity, structure deficiency, native vacancies or other imperfections (for more detailed considerations, see [46-49].

5.2.4. Late diffusional stage of layer growth

Growth kinetics of boride layers at the diffusional stage of their formation, usually observed in practice, are somewhat more complicated than merely parabolic and more adequately be described by a system of two differential equations

$$\frac{dx}{dt} = \frac{k_B}{x} - \frac{rg}{p}\frac{k_{Fe}}{y}, \qquad (5.6_1)$$

$$\frac{dy}{dt} = \frac{k_{Fe}}{y} - \frac{q}{sg}\frac{k_B}{x}, \qquad (5.6_2)$$

following from the system of equations (5.1) at high values of time and accordingly layer thicknesses. In such a case, unity can be neglected in comparison with the terms of the type $k_0 x/k_1$ and $k_0 y/k_1$. As the outer FeB layer grows at the expense of diffusion of boron atoms across its bulk and their subsequent reaction with the Fe_2B compound, while the inner Fe_2B layer grows at the expense of diffusion of iron atoms across its bulk and their subsequent reaction with the FeB compound, simplified designations of the growth-rate constants k_B and k_{Fe} are employed.

System of equations (5.6) describes the *diffusion controlled stage* of growth of boride layers when the rates of diffusion of iron and boron atoms across layer bulks are so small that their effect on the overall rates of formation of the layers prevails over that of the rates of subsequent chemical transformations taking place at phase interfaces. As the layers thicken with passing time, the effect of diffusion increases progressively, while that of chemical transformations decreases and eventually becomes negligible by comparison.

Experimental kinetic data for Fe–10% Cr, Fe–15% Cr, Fe–25% Cr and Fe–30% Cr alloys and a 13% Cr steel were treated using both parabolic relations and the system of equations (5.6). Plots of layer thickness (left) and squared layer thickness (right) against the time for boride layers formed at the interface of Fe–15% Cr and Fe–30% Cr alloys with boron at a temperature of 850–950 °C are presented in Fig. 5.2 and 5.3 as an example of typical dependences. Even though the boride layers have different types of microstructure, these dependences are similar.

Values of the derivatives dx/dt and dy/dt entering into the system of equations (5.6) were found from the experimental layer thickness-time dependences by the numerical three-point method. Calculations were carried out in a linear approximation using an Excel computer program (for more detail, see www.dybkov.kiev.ua). To find a derivative for a given experimental point, (x_i, t_i), like those on left-hand plots of Figs 5.2 and 5.3, data for its two neighboring points, (x_{i-1}, t_{i-1}) and (x_{i+1}, t_{i+1}), including the point $x_0 = 0$ at $t_0 = 0$, were used. Left-hand and right-hand derivatives, $(x_i - x_{i-1})/(t_i - t_{i-1})$ and $(x_{i+1} - x_i)/(t_{i+1} - t_i)$, were first found for this point and a mean value was then calculated. The derivatives could thus be found for all experimental points, excepting clearly the last one, for which a next neighboring point is lacking.

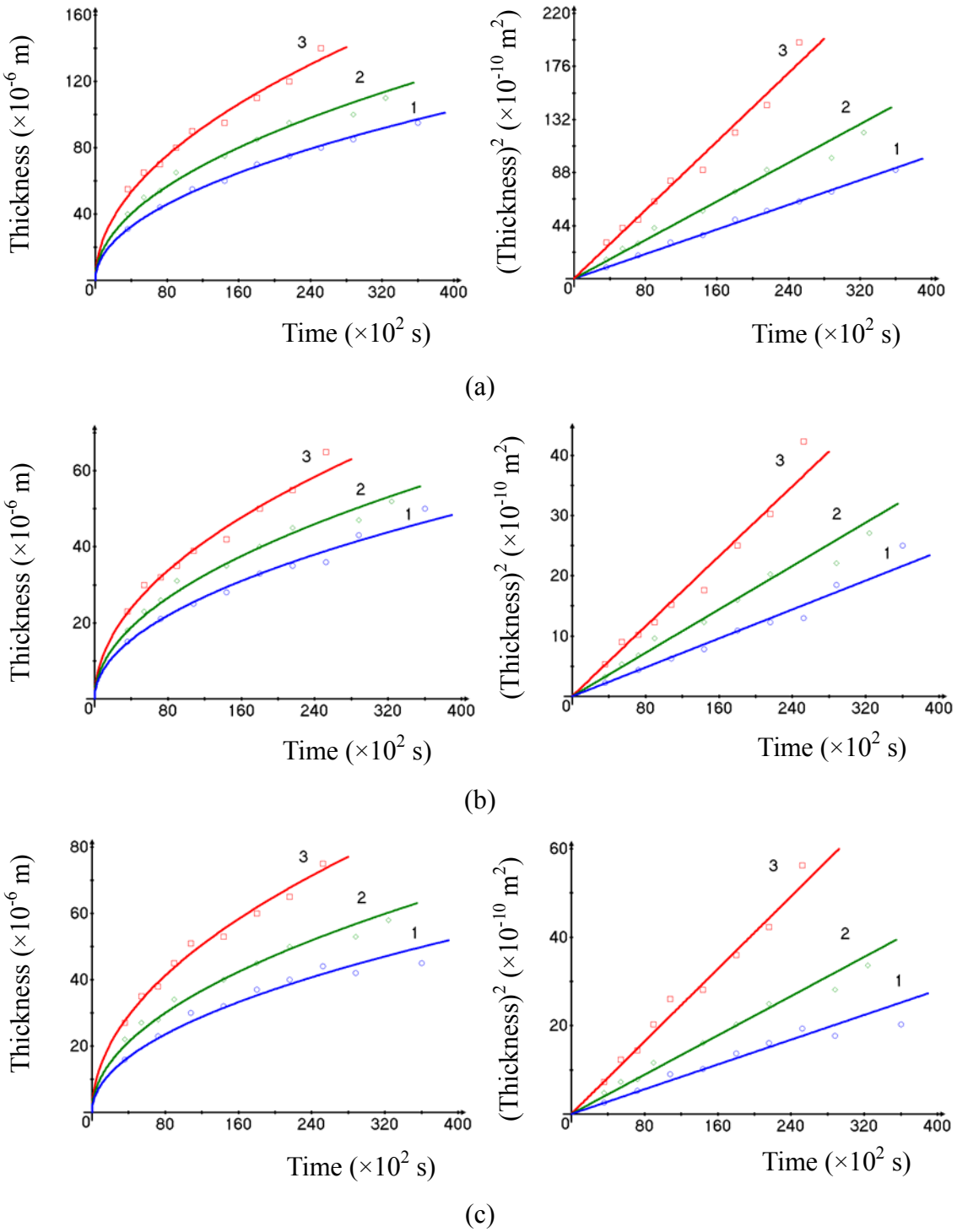

Fig. 5.2. Plots of layer thickness (left) and squared layer thickness (right) against time for (a) both boride layers, (b) the FeB layer and (c) the Fe_2B layer formed between a Fe–15% Cr alloy and boron at a temperature of 850 °C (1), 900 °C (2) and 950 °C (3).

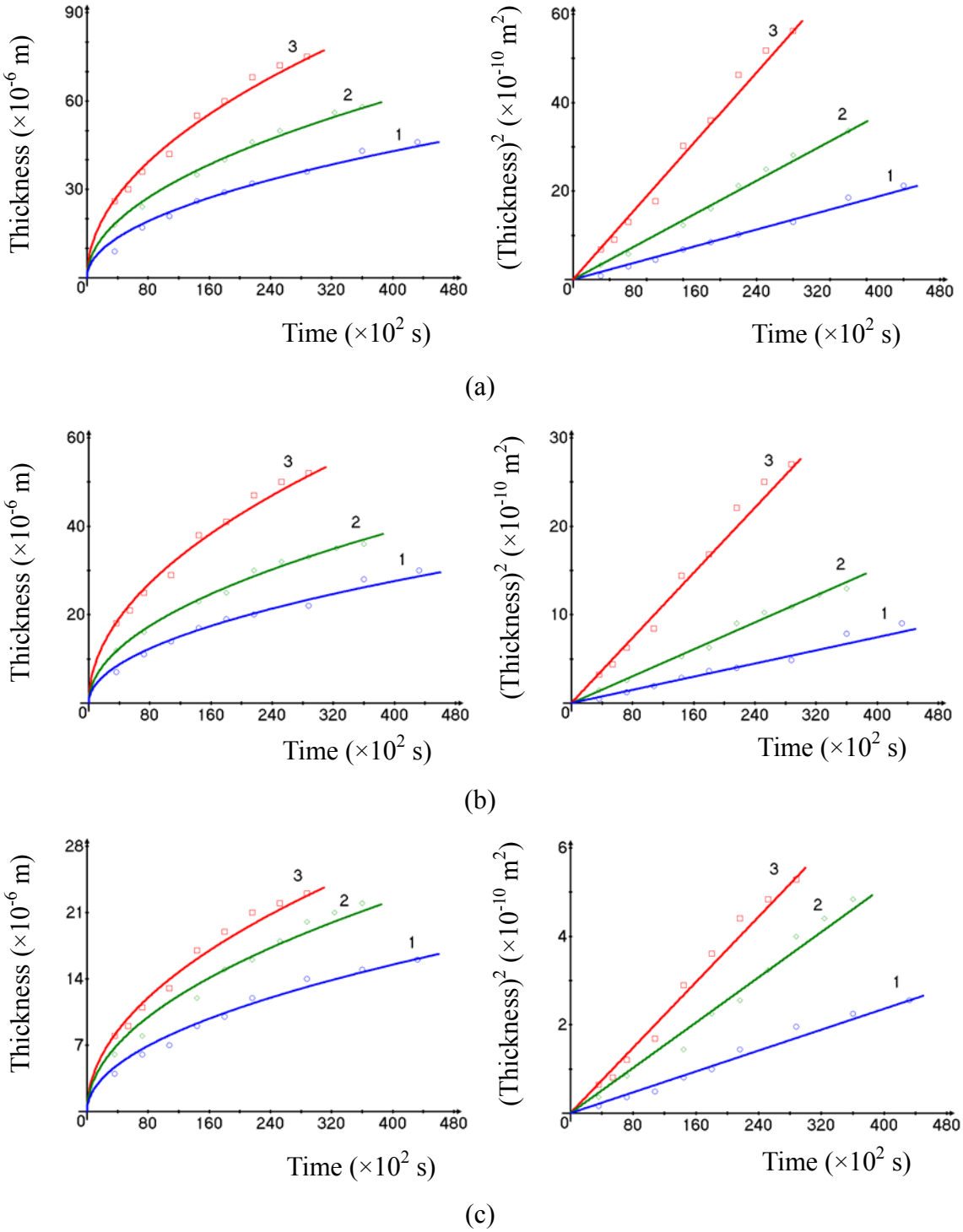

Fig. 5.3. Plots of layer thickness (left) and squared layer thickness (right) against time for (a) both boride layers, (b) the FeB layer and (c) the Fe_2B layer formed between a Fe–30% Cr alloy and boron at a temperature of 850 °C (1), 900 °C (2) and 950 °C (3).

The results of calculations for Fe–10% Cr, Fe–15% Cr, Fe–25% Cr and Fe–30% Cr alloys and a 13% Cr steel are provided in Tables 5.3-5.7 where the experimental layer thicknesses are also given. Average values of the growth-rate constants are summarized in Table 5.8.

The accuracy of calculations is strongly dependent upon a scatter of experimental points. To avoid this, preliminary approximation of the experimental data with any suitable analytical function is advisable. For example, application of parabolic relations to approximate the layer thickness-time dependences and then to find the derivatives yields another set of values of k_B and k_{Fe} also provided in Tables 5.3-5.8. Physically, k_B is the reaction-diffusion coefficient of boron atoms in the FeB layer, whereas k_{Fe} is the reaction-diffusion coefficient of iron atoms in the Fe_2B layer.

Comparing these with the average values of k_B and k_{Fe} found directly from the experimental points, it may be concluded that both sets of the constants agree fairly well, providing evidence for the validity of the analytical treatment employed. Note that, in order to avoid a large computational uncertainty and to obtain acceptable results, the optimum number of experimental points must generally be nine or more.

Temperature dependence of layer growth-rate constants K is described in the 850-950 °C range by a relation of the Arrhenius type. Plots of ln K against T^{-1} for Fe–15 % Cr and Fe–30 % Cr alloys having different types of microstructure are shown in Figs 5.4 and 5.5 as examples. Values of the pre-exponential factor K_0 and the activation energy E found by the least-squares fit method are listed in Table 5.9.

These are typical of diffusion-controlled processes [44-49, 81, 82] and can be used in practice to evaluate the values of growth-rate constants of boride layers at intermediate temperatures. In view of the rather limited number of Fe–Cr alloys investigated, it was hardly possible to establish any correlation between their chromium content and the value of the activation energy.

With a 25% Cr steel, kinetic data were treated using only parabolic equations and the values of the total thickness of both layers because the thickness of each of them could hardly be measured separately with a sufficient accuracy due to their extreme irregularity. In this case, the value of the diffusional constant k_1 was found to be 0.72×10^{-14} m^2 s^{-1} at 850 °C, 1.36×10^{-14} m^2 s^{-1} at 900 °C and 2.40×10^{-14} m^2 s^{-1} at 950 °C.

These constants can be employed to estimate the boride layer thickness at intermediate values of time. For the total thickness of both boride layers formed on the surface of 25% Cr steel samples, the Arrhenius-type equation is

$$k_1 = 1.72\times10^{-8}\ \exp(-137.1\ \text{kJ mol}^{-1}/RT)\ \text{m}^2\ \text{s}^{-1}.$$

A plot of ln k_1 against T^{-1} for this steel is provided in Fig. 5.6. It is seen to be similar to that of Fig. 5.1 exhibiting the temperature dependence of the growth-rate constant of the Fe_2B layer in the absence of the FeB layer from the Fe–5% Cr alloy-boron interface.

Table 5.3. Thickness and growth-rate constants of boride layers formed at the Fe–10% Cr alloy-boron interface.

Temperature (°C)	Time ($\times 10^2$ s)	Layer thickness ($\times 10^{-6}$ m)			k_1 ($\times 10^{-14}$ m^2 s^{-1}) from the equation $x^2 = 2k_1t$			k ($\times 10^{-14}$ m^2 s^{-1}) from the system of equations (5.6)	
		total	FeB	Fe_2B	total	FeB	Fe_2B	k_B	k_{Fe}
850	36	38	17	21	20.0	4.0	6.1	20.6	31.1
	72	50	23	27	17.4	3.7	5.1	16.5	24.1
	108	65	30	35	19.5	4.0	5.7	18.9	27.1
	144	80	35	45	22.2	4.2	7.0	14.7	23.2
	180	85	38	47	20.1	4.0	6.1	9.25	11.5
	216	90	42	48	18.8	4.1	5.3	14.2	18.1
	288	110	50	60	21.0	4.3	6.3	23.0	30.0
	360	120	55	65	20.0	4.2	5.9	14.4	16.5
	432	130	60	70	19.6	4.2	5.7	-	-
900	36	45	Absent	45	28.1	-	-	-	-
	72	65	30	35	29.3	6.3	8.5	30.3	42.7
	108	80	35	45	29.6	5.7	9.4	18.4	29.0
	144	95	40	50	31.3	5.6	8.7	23.2	31.1
	180	105	50	55	30.6	6.9	8.4	29.1	34.2
	216	115	55	60	30.6	7.0	8.3	24.3	30.4
	252	125	60	65	31.0	7.1	8.4	26.6	32.9
	288	135	65	70	31.6	7.3	8.5	24.3	31.4
	360	150	70	80	31.3	6.8	8.9	-	-
950	36	70	Absent	70	68.1	-	-	-	-
	54	85	35	50	66.9	11.3	23.1	72.9	124.0
	72	105	45	60	76.6	14.1	25.0	50.3	75.7
	90	110	48	62	67.2	12.8	21.4	47.8	59.9
	108	125	60	65	72.3	16.7	19.6	72.4	79.5
	126	135	65	70	72.3	16.8	19.4	68.3	90.3
	144	150	70	80	78.1	17.0	22.2	58.1	82.9
	180	160	75	85	71.1	15.6	20.1	60.2	74.3
	216	185	90	95	79.2	18.8	20.9	-	-

Table 5.4. Thickness and growth-rate constants of boride layers formed at the Fe–15% Cr alloy-boron interface.

Temperature (°C)	Time ($\times 10^2$ s)	Layer thickness ($\times 10^{-6}$ m)			k_1 ($\times 10^{-14}$ m^2 s^{-1}) from the equation $x^2 = 2k_1t$			k ($\times 10^{-14}$ m^2 s^{-1}) from the system of equations (5.6)	
		total	FeB	Fe_2B	total	FeB	Fe_2B	k_B	k_{Fe}
850	36	31	15	16	13.3	3.1	3.6	18.4	25.0
	72	44	21	23	13.4	3.1	3.7	16.3	24.4
	108	55	25	30	14.0	2.9	4.2	8.58	12.3
	144	60	28	32	12.5	2.7	3.6	9.45	12.1
	180	70	33	37	13.6	3.0	3.8	10.8	14.1
	216	75	35	40	13.0	2.8	3.7	5.81	8.29
	252	80	36	44	12.7	2.6	3.8	8.57	9.30
	288	85	43	42	12.5	3.2	3.1	12.8	10.7
	360	95	50	45	12.5	3.5	2.8	-	-
900	36	40	18	22	22.2	4.5	6.7	22.0	30.6
	54	50	23	27	23.1	4.9	6.8	12.5	14.4
	72	54	26	28	20.3	5.1	5.4	14.5	15.7
	90	65	31	34	23.5	5.3	6.4	17.0	21.2
	144	75	35	40	19.5	4.3	5.6	13.8	19.2
	180	85	40	45	20.1	4.4	5.6	16.0	19.7
	216	95	45	50	20.9	4.7	5.8	10.5	12.4
	288	100	47	53	17.4	3.8	5.2	10.9	13.2
	324	110	52	58	18.7	4.2	5.2	-	-
950	36	55	23	27	34.7	7.3	10.1	50.3	75.2
	54	65	30	35	39.1	8.3	11.3	24.4	32.9
	72	70	32	38	34.0	7.1	10.0	14.2	19.2
	90	80	35	45	35.6	6.8	11.3	21.1	30.7
	108	90	39	51	37.5	7.0	12.0	17.0	24.2
	144	95	42	53	31.3	6.1	9.7	19.1	26.6
	180	110	50	60	33.6	7.0	10.0	25.9	33.7
	216	120	55	65	33.3	7.0	9.8	29.7	35.9
	252	140	65	75	38.9	8.4	11.2	-	-

Table 5.5. Thickness and growth-rate constants of boride layers formed at the Fe–25% Cr alloy-boron interface.

Temperature (°C)	Time ($\times 10^2$ s)	Layer thickness ($\times 10^{-6}$ m)			k_1 ($\times 10^{-14}$ m^2 s^{-1}) from the equation $x^2 = 2k_1t$			k ($\times 10^{-14}$ m^2 s^{-1}) from the system of equations (5.6)	
		total	FeB	Fe_2B	total	FeB	Fe_2B	k_B	k_{Fe}
850	36	19	10	9	5.0	1.4	1.1	7.80	8.58
	72	28	15	13	5.1	1.6	1.2	7.06	7.78
	108	33	18	15	5.0	1.5	1.0	5.18	4.42
	144	40	23	17	5.5	1.8	1.0	6.36	5.08
	180	45	25	20	5.6	1.7	1.1	5.53	5.06
	216	50	28	22	5.7	1.8	1.1	4.73	4.15
	288	55	30	25	5.3	1.6	1.1	3.32	3.16
	360	60	33	27	5.0	1.5	1.0	3.65	3.42
	432	65	35	30	5.7	1.4	1.0	-	-
900	36	25	15	10	8.7	3.1	1.4	12.0	8.74
	72	35	20	15	8.5	2.8	1.6	8.85	7.59
	108	45	25	20	9.4	2.9	1.9	8.16	7.64
	144	50	27	23	6.9	2.5	1.8	9.71	8.46
	180	60	35	25	8.3	3.4	1.7	13.0	9.08
	216	65	38	27	9.8	3.3	1.7	9.04	6.64
	288	75	45	30	9.8	3.5	1.7	9.96	7.59
	360	80	48	37	8.9	3.2	1.9	7.30	7.24
	432	90	50	40	9.4	2.9	1.9	-	-
950	18	23	13	10	14.6	4.7	2.8	20.9	17.5
	36	35	20	15	17.0	5.6	3.1	18.3	14.5
	72	50	30	20	17.4	6.2	2.8	14.3	9.84
	108	55	33	22	14.0	5.0	2.2	10.0	8.61
	144	65	35	30	14.7	4.3	3.1	14.3	15.6
	180	75	40	35	15.6	4.4	3.4	13.5	13.2
	216	80	43	37	14.8	4.2	3.2	15.0	13.8
	288	100	55	45	17.4	5.3	3.5	18.9	16.9
	360	110	60	50	16.8	5.0	3.5	6.64	6.33
	432	125	70	55	18.1	5.7	3.5	-	-

Table 5.6. Thickness and growth-rate constants of boride layers formed at the Fe–30% Cr alloy-boron interface.

Temperature (°C)	Time ($\times 10^2$ s)	Layer thickness ($\times 10^{-6}$ m)			k_1 ($\times 10^{-14}$ m^2 s^{-1}) from the equation $x^2 = 2k_1t$			k ($\times 10^{-14}$ m^2 s^{-1}) from the system of equations (5.6)	
		total	FeB	Fe_2B	total	FeB	Fe_2B	k_B	k_{Fe}
850	36	9	7	4	1.68	0.68	0.22	3.29	2.12
	72	17	11	6	2.00	0.84	0.25	3.41	2.13
	108	21	14	7	2.04	0.91	0.19	3.02	1.55
	144	26	17	9	2.34	1.00	0.28	3.20	1.78
	180	29	19	10	2.34	1.00	0.28	2.52	1.52
	216	32	20	12	2.37	0.93	0.33	2.10	1.55
	288	36	22	14	2.25	0.84	0.34	2.98	1.87
	360	43	28	15	2.57	1.09	0.21	3.56	1.79
	432	46	30	16	2.45	1.04	0.30	-	-
900	36	18	12	6	4.50	2.00	0.50	6.91	3.53
	72	24	16	8	4.00	1.78	0.44	4.91	2.71
	144	35	23	12	4.25	1.84	0.50	6.17	3.84
	180	40	25	15	4.44	1.74	0.52	6.50	4.07
	216	46	30	16	4.90	2.08	0.59	7.30	3.90
	252	50	32	18	4.96	2.03	0.64	4.25	2.73
	288	53	33	20	4.88	1.89	0.69	3.56	2.21
	324	56	35	21	4.83	1.89	0.68	3.49	2.03
	360	58	36	22	4,67	1.80	0.67	-	-
950	36	26	18	8	9.39	4.50	0.89	17.3	8.39
	54	30	21	9	8.33	4.08	0.75	9.53	3.89
	72	36	25	11	9.00	4.34	0.84	9.96	4.25
	108	42	29	13	8.17	3.89	0.78	13.3	6.04
	144	55	38	17	10.5	5.01	1.00	16.4	7.51
	180	60	41	19	10.0	4.67	1.00	12.9	6.03
	216	68	47	21	10.7	5.11	1.02	13.7	5.79
	252	72	50	22	10.2	4.96	0.96	7.75	3.13
	288	75	52	23	9.77	4.69	0.92	-	-

Table 5.7. Thickness and growth-rate constants of boride layers formed at the 13% Cr steel-boron interface.

Temperature (°C)	Time ($\times 10^2$ s)	Layer thickness ($\times 10^{-6}$ m)			k_1 ($\times 10^{-14}$ m^2 s^{-1}) from the equation $x^2 = 2k_1t$			k ($\times 10^{-14}$ m^2 s^{-1}) from the system of equations (5.6)	
		total	FeB	Fe_2B	total	FeB	Fe_2B	k_B	k_{Fe}
850	36	25	12	13	8.7	2.0	2.3	11.6	16.3
	72	35	15	20	8.5	1.6	2.8	8.51	16.4
	144	50	20	30	8.7	1.4	3.1	5.26	9.67
	216	60	25	35	8.3	1.5	2.8	5.26	9.03
	288	70	28	42	8.5	1.4	3.1	5.73	10.9
	324	75	30	45	8.7	1.4	3.1	6.64	11.4
	360	80	33	47	8.9	1.5	3.1	7.30	11.9
	396	85	35	50	9.1	1.5	3.2	8.52	12.2
	432	90	40	50	9.4	1.9	2.9	-	-
900	36	35	17	18	17.0	4.0	4.5	18.4	23.0
	72	50	23	27	17.4	3.7	5.1	11.6	17.7
	108	60	25	35	16.7	2.9	5.7	10.2	18.2
	144	70	30	40	17.0	3.1	5.6	13.3	20.3
	180	80	35	45	17.8	3.4	5.6	15.5	22.8
	216	90	40	50	18.8	3.7	5.8	17.7	25.3
	252	100	45	55	17.4	3.5	5.3	19.9	27.8
	288	110	50	60	16.8	3.5	5.0	16.6	22.8
	360	120	55	65	16.7	3.5	4.9	-	-
950	36	45	20	25	28.1	5.6	8.7	28.2	41.4
	72	65	30	35	29.3	6.3	8.5	22.4	31.4
	108	80	35	45	29.6	5.7	9.3	18.4	29.0
	144	90	40	50	28.1	5.6	8.7	17.7	25.3
	180	100	45	55	27.8	5.6	8.4	19.9	27.8
	216	110	50	60	28.0	5.8	8.3	20.1	26.2
	288	125	60	65	27.1	6.3	7.3	19.9	24.7
	360	140	65	75	27.2	5.9	7.8	9.89	14.7
	432	155	75	80	27.8	6.5	7.4	-	-

Table 5.8. Average values of layer growth-rate constants of Fe–Cr alloys (10–30% Cr) and a 13% steel.

Alloy or steel	Temperature (°C)	k_1 ($\times 10^{-14}$ m^2 s^{-1}) from the equation $x^2 = 2k_1t$			k ($\times 10^{-14}$ m^2 s^{-1}) from the system of equations (5.6) using experimental points		k ($\times 10^{-14}$ m^2 s^{-1}) from the system of equations (5.6) using approximated thickness-time dependences	
		total	FeB	Fe_2B	k_B	k_{Fe}	k_B	k_{Fe}
10 % Cr alloy	850	19.8	4.1	5.9	16.4	22.7	14.0	19.9
	900	30.4	6.6	8.6	25.2	33.1	22.2	29.6
	950	72.4	15.4	21.4	61.4	83.7	52.4	72.6
15 % Cr alloy	850	13.1	2.9	3.6	11.3	14.5	9.64	12.5
	900	20.6	4.6	5.9	14.7	18.3	15.4	20.4
	950	35.3	7.2	10.6	22.4	30.9	24.8	35.6
25 % Cr alloy	850	5.3	1.6	1.1	5.45	5.21	4.77	4.38
	900	8.9	3.1	1.7	9.76	7.88	8.92	7.18
	950	16.0	5.0	3.1	14.6	12.9	14.7	12.7
30 % Cr alloy	850	2.23	0.93	0.27	3.01	1.79	2.45	1.37
	900	4.60	1.90	0.58	5.39	3.13	5.04	2.89
	950	9.56	4.58	0.82	11.2	5.00	11.4	4.84
13 % Cr steel	850	8.8	1.6	3.0	7.35	12.2	5.81	9.60
	900	17.3	3.5	5.3	15.4	22.2	12.1	17.7
	950	28.1	5.9	8.3	19.6	27.6	20.1	28.1

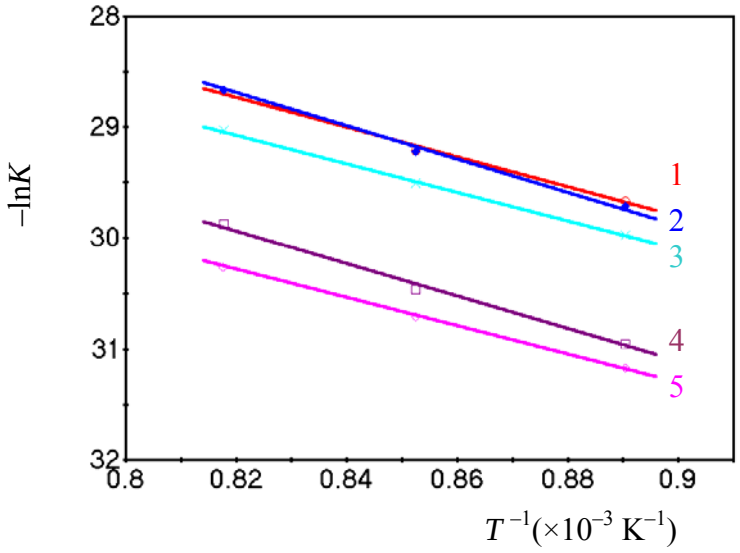

Fig. 5.4. Temperature dependence of the layer growth-rate constants K for a Fe–15% Cr alloy: 1, k_1 from the equation $x^2 = 2k_1t$ for both boride layers; 2, k_{Fe} from the system of equations (5.6); 3, k_B; 4, k_1 for the Fe_2B layer; 5, k_1 for the FeB layer.

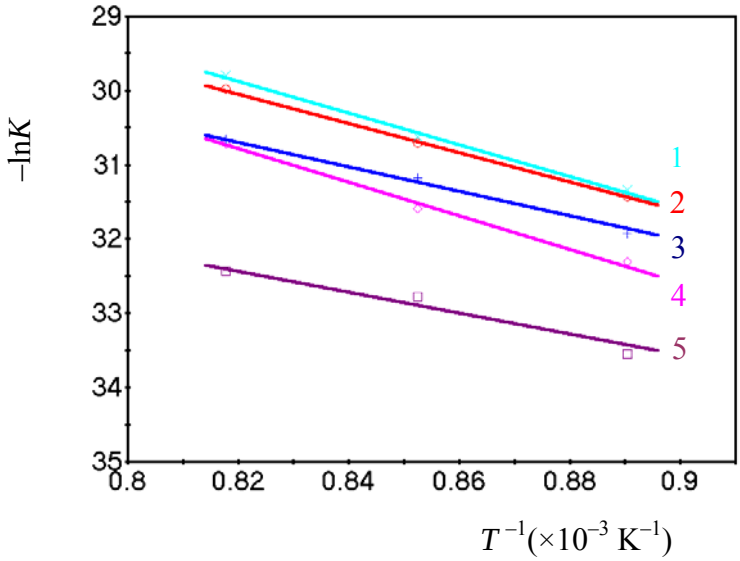

Fig. 5.5. Temperature dependence of the layer growth-rate constants K for a Fe–30% Cr alloy: 1 , k_B from the system of equations (5.6); 2 , k_1 from the equation $x^2 = 2k_1t$ for both boride layers; 3 , k_{Fe} ; 4, k_1 for the FeB layer; 5, k_1 for the Fe_2B layer.

Table 5.9. Values of K_0 and E of a relation of the Arrhenius type $K = K_0 \exp(-E/RT)$, where K stands for any layer growth-rate constant, K_0 is the pre-exponential factor, E is the activation energy, R is the gas constant (8.314 J mol^{-1} K^{-1}) and T is the absolute temperature, describing the temperature dependence of growth-rate constants of boride layers (K_0 is expressed in m^2 s^{-1}, E in kJ mol^{-1}).

Alloy or steel	k_1						k_B		k_{Fe}	
	Total		FeB		Fe_2B					
	K_0	E	K_0	E	K_0	E	K_0	E	K_0	E
10% Cr alloy	12.8 $\times10^{-7}$	147.2	3.78 $\times10^{-7}$	150.5	3.34 $\times10^{-7}$	146.1	12.2 $\times10^{-7}$	149.9	12.3 $\times10^{-7}$	146.8
15% Cr alloy	2.32 $\times10^{-8}$	113.0	1.95 $\times10^{-9}$	103.8	1.88 $\times10^{-8}$	123.1	1.00 $\times10^{-8}$	107.9	4.38 $\times10^{-8}$	119.4
25% Cr alloy	3.78 $\times10^{-8}$	126.0	1.91 $\times10^{-8}$	130.5	3.27 $\times10^{-9}$	118.0	4.70 $\times10^{-8}$	128.8	1.90 $\times10^{-8}$	121.4
30% Cr alloy	1.18 $\times10^{-8}$	166.2	2.53 $\times10^{-8}$	181.7	2.48 $\times10^{-9}$	127.7	3.42 $\times10^{-8}$	175.4	7.45 $\times10^{-9}$	144.6
13% Cr steel	1.37 $\times10^{-8}$	132.9	1.49 $\times10^{-7}$	149.5	7.90 $\times10^{-9}$	116.4	2.44 $\times10^{-7}$	142.2	5.09 $\times10^{-8}$	122.9

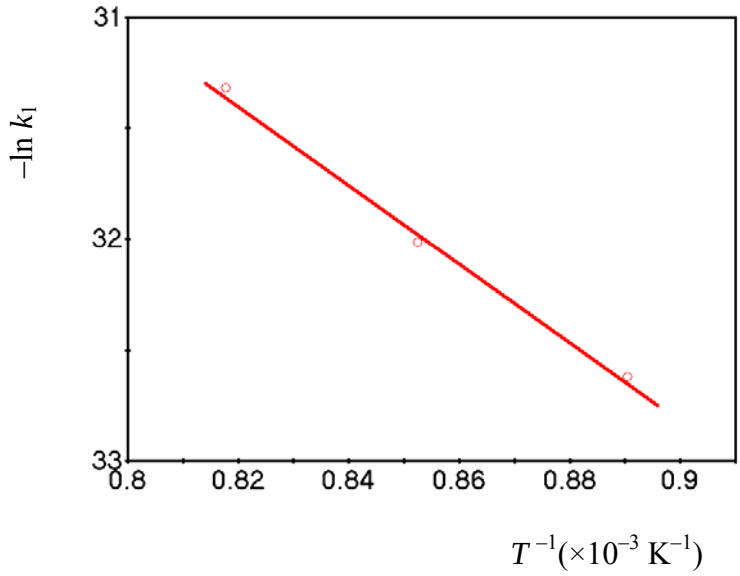

Fig. 5.6. Temperature dependence of the layer growth-rate constant calculated using the total thickness of both boride layers formed on the surface of 25% Cr steel samples.

5.3. Degradation of boride layers at their heat treatment in the absence of boron

Heat treatment of an as-received borided Fe–10% Cr alloy sample (Fig. 5.7a) in the absence of boriding media (a mixture of boron powder and KBF_4) results in a decrease of the thickness of the FeB layer and an appropriate increase of the thickness of the Fe_2B layer. As seen in Fig. 5.7b, 21600 s (6 h) holding at 950 °C causes the full disappearance of the FeB layer, about 90 μm thick initially. Further heat treatment of this sample leads to gradual disintegration of the Fe_2B layer into separate grains. As evidenced in Fig. 5.7c, grain-boundary diffusion appears to play a significant, if not decisive, role in this process. Boride layers formed on the surface of 13% steel samples degrade (disintegrate) similarly but somewhat slower (Fig. 5.8). Some amount of the FeB phase in the form of separate grains remains even after 43200 s (12 h) holding (Fig. 5.8c).

Note that the FeB layer decomposes as a whole at the interface with the adjacent Fe_2B layer, with its compactness retaining and thickness decreasing, without any change of chemical composition. It is typical of compound layers with the microstructure of the fist type (a homogeneous phase without any homogeneity range) observed for Fe–Cr alloys (5–15% Cr) and a13% steel.

Boride layers with the microstructure of the second type (two-phase) behave somewhat differently, as illustrated in Fig. 5.9 for a borided Fe–25% Cr alloy sample. As seen in Fig. 5.9b and c, the FeB layer, initially compact and around 40 μm thick, disintegrates into separate grains during the heat treatment of this sample in vacuum at 950°C, and after 43200 s (12 h) holding disappears almost completely as a result of chemical reaction between iron and FeB to form more Fe_2B.

Micrographs of the transition zone between the reactants of borided Fe–10% Cr alloy, 13% steel and Fe–25% Cr alloy samples after their heat treatment at a temperature of 950 °C for 21600 s (6 h) in the absence of boriding media are presented in Fig.5.10 where the available phases are indicated for easy comparison. Figure 5.11 provides backscattered and secondary electron images (BEI and SEI) of the same area of the transition zone between the reactants of a borided Fe–10% Cr alloy sample after its heat treatment at a temperature of 950 °C for 21600 s (6 h) in the absence of boriding media. BEI visualizes the difference in chemical composition of the reacting phases, while SEI shows their relief.

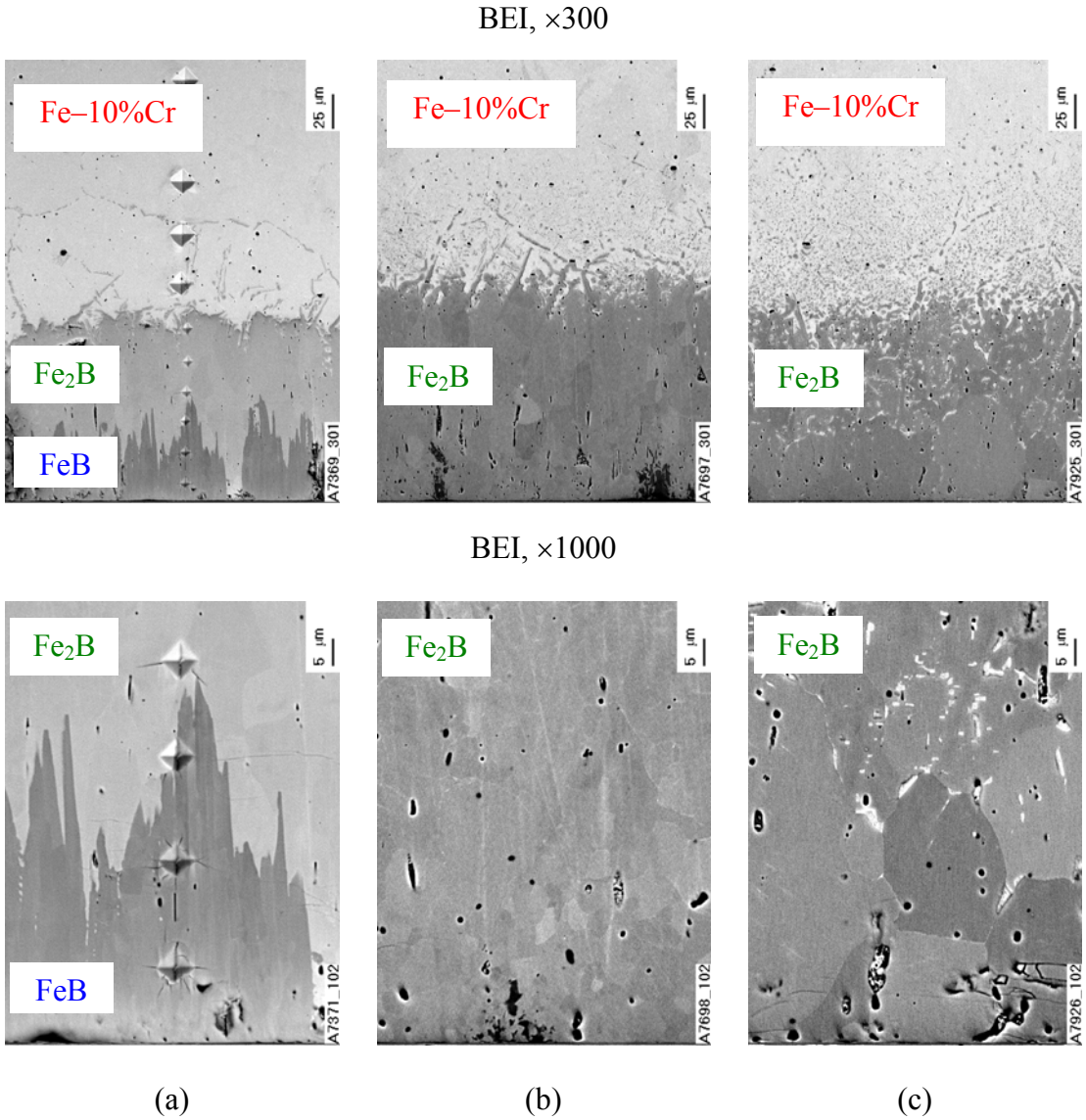

Fig. 5.7. Degradation of boride layers formed on the surface of a borided Fe–10% Cr alloy sample during its heat treatment at a temperature of 950 °C in the absence of boriding media: (a) as-received condition, (b) 21600 s (6 h) reaction time and (c) 43200 s (12 h) reaction time. BEI – backscattered electron image, magnifications ×300 and ×1000.

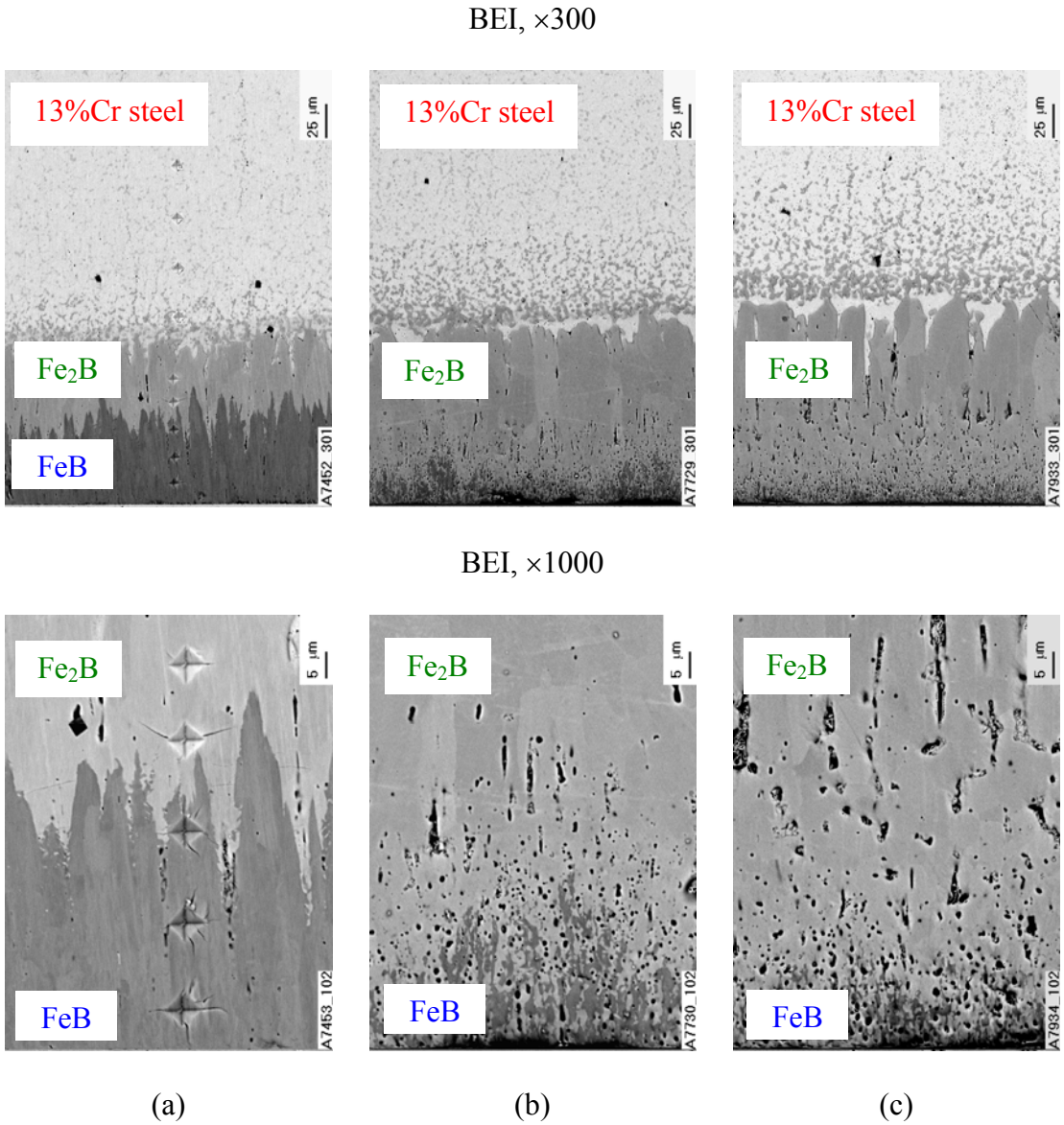

Fig. 5.8. Degradation of boride layers formed on the surface of a borided 13% Cr steel sample during its heat treatment at a temperature of 950 °C in the absence of boriding media: (a) as-received condition, (b) 21600 s (6 h) reaction time and (c) 43200 s (12 h) reaction time. BEI – backscattered electron image, magnifications ×300 and ×1000.

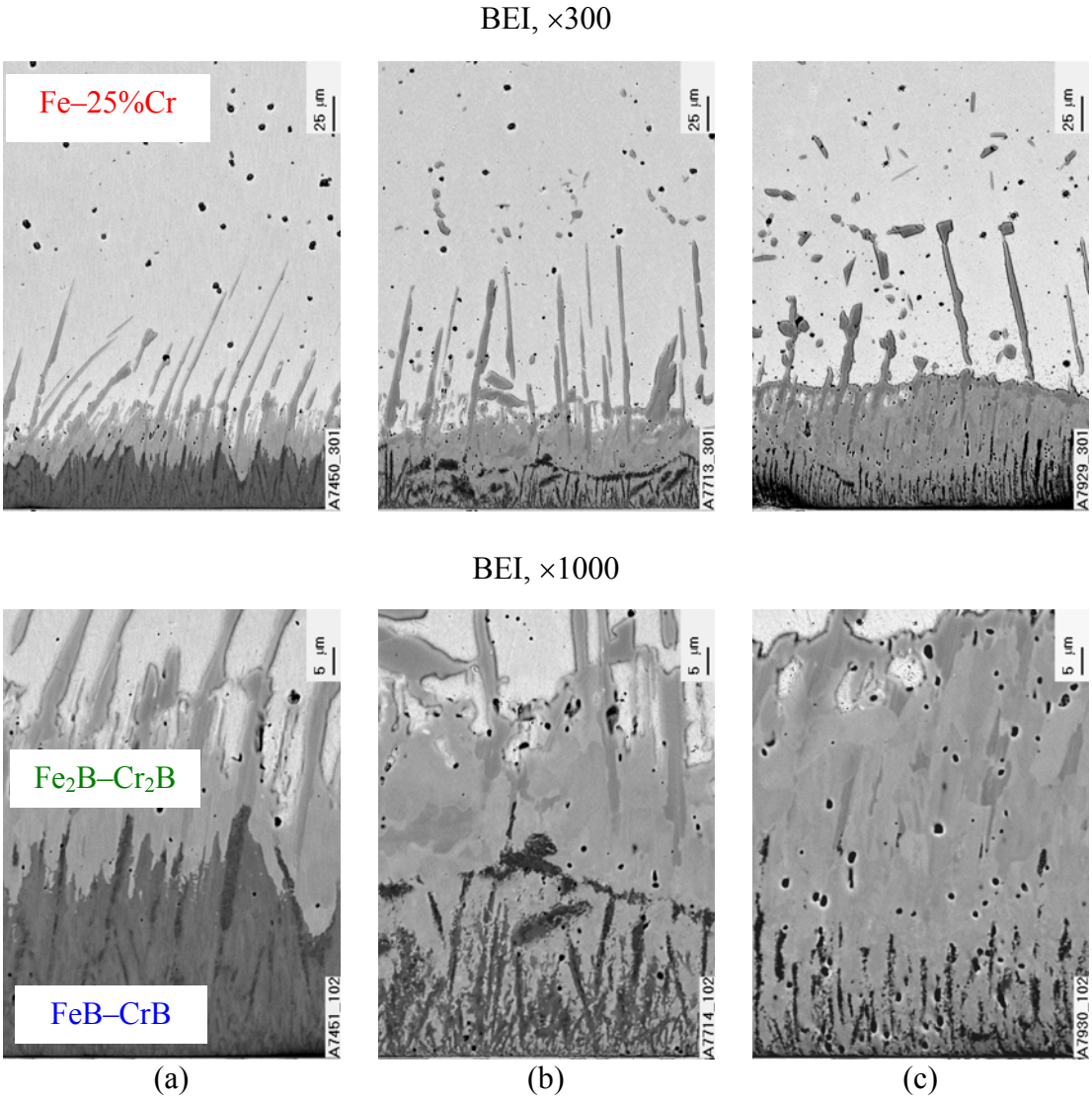

Fig. 5.9. Degradation of boride layers formed on the surface of a borided Fe–25%Cr alloy sample during its heat treatment at a temperature of 950 °C in the absence of boriding media: (a) as-received condition, (b) 21600 s (6 h) reaction time and (c) 43200 s (12 h) reaction time. The brighter phase of the Fe_2B–Cr_2B layer is Fe_2B, while the darker is Cr_2B. The brighter phase of the FeB–CrB layer is FeB, while the darker is CrB. BEI – backscattered electron image. Magnification: ×300 and ×1000.

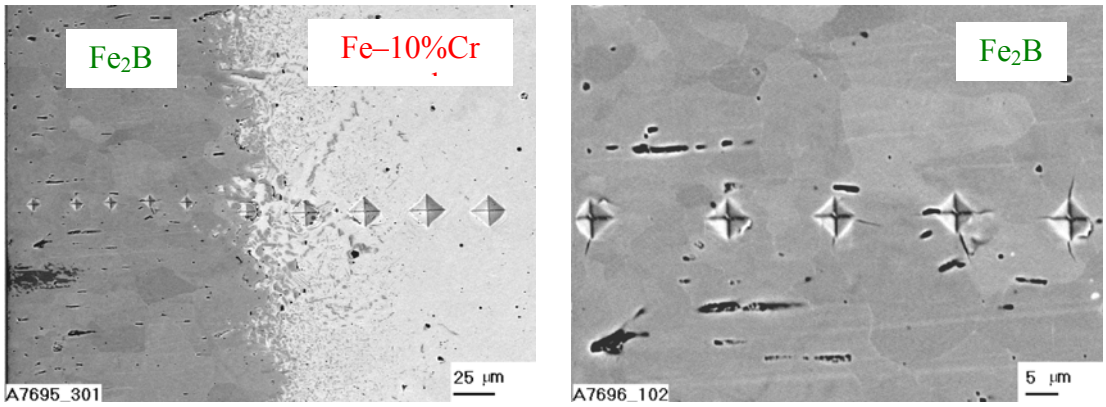

×300 ×1000

(a)

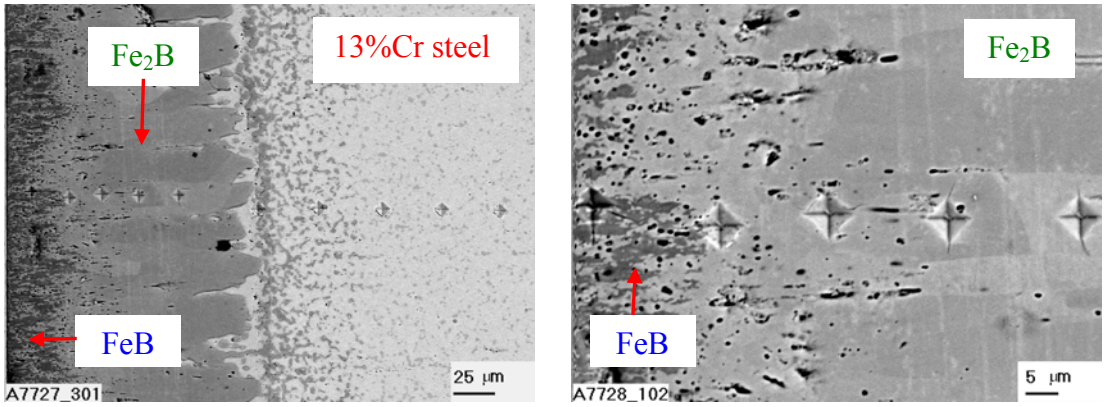

×300 ×1000

(b)

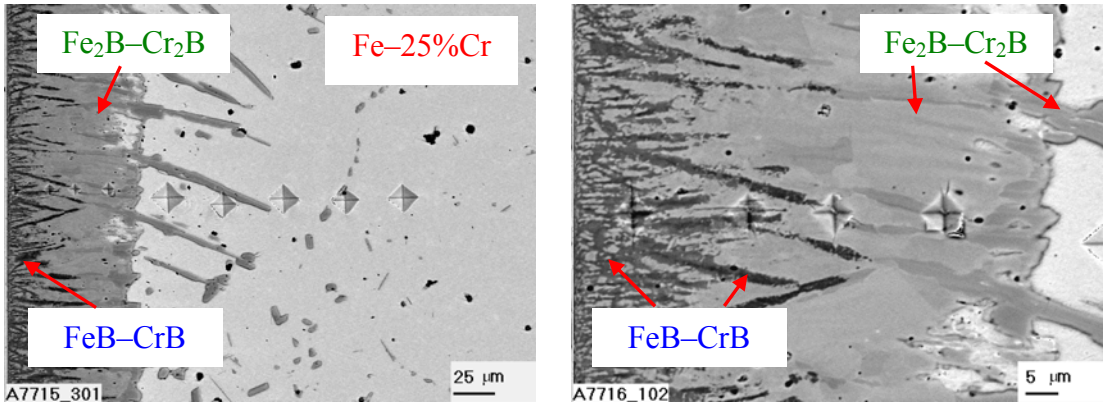

×300 ×1000

(c)

Fig. 5.10. Microstructure (BEI – backscattered electron images) of the transition zone between the reactants of borided (a) Fe–10% Cr alloy, (b) 13% steel and (c) Fe–25% Cr alloy samples after their heat treatment at a temperature of 950 °C for 21600 s (6 h) in the absence of boriding media. Magnifications ×300 and ×1000.

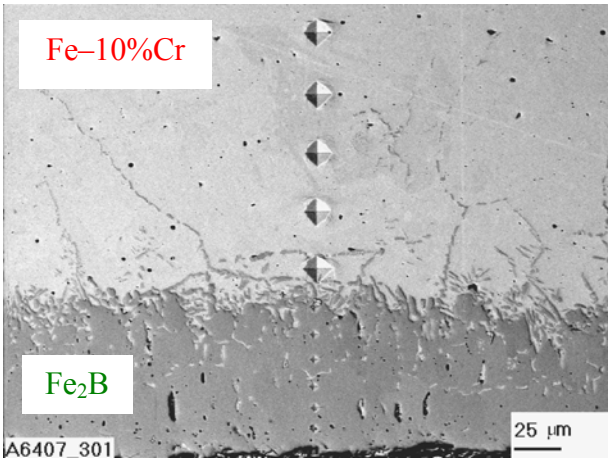

BEI

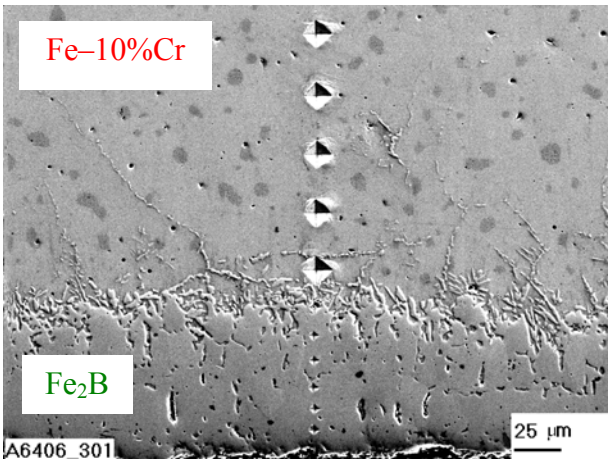

SEI

Fig. 5.11. Backscattered (BEI) and secondary (SEI) electron images of the same area of the transition zone between the reactants of a borided Fe–10% Cr alloy sample after its heat treatment at a temperature of 950 °C for 21600 s (6 h) in the absence of boriding media. The FeB layer disappeared completely as a result of chemical reaction between Fe and FeB to form more Fe_2B. Magnification ×300.

This kind of consumption is characteristic of non-homogeneous layers. The first phase to disappear is seen in Fig. 5.9b and c to be (Fe,Cr)B because the remaining crystals of the outer (Fe,Cr)B–(Cr,Fe)B layer are blackish. This is confirmed by EPMA measurements. The chemical composition of blackish crystals of the outer (Fe,Cr)B–(Cr,Fe)B layer in Fig. 5.9c is 50 ± 2 at.% B, 17 ± 3 at.% Fe and 33 ± 4 at.% Cr. Wherever remained between blackish crystals, the more light (Fe,Cr)B phase has a composition of 50 ± 2 at.% B, 35 ± 3 at.% Fe and 15 ± 3 at.% Cr. Darker crystals of the inner $(Fe,Cr)_2B$–$(Cr,Fe)_2B$ layer have a composition of 33 ± 2 at.% B, 22 ± 5 at.% Fe and 45 ± 5 at.% Cr. Brighter crystals of this layer contain 33 ± 2 at.% B, 25 ± 3 at.% Cr and 42 ± 3 at.% Fe.

It should be noted that elongated crystals of the $(Cr,Fe)_2B$ phase penetrating deep into the Fe–25%Cr alloy base actually do not grow in the absence of boriding media. The boron atoms released according to the reaction $2FeB = Fe_2B + B_{dif}$ at the interface between two boride layers, then diffuse across the Fe_2B layer and react with iron from the alloy base by the reaction $B_{dif} + 2Fe = Fe_2B$ to form more Fe_2B at the Fe_2B-alloy interface. The thinner the Fe_2B layer at a certain place, the shorter is the diffusion path and hence the higher is the supply of diffusing boron atoms to that place. Therefore, at thinner places the growth rate of the Fe_2B layer is higher than at thicker ones. As a result, the Fe_2B-alloy interface flattens with passing time, as evidenced in Fig. 5.9b and c.

These experiments clearly show the essential, if not decisive, role of diffusion of a gaseous boron-containing phase, probably BF_3 [1, 43], in the course of boriding of Fe–Cr alloy and steel samples in a mixture of boron powder and KBF_4 under reduced pressure. Defects of a certain kind and probably some solid-state transformation in the alloy base, providing the paths of rapid diffusion for the gaseous boriding agent, are responsible for the deep penetration of the $(Cr,Fe)_2B$ crystals into the sample bulk. It can hardly be solely a result of peculiarities of the crystal structure of iron and chromium borides, as is usually explained [1]. The regular arrangement of the constituting phases in both boride layers provides evidence for an additional solid-state transformation. It may either take place simultaneously with the layer growth or precede or follow it. This transformation may be closely connected with the occurrence of hot cracks that boron (> 0.007%) is known to cause in steels at elevated temperatures [83].

6. Microhardness and abrasive wear resistance of boride layers

6.1. Microhardness of boride phases

Plots of microhardness against distance across the reacting phases for Fe–10% Cr and Fe–30% Cr alloys are shown in Fig. 6.1 and 6.2 as examples for alloys with two different types of microstructure. Numerical values of microhardness HV_{100} for all alloys and steels investigated are presented in Table 6.1. Microhardness was found to vary considerably within both boride layers, especially those with the second type of microstructure in view of their non-homogeneity. The difference in microhardness of near-boride and far-away regions of the alloys or steels was insignificant (around 0.2 GPa).

For steels, the values obtained are close to those reported in the literature [1]. Somewhat higher values for Fe–25% Cr and Fe–30 % Cr alloys compared to Fe–5% Cr, Fe–10% Cr and Fe–15 % Cr alloys are probably due to the difference in their microstructures, the two-phase microstructure being more rigid and therefore harder than the single-phase homogeneous one.

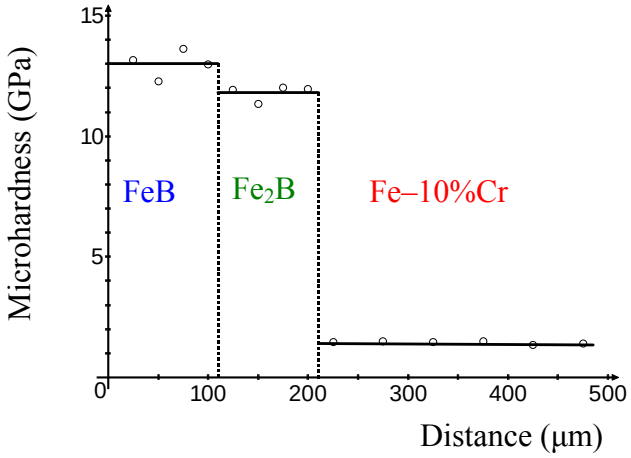

Fig. 6.1. A plot of microhardness HV_{100} against distance within reacting phases for a Fe–10% Cr alloy. Boriding conditions: temperature 950 °C, reaction time 21600 s (6 h).

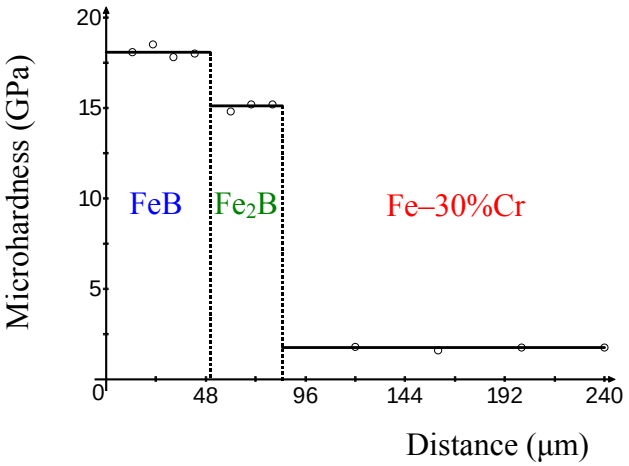

Fig. 6.2. A plot of microhardness HV_{100} against distance within reacting phases for a Fe–30% Cr alloy. Boriding conditions: temperature 950 °C, reaction time 28800 s (8 h).

Table 6.1. Microhardness (GPa) of boride layers, iron-chromium alloys and steels

Alloy or steel	FeB	Fe_2B	Base
5% Cr alloy	15.6	13.0	0.87
10% Cr alloy	13.0	11.8	0.95
15% Cr alloy	17.4	14.4	1.30
25% Cr alloy	21.0	18.0	1.35
30% Cr alloy	19.1	16.2	1.75
13% Cr steel	17.9	16.1	5.9
25% Cr steel	17.8	15.9	1.70

6.2. Dry abrasive wear resistance of boride layers

Boriding the alloy and steel tablets for dry abrasive wear resistance tests was carried out at 950°C for 21600 s (6 h). The data obtained for borided Fe–10% Cr and Fe–25% Cr alloy 13% Cr steel samples are presented in Tables 6.2-6.4 as an example. Wear resistance values are seen to be greater for the middle part of the layers than for their borders with adjacent phases due to its more developed texture and more ordered microstructure.

Comparative data on the wear resistance of the outer boride layer for the alloys and steels investigated are provided in Table 6.5. Its values proved to increase disproportionately with increasing chromium content of the alloys and steels. Borided materials with the layers of type I microstructure consisting of a homogeneous solid solution of chromium in the FeB compound or in the Fe_2B compound exhibit a rather moderate increase in wear resistance compared to their bases. As seen from Tables 6.2 and 6.3 it is 5-15 times for a Fe–10% Cr alloy and 6-27 times for a 13% Cr steel. A much greater increase is observed if the boride layers with a microstructure of type II are formed. Table 6.4 indicates that for a Fe–25% Cr alloy it varies from 150 to 350 times. Boride layers with a microstructure of type II are so wear resistant that it is impossible to reach not only the alloy or steel base but even the inner layer by carrying out a reasonable number of tests. For this reason, comparison of the wear resistance values in Table 6.5 is restricted to the data for the outer boride layers.

In boride layers with type II microstructure, the (Cr,Fe)B phase (thin platelets, less than 100 nm thick) forms a rigid framework filled with the (Fe,Cr)B phase. Such network-platelet morphology results in enhanced wear resistance of the outer boride layer. The same applies to the inner boride layer consisting of $(Cr,Fe)_2B$ platelets embedded into the $(Fe,Cr)_2B$ matrix.

Table 6.2. Results of abrasive wear resistance tests of borided Fe–10% Cr alloy samples. Three consecutive tests were carried out on each of the samples until the alloy base was reached. Wear resistance of a non-borided sample (n/b) is given in the last line of the table for comparison. Boriding conditions: temperature 950 °C, reaction time 21600 s (6 h).

Borided sample number	Test number	Δm (g)	r	Δh (mm)	Phase
1	1	0.03470	11.4	0.060	(Fe,Cr)B
	2	0.02740	16.0	0.050	(Fe,Cr)B + $(Fe,Cr)_2B$
	3	0.06920	5.7	0.090	$(Fe,Cr)_2B$
2	1	0.03415	11.6	0.055	(Fe,Cr)B
	2	0.02485	15.9	0.045	(Fe,Cr)B + $(Fe,Cr)_2B$
	3	0.06925	5.7	0.095	$(Fe,Cr)_2B$
3	1	0.03995	9.9	0.060	(Fe,Cr)B
	2	0.02585	15.3	0.045	(Fe,Cr)B + $(Fe,Cr)_2B$
	3	0.06605	6.0	0.085	$(Fe,Cr)_2B$
n/b	1	0.39500	1.0	0.50	Fe–10% Cr alloy

Note: Δm and Δh are changes in mass and height, respectively, of a sample;
r is an increase in wear resistance in comparison with the alloy base.

Table 6.3. Results of dry abrasive wear resistance tests of borided 13% Cr steel samples. Six consecutive tests were carried out on each of three borided samples until the steel base was reached. Wear resistance of a non-borided sample (n/b) is given in the last line of the table for comparison. Boriding conditions: temperature 950 °C, reaction time 21600 s (6 h).

Borided sample number	Serial test number	Δm (g)	r	Δh (mm)	Phase
1	1	0.03035	11.0	0.035	(Fe,Cr)B
	2	0.01245	26.7	0.020	(Fe,Cr)B
	3	0.02140	15.6	0.030	(Fe,Cr)B
	4	0.02195	15.2	0.035	(Fe,Cr)B–$(Fe,Cr)_2B$
	5	0.03360	9.9	0.040	(Fe,Cr)B–$(Fe,Cr)_2B$
	6	0.05400	6.2	0.050	$(Fe,Cr)_2B$
2	1	0.03210	10.4	0.035	(Fe,Cr)B
	2	0.01315	25.3	0.020	(Fe,Cr)B
	3	0.02140	15.6	0.030	(Fe,Cr)B
	4	0.02195	15.2	0.035	(Fe,Cr)B–$(Fe,Cr)_2B$
	5	0.03165	10.5	0.040	(Fe,Cr)B–$(Fe,Cr)_2B$
	6	0.04385	7.6	0.050	$(Fe,Cr)_2B$
3	1	0.02315	14.4	0.025	(Fe,Cr)B
	2	0.01310	25.4	0.020	(Fe,Cr)B
	3	0.01290	25.8	0.020	(Fe,Cr)B
	4	0.01960	17.0	0.030	(Fe,Cr)B–$(Fe,Cr)_2B$
	5	0.03165	10.5	0.040	(Fe,Cr)B–$(Fe,Cr)_2B$
	6	0.05405	6.2	0.050	$(Fe,Cr)_2B$
n/b	1	0.3329	1	0.40	13% Cr steel

Note: Δm and Δh are changes in mass and height, respectively, of a sample;
r is an increase in wear resistance in comparison with the steel base.

Table 6.4. Results of abrasive wear resistance tests of borided Fe–25% Cr alloy samples. Wear resistance of a non-borided sample (n/b) is given in the last line of the table for comparison. Boriding conditions: temperature 950°C, reaction time 21600 s (6 h).

Borided sample number	Test number	Δm (g)	r	Δh (mm)	Phase
1	1	0.00190	154	~ 0.01	(Fe,Cr)B–(Cr,Fe)B
	2	0.00095	307	< 0.01	(Fe,Cr)B–(Cr,Fe)B
2	1	0.00195	150	~ 0.01	(Fe,Cr)B–(Cr,Fe)B
	2	0.00085	344	< 0.01	(Fe,Cr)B–(Cr,Fe)B
3	1	0.00200	146	~ 0.01	(Fe,Cr)B–(Cr,Fe)B
	2	0.00085	344	< 0.01	(Fe,Cr)B–(Cr,Fe)B
n/b	1	0.29200	1	0.36	Fe–25% Cr alloy

Note: Δm and Δh are changes in mass and height, respectively, of a sample;
r is an increase in wear resistance in comparison with the alloy base.

Table 6.5. Comparison of wear resistance values of the outer FeB layer for the Fe–Cr alloys and chromium steels investigated.

Alloy or steel	5% Cr alloy	10% Cr alloy	13% Cr steel	15% Cr alloy	25% Cr steel	25% Cr alloy	30% Cr alloy
	Microstructure of type I				Microstructure of type II		
Δm_{base} (g)	0.42335	0.32130	0.24335	0.31060	0.25730	0.29910	0.27740
Δh_{base} (mm)	0.47	0.43	0.30	0.41	0.31	0.38	0.37
r_1	1	1.32	1.74	1.36	1.65	1.42	1.53
$\Delta m_{boride\ layer}$ (g)	0.03853	0.02875	0.02645	0.00695	0.00100	0.00095	0.00090
$\Delta h_{boride\ layer}$ (mm)	0.040	0.035	0.030	0.010	~.0.003	~0.003	~0.003
r_2	11.0	11.2	9.2	44.7	257.3	314.8	308.5
r_3	1	1.34	1.46	5.54	38.5	40.6	42.8

Note: Δm and Δh are changes in mass and height, respectively, of a sample;
$r_1 = \Delta m_{\text{ base of a 5\% Cr alloy}} / \Delta m_{\text{ base of a given material}}$;
$r_2 = \Delta m_{\text{ base of a given material}} / \Delta m_{\text{ boride layer on a given material}}$;
$r_3 = \Delta m_{\text{ boride layer on a 5\% Cr alloy}} / \Delta m_{\text{ boride layer on a given material}}$.

Thus, in order to increase the wear resistance of any product or part made of an ordinary iron-base alloy or steel, it is advisable first to cover its surface, for example galvanically, with a Fe–Cr alloy containing 25±5% chromium. Then, it is borided under carefully controlled temperature-time conditions based on the available kinetic data to ensure the necessary thickness and quality of a boride coating. If too high, brittleness of the coating obtained may be lowered by its alloying with Al, Si and other elements.

Conclusions

Two boride layers occur at the interface of Fe–Cr alloys (5–30% Cr) and chromium steels (10 and 25% Cr) with boron in the temperature range of 850–950 ^{o}C and reaction times up to 43200 s (12 h).

In the case of Fe–5% Cr, Fe–10% Cr and Fe–15% Cr alloys and a 13% Cr steel, the outer boride layer bordering the boriding agent consists of the (Fe,Cr)B phase, whereas the inner boride layer adjacent to the solid substrate consists of the $(Fe,Cr)_2B$ phase. Each layer is a homogeneous phase (microstructure of type I).

With Fe–5% Cr and Fe–10% Cr alloys, thermochemical boriding during 3600 s results in the formation of a single $(Fe,Cr)_2B$ layer. The next (Fe,Cr)B layer occurs after the first-occurred $(Fe,Cr)_2B$ layer has reached, depending on the temperature, a thickness of 100-180 μm.

With other alloys and steels, a reaction time of 3600 s is sufficient for both boride layers (Fe,Cr)B and $(Fe,Cr)_2B$ to form.

Each of two boride layers formed on the surface of Fe–25% Cr and Fe–30% Cr alloys and a 25% Cr steel consists of two phases and has a regular network-platelet morphology. The outer boride layer comprises the (Fe,Cr)B and (Cr,Fe)B phases, while the inner consists of the $(Fe,Cr)_2B$ and $(Cr,Fe)_2B$ phases (microstructure of type II).

The characteristic feature of both layers is a pronounced texture, the strongest reflections being {002} and {020} for the FeB phase and {002} for the Fe_2B phase.

Mechanism of formation of the layers generally includes the counter-diffusion of boron and iron (chromium) atoms across their bulks followed by subsequent chemical transformations at layer interfaces.

Diffusional growth kinetics of boride layers are close to parabolic and can more adequately be described by a system of two non-linear differential equations. With the alloys and steels investigated, both approaches yield a good fit to the experimental data.

Temperature dependence of layer growth-rate constants obeys a relation of the Arrhenius type. Values of the activation energy obtained are typical of diffusion-controlled chemical reactions.

Boride layers with the microstructure of the second type exhibit a much higher wear resistance than those with the microstructure of the first type, the difference exceeding an order of magnitude.

References

1. L.G. Voroshnin, L.S. Lyakhovich. Boriding of Steel.- Moskwa: Metallurgiya.- 1978.- 240 p.- In Russian.

2. A.G. Matuschka. Boronizing.- Munchen: Carl Hanser Verlag. - 1980.

3. L.G. Voroshnin. Boriding of Industrial Steels and Cast Irons. – Minsk: Belarus.- 1981. – 205 p.- In Russian.

4. A.K. Sinha. Boriding (Boronizing).- In: A.K. Sinha (Ed.), Metals Handbook, ASM International, Metals Park, Ohio.- 1982.- P. 844.

5. H. Kunst, B. Haase, J.C. Malloy, K. Wittel, M.C. Nestler, A.R. Nicoll, U. Erning, G. Rauscher. Metals, Surface Treatment.- In: Ullmann's Encyclopedia of Industrial Chemistry.- Weinheim: Viley–VCH.- 2006. DOI:10.1002/14356007.a16_403.pub2.

6. K. Holmberg, A. Matthews. Coatings Tribology.- Amsterdam: Elsevier.- 2009.

7. M. Hansen. Constitution of Binary Alloys.- New-York: McGraw-Hill.- 1958.

8. A.E. Vol. Structure and Properties of Binary Metallic Systems.- V.1.- Moskwa: Fizmatgiz.- 1962.- P. 679. - In Russian.

9. T.B. Massalski, J.L. Murray, L.H. Bennett, H. Baker. Binary Alloy Phase Diagrams, V. 1, American Society of Metals, Metals Park, Ohio.- 1986.- P. 351.

10. H. Okamoto. B-Fe (Boron-Iron) // J. Phase Equil. Diffusion. – 2004.- v. 25.- P. 297-298.

11. P. Goeuriot, R. Fillit, F. Thevenot, J. H. Driver, H. Bruyas. The influence of alloying element additions on the boriding of steels.- Mater. Sci. Eng. – 1982.- V. 55, No. 1.- P. 9-19.

12. G. Palombarini, M. Carbucicchio, L. Cento. Electron probe microanalysis of nickel and chromium in Fe-Cr-Ni and Fe-C-Cr alloys borided at 850ºC // J. Mater. Sci. – 1984.- V. 19, No. 11.- P. 3732-3738.

13. M. Carbucicchio, G. Sambogna. Influence of chromium on boride coatings produced on iron alloys // Thin Solid Films.- 1985.- V. 126, No 3-4.- P. 299-305.

14. M. Carbucicchio, G. Palombarini. Effects of alloying elements on the growth of iron boride coatings // J. Mater. Sci. Lett. – 1987.- V. 6, No. 10.- P. 1147-1149.

15. C.M. Brakman, A.W.J. Gommers, E.I. Mittemeijer. Boriding of Fe and Fe-C, Fe-Cr and Fe-Ni Alloys. Boride-layer growth kinetics // J. Mater. Res.- 1989.- V. 4, No. 6.- P.1354-1370.

16. R. Iakovou, L. Bourithis, G. Papadimitriou. Synthesis of boride coatings on steel using plasma transferred arc (PTA) process and its wear performance // Wear.- 2002.- V. 252, No. 11-12.- P. 1007-1015.

17. C. Meric, C. Sahin, B. Backir, N.C. Kokcal. Vliyaniye borirovaniya na abrazivniy iznos chugunov // Metalloved. Term. Obrab. Metallov.- 2003.- No. 9.- P. 26-30.

18. I.G. Sizov. Mossbauerskaya spectroscopiya boridnogo sloya posle elecrtonno-luchevoy obrabotki // Metalloved. Term. Obrab. Metallov.- 2003.- No. 9.- P. 22-25.

19. I. Campos, J. Oseguera, U. Figueroa, J. A. García, O. Bautista and G. Kelemenis. Kinetic study of boron diffusion in the paste-boriding process // Mater. Sci. Eng. A.- 2003.- V. 352, No. 1-2.- P. 261-265.

20. K. Genel, I. Ozbek, C. Bindal. Kinetics of boriding of AISI W1 steel // Mater. Sci. Eng. A.- 2003.- V. 347, No. 1-2.- P. 311-314.

21. M.Kulka, P. Pertek. Microstructure and properties of borided 41Cr4 steel after laser surface modification with re-melting // Appl. Surf. Sci..- 2003.- V. 214.- P.278-288.

22. C. Martini, G. Palombarini, M. Carbucicchio. Mechanism of thermochemical growth of iron borides on iron // J. Mater. Sci. – 2004.- V. 39, No. 3.- P. 933-937.

23. A. A. Novakova, I. G. Sizov, D. S. Golubok, T. Yu. Kiseleva, P. O. Revokatov. Electron-beam boriding of low-carbon steel // J. Alloys Compd.- 2004.- V. 383, No 1-2.- P. 108-112.

24. L.G. Yu, X.J. Chen, K.A. Khor, G. Sundararajan. FeB/Fe_2B phase transformation during SPS pack-boriding: Boride layer growth kinetics // Acta Mater. - 2005.- V. 53, No.8.- P. 2361-2368.

25. M. Keddam, S.M. Chentouf. A diffusion model for describing the bilayer growth (FeB/Fe_2B) during the iron powder-pack boriding // Appl. Surf. Sci. – 2005.- V. 252, No. 2.- P. 393-399.

26. L. Avril, B. Courant, J.-J. Hantzpergue. Tribological performance of α-Fe(Cr)-Fe_2B-FeB and α-Fe(Cr)-h-BN coatings obtained by laser melting // Wear.- 2006.- V. 260, No. 4-5.- P. 351-360.

27. E. Galvanetto, F. Borgioli, T. Bacci, G. Pradelli. Wear behaviour of iron boride coatings produced by VPS technique on carbon steels // Wear.- 2006.- V. 260, No. 7-8.- P. 825-831.

28. S. Taktak. A study on the diffusion kinetics of borides on boronized Cr-based steels // J. Mater. Sci.- 2006.- V. 41, No. 22.- P. 7590-7596.

29. I. Campos, G. Ramírez, C. VillaVelázqueza, U. Figueroa, G. Rodríguez. Study of microcracks morphology produced by Vickers indentation on AISI 1045 borided steels // Mater. Sci. Eng. A.- 2008.- V. 475, No. 1-2.- P. 285-292.

30. I. Campos, R. Rosas, U. Figueroa, C. VillaVelázquez, A. Meneses, A. Guevara. Fracture toughness evaluation using Palmqvist crack models on AISI 1045 borided steels // Mater. Sci. Eng. A.- 2008.- V. 488, No. 1-2.- P. 562-568.

31. X. Tian, Y. Lu, S.J. Sun, Z.G. Wang, W.Q. Hao, X.D. Zhu, Y.L. Yang. Effect of boronising on mechanical properties, wear and corrosion of N80 steel // Mater. Sci. Techn.- 2008.- V. 24, No. 3.- P. 314-319(6).

32. M. Keddam. Simulation of the growth kinetics of FeB and Fe_2B phases on the AISI M2 borided steel: Effect of the paste thickness // Intern. J. Mater. Res.- 2009.- V. 100, No. 6.- P. 901-905.

33. S. Sahin. Effects of boronizing process on the surface roughness and dimensions of AISI 1020, AISI 1040 and AISI 2714 // J. Mater. Process. Technol. - 2009.- V. 209, No. 4. P. 1736-1741.

34. M. Tabur, M. Izciler, F. Gul, I. Karacan. Abrasive wear behavior of boronized AISI 8620 steel // Wear.- 2009.- V. 266, No 11–12.- P.1106-1112.

35. I. Campos-Silva, M. Ortiz-Dominguez, M. Keddam, N. Lapez-Prrusquia, A. Carmona-Vargas, M. Elias-Espinosa. Kinetics of the formation of Fe_2B layers in gray cast iron: Effects of boron concentration and boride incubation time // Appl. Surf. Sci.- 2009.- V. 255, No. 22.- P. 9290-9295.

36. C.K.N. Oliveira, L.C. Casteletti, A. Lombardi Neto, G.E. Totten, S.C. Heck. Production and characterization of boride layers on AISI D2 tool steel // Vacuum.- 2010.- V. 84, No.6.- P. 792-796.

37. I. Campos-Silva, M. Ortiz-Domínguez, N. López-Perrusquia, A. Meneses-Amador, R. Escobar-Galindo, J. Martínez-Trinidad. Characterization of AISI 4140 borided steels // Appl. Surf. Sci.- 2010.- V. 256, No. 8.- P. 2372-2379.

38. H. Tavakoli, S.M. Mousavi Khoie. An electrochemical study of the corrosion resistance of boride coating obtained by thermo-reactive diffusion // Mater. Chem. Phys.- 2010.- V. 124, No. 2–3.- P. 1134-1138.

39. Y. Kayali, Y. Yalcin, S.Taktak. Adhesion and wear properties of boro-tempered ductile iron // Mater. Design.- 2011.- V. 32, No. 8–9.- P. 4295-4303.

40. J. Jiang, Y. Wang, Q. Zhong, Q. Zhou, L. Zhang. Preparation of Fe_2B boride coating on low-carbon steel surfaces and its evaluation of hardness and corrosion resistance // Surf. Coat. Techn. – 2011.- V. 206, No. 2-3. – P. 473-478.

41. N. Kiratli, F. Findik. Research on wear characteristics of AISI 1035 steel boronized at various parameters // Industr. Lubr. Tribology .- 2011.- V. 63, No. 2.- P. 127-133.

42. I. Campos-Silva. The boriding process: growth kinetics and mechanical characterization of boride layers // JESTECH. - 2012.- V. 15, No 2.- P. 53-61.

43. J. Brandstötter, W. Lengauer. Multiphase Reaction Diffusion in Transition Metal-Boron Systems // J. Alloys Compd.- 1997.- V. 262-263.- P. 390-396.

44. K.P. Gurov, B.A. Kartashkin, Yu.E. Ugaste. Vzaimnaya diffusiya v mnogofaznikh metallicheskikh sistemakh.- Moskwa: Nauka, 1981.- 352 p. In Russian.

45. A.M. Gusak, T.V. Zaporozhets, Yu.O. Lyashenko, S.V. Kornienko, M.O. Pasichnyy, A.S. Shirinyan. Diffusion-controlled solid state reactions: In alloys, thin-films and nanosystems.- Berlin: Wiley-VCH, 2010. - 498 p.

46. V.I. Dybkov. Reaction diffusion and solid state chemical kinetics, 1st ed.- Kyiv: IPMS Publications, 2002. - 298 p.

47. V.I. Dybkov. Reaction diffusion and solid state chemical kinetics, 2nd ed.- Zuerich: Trans Tech Publications, 2010. - 334 p.

48. V.I. Dybkov. Solid state reaction kinetics.- Kyiv: IPMS Publications, 2013. - 398 p.

49. V.I. Dybkov. Chemical kinetics.- Kyiv: IPMS Publications, 2013. - 286 p.

50. A. A. Bondar. Boron-chromium-iron / In: Landolt-Börnstein, Numerical Data and Functional Relationships in Science and Technology, (New Series) Group IV: Physical Chemistry. Ed. W. Martinsen, Ternary Alloy Systems. Phase Diagrams, Crystallographic

and Thermodynamic Data Critically Evaluated by MSIT, Eds. G. Effenberg, S. Ilyenko Vol. 11D1, Berlin-Heidelberg: Springer, 2007.- P. 320-343.

51. V.I. Dybkov, W. Lengauer, K. Barmak. Formation of boride layers at the Fe–10%Cr alloy-boron interface // J.Alloys Compd.- 2005.- V. 398, No.1-2.- P.113-122.

52. V.I. Dybkov, W. Lengauer, K. Barmak. Abrasive wear resistance of pack-borided iron-chromium alloys / Proc. 16th Plansee Seminar, Eds. G. Kneringer et al., May 30-June 4, 2005, Reutte, Austria.- P. 999-1009.

53. V.I. Dybkov. Diffusional growth kinetics of boride layers at the 13% Cr steel interface with amorphous boron / Abstr. IX Seminar "Diffusion and Termodynamics of Materials" D&T-06, September 13-15, 2006, Brno, Czech Republic.- P. 48.

54. V.I. Dybkov. Diffusional growth kinetics of boride layers at the 13% Cr steel interface with amorphous boron // Defect Diffusion Forum.- 2007.- V. 263.-P.183-188.

55. V.I. Dybkov. Growth of boride layers on the 13% Cr steel surface in a mixture of amorphous boron and KBF_4 // J. Mater. Sci.- 2007.- V. 42, No.16.- P.6614-6627.

56. V.I. Dybkov, V.G. Khoruzha, K.A. Meleshevich. Formation kinetics of boride coatings on iron-chromium alloys (10 and 25% Cr) and their abrasive wear resistance / Proc. Fourth Intern. Conf. "Materials and coatings for extreme performances: investigations, applications, ecologically safe technologies for their production and utilization" MEE-2006, September 18-23, 2006, Zhukovka, Crimea, Ukraine.- P. 284.

57. V.I. Dybkov, L.V. Goncharuk, V.G. Khoruzha, K.A. Meleshevich, A.V. Samelyuk, V.R. Sidorko. Growth kinetics of boride layers on iron-chromium alloys and their dry abrasive wear resistance / Proc. Mater. Sci. Technol. Conf. MS&T-2007, 16-20 September 2007, Detroit, USA, Fundamentals and Characterization: Phase Stability, Diffusion and Their Applications.- P. 513-524.

58. V.I. Dybkov, L.V. Goncharuk, V.G. Khoruzha, K.A. Meleshevich, A.V. Samelyuk, V.R. Sidorko. Formation of boride coatings on iron-chromium alloys and their dry abrasive wear resistance / Abstr. Europ. Congr. Adv. Mater. Processes EUROMAT-2007, 10-13 September, 2007, Nuremberg, Germany, C52-196.- P. 73.

59. V.I. Dybkov, L.V. Goncharuk, V.G. Khoruzha, K.A. Meleshevich, A.V. Samelyuk, V.R. Sidorko. Boride coatings on iron-chromium alloys and their dry abrasive wear resistance / Proc. HighMatTech-2007 Intern. Conf., 15-19 October, 2007, Kyiv, IPMS, Ukraine.- P. 128.

60. V.I. Dybkov, L.V. Goncharuk, V.G. Khoruzha, K.A. Meleshevich, A.V. Samelyuk, V.R. Sidorko. Diffusional growth kinetics of boride layers on iron-chromium alloys // Solid State Phenomena.- 2008.- V. 138. - P. 181-187.

61. V.I. Dybkov, L.V. Goncharuk, V.G. Khoruzha, K.A. Meleshevich, A.V. Samelyuk, V.R. Sidorko. Wear resistance of boride phases on iron-chromium alloys / Abstr. I G.V. Samsonov Intern. Conf. "Materials Science of Refractory Compounds: Achievements and Problems" MSRC-08, May 27-29, 2008, Kyiv, IPMS, Ukraine.- P. 211.

62. V.I. Dybkov, L.V. Goncharuk, V.G. Khoruzha, K.A. Meleshevich, A.V. Samelyuk, V.R. Sidorko. Abrasive wear resistance of boride coatings on iron-chromium alloys / Proc. II G.V.

Samsonov Intern. Conf. “Materials Science of Refractory Compounds” MSRC-2010, May 18-20, 2010, Kyiv, IPMS, Ukraine.- P. 110.

63. V.I. Dybkov, L.V. Goncharuk, V.G. Khoruzha, K.A. Meleshevich, A.V. Samelyuk, V.R. Sidorko. Growth kinetics of boride coatings on iron-chromium alloys/ Proc. II G.V. Samsonov Intern. Conf. “Materials Science of Refractory Compounds” MSRC-2010, May 18-20, 2010, Kyiv, IPMS, Ukraine.- P. 111.

64. V.I. Dybkov, L.V. Goncharuk, V.G. Khoruzha, A.V. Samelyuk, V.R. Sidorko. Dry abrasive wear resistance of boride layers on iron-chromium alloys and steels / Abstr. 49-th Intern. Conf. “Actual Problems of Strength” APS-2010, June 14-18, 2010, Kyiv, IPMS, Ukraine.- P. 275.

65. V.I. Dybkov, L.V. Goncharuk, V.G. Khoruzha, K.A. Meleshevich, A.V. Samelyuk, V.R. Sidorko. Microstructure and wear resistance of boride coatings on chromium-containing alloys and steels / Abstr. Sixth Intern. Conf. “Materials and Coatings for Extreme Performamces: Investigations, Applications, Ecologically Safe Technologies for their Production and Utilization” MEE-2010, September 20-24, 2010, Big Yalta, Ponizovka, Crimea, Ukraine.- P. 270.

66. V.I. Dybkov, V.R. Sidorko, V.G. Khoruzha, A.V. Samelyuk, L.V. Goncharuk. Interaction of 25% chromium steel with boron powder // Poroshkovaya Metallurgiya.- 2011.- No. 7/8.- P. 222-230.

67. V.I. Dybkov, V.R. Sidorko, V.G. Khoruzha, A.V. Samelyuk, L.V. Goncharuk. Microstructure, growth kinetics and wear resistance of boride phases on iron-chromium alloys and steels / Proc.3-rd International Conference HighMatTech-2011, October 3-7, 2011, Kiev, IPMS, Ukraine. - P.107.

68. V.I. Dybkov, L.V. Goncharuk, V.G. Khoruzha, A.V. Samelyuk, V.R. Sidorko. Growth kinetics and abrasive wear resistance of boride layers on Fe–15% Cr alloy // Mater. Sci. Technol. – 2011.- V. 27, No. 10.- P. 1502-1512.

69. V.I. Dybkov, V.R. Sidorko, A.V. Samelyuk, L.V. Goncharuk, V.G. Khoruzha. Thermochemical boriding of Fe–Cr alloys and chromium steels / Proc. III G.V. Samsonov Intern. Conf. “Materials Science of Refractory Compounds” MSRC-2012, May 23-25, 2012, Kyiv, IPMS, Ukraine.- P. 139.

70. V.I. Dybkov, V.R. Sidorko, L.V. Goncharuk, V.G. Khoruzha, A.V. Samelyuk. Microstructure, growth kinetics and abrasive wear resistance of boride layers on Fe–30% Cr alloy // Poroshkovaya Metallurgiya.- 2012.- No. 9/10.- P. 24-37.

71. V.I. Dybkov. Effect of microstructure on the wear resistance of borided Fe–Cr alloys // Intern. J. Mater. Res. IJMR.- 2013.- V. 104, No. 7. - P. 617-629; DOI: 10.3139/146.110915.

72. V.I. Dybkov. Thermochemical boriding of Fe–5% Cr alloy // Poroshkovaya Metallurgiya.- 2015.- (In Press).

73. L.I. Mirkin. Handbook on X-ray Analysis of Polycrystals.- Moskwa Fizmatgiz, 1961.- 864 p. - In Russian.

74. S.S. Gorelik, L.N. Rastorguev, Yu.A. Skakov. X-ray and Electron-optical Analysis: Appendixes.- Moskwa: Metallurgiya, 1970.- 106 p. - In Russian.

75. Barinov V.A., G.A. Dorofeev, L.V. Ovechkin, E.P. Elsukov, A.E. Ermakov. Structure and magnetic properties of the α-FeB phase obtained by mechanical working // Physica Status Solidi: A.- 1991.- V. 123.- P. 527-534.

76. C. Gianoglio, C.Badini. Distribution equilibria of iron and nickel in two phase fields of the Fe-Ni-B system // J. Mater. Sci.- 1986.- V. 21.- P. 4331-4334.

77. S. Okada, T. Atoda, I. Higashi. Structural investigation of Cr_2B_3, Cr_3B_4, and CrB by single-crystal diffractometry // J. Solid State Chemistry.- 1987.- V. 68.- P. 61-67.

78. C. Gianoglio, G. Pradelli, M. Vallino. Solid state equilibria in the Cr-Fe-B system at the temperature of 1373 K // Metallurg. Sci. Technology. - 1983.- V. 1.- P. 51-57.

79. M. Keddam. A kinetic model for the borided layers by the paste-boriding process // Appl. Surf. Sci. – 2004 – V. 236, No. 1.- P.:451-455.

80. M. Keddam. Simulation of the growth kinetics of FeB and Fe_2B phases onthe AISI M2 borided steel: Effect of the paste thickness // Intern. J. Mater. Res. IJMR.- 2009.- Vol. 100, No. 6.- P. 901-905.

81. H. Schmalzried. Chemical kinetics of solids.- Weinheim: Verlag Chemie.- 1995.

82. H. Mehrer. Diffusion in Solids: Fundamentals, Methods, Materials, Diffusion-Controlled Processes, 2nd ed.- Berlin-Heidelberg: Springer.- 2010.

83. G. V. Motovilin, M. A. Masino, O. M. Suvorov. Automobile Materials.- Moskwa: Transport.- 1989.- In Russian.

Collaborators

The invaluable help of V.R. Sidorko, V.G. Khoruzha, L.V. Goncharuk, A.V. Samelyuk, V.V. Berezutsky, S.V. Bykova, L.A. Duma, I.G. Kondratenko, K.A. Meleshevich, E.S. Rabotina, D.M. Pashko and V.M. Petukh with preliminary work, maintenance of equipment and carrying out experiments is acknowledged with sincere gratitude.

L.A. Duma

V.R. Sidorko
05.08.1938-22.09.2014

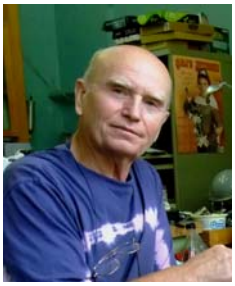

V.M. Petukh

A.V. Samelyuk

V.V. Berezutsky

E.S. Rabotina

L.V. Goncharuk

V.G. Khoruzha

Producers

This book is a result of consolidated efforts of the workers of Dybkov Production Group, Unlimited.
Contribution of smallest creatures is most essential.

W, M, GM

W = wife, M = mother,
GM = grandmother

S = son,
DL = daughter-in-law

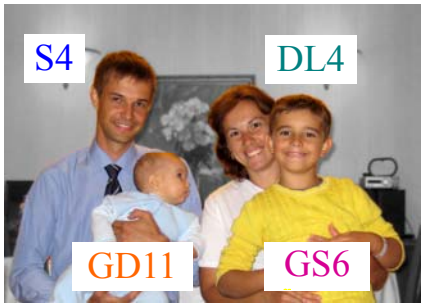

GS = grandson

GD = granddaughter

(Executive Producer)

<Необмежена продюсерська група **ДИБКОВ** – **DYBKOV** production group, Unlimited>

Наукове видання

В. І. Дибков

V. I. Dybkov

Термохімічне борування залізохромових сплавів

Thermochemical Boriding of Iron–Chromium Alloys

(англійською мовою)

(In English)

Авторський оригінал

Electronic version

Надруковано в Україні

Printed in Ukraine